

AD 740 813

UNIVERSITY OF CALIFORNIA, SAN DIEGO
MARINE PHYSICAL LABORATORY OF THE
SCRIPPS INSTITUTION OF OCEANOGRAPHY
SAN DIEGO, CALIFORNIA 92152

STUDIES OF DEEP SEA EROSION
USING DEEP-TOWED INSTRUMENTATION

David A. Johnson

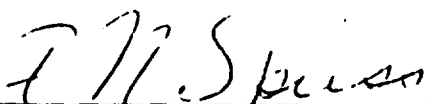
Sponsored by
National Science Foundation
Grant GA 20014
Office of Naval Research
N00014-69-A-0200-6002
NR 260-103
and
The International
Nickel Company

SIO REFERENCE 71-24

1 September 1971

Reproduction in whole or in part is permitted
for any purpose of the U.S. Government

Document cleared for public release
and sale; its distribution is unlimited


F.N. SPIESS, DIRECTOR
MARINE PHYSICAL LABORATORY

Details of illustrations in
this document may be better
studied on microfiche

UNCLASSIFIED

Security Classification

DOCUMENT CONTROL DATA - R & D

(Security classification of title, body of abstract and indexing annotation must be entered when the overall report is classified)

1. ORIGINATING ACTIVITY (Corporate author) University of California, San Diego, Marine Physical Laboratory of the Scripps Institution of Oceanography San Diego, California 92152		2a. REPORT SECURITY CLASSIFICATION Unclassified	
		2b. GROUP	
3. REPORT TITLE STUDIES OF DEEP SEA EROSION USING DEEP-TOWED INSTRUMENTATION			
4. DESCRIPTIVE NOTES (Type of report and inclusive dates) Summary			
5. AUTHOR(S) (First name, middle initial, last name) David A. Johnson			
6. REPORT DATE 1 September 1971	7a. TOTAL NO. OF PAGES 155	7b. NO. OF REFS 126	
8a. CONTRACT OR GRANT NO. NSF Grant GA 20014, ONR N00014-69-A-0200-6002 NR 260-103, and The International Nickel Company		8b. ORIGINATOR'S REPORT NUMBER(S) SIO Reference 71-24	
		9. OTHER REPORT NO(S) (Any other numbers that may be assigned this report) MPL-U-65/71	
10. DISTRIBUTION STATEMENT Document cleared for public release and sale; its distribution is unlimited.			
11. SUPPLEMENTARY NOTES		12. SPONSORING MILITARY ACTIVITY Office of Naval Research	
13. ABSTRACT Detailed geological and geophysical studies were conducted in a region of the equatorial Pacific (near 0° 40' N, 134° 00' W), using the deep-towed instrumentation of the Marine Physical Laboratory. Sediment cores and near-bottom reflection profiles show a sharp angular unconformity a few cm beneath the sea floor, which separates a thin upper layer of Holocene sediment from a chert of Tertiary age. This unconformity is interpreted as a Pleistocene erosion surface which truncates sediments ranging in age from Upper Eocene to Middle Miocene. Bottom currents have evidently caused the erosion and redistribution of sediment tens to hundreds of meters in thickness. Much of the eroded material has been redeposited into a large (15 km x 25 km) topographic basin containing sediments which are considerably thicker than those in the surrounding region. Prominent channels feed into the basin from the areas where erosion has taken place. Significant ocean floor erosion in the central Pacific did not begin until the late Tertiary, and was perhaps restricted to the glacial stages of the Pleistocene when bottom currents may have been considerably stronger than those present today. During successive episodes of high current speeds the erosion surface deepened and became increasingly irregular. The prominent unconformity which is observed today represents only the shape of the erosion surface when current speeds most recently decreased to the point where erosion could no longer take place. The results of this study are comparable with observations in other widely separated regions in the central Pacific, suggesting that some of the processes responsible for erosion in the deep-tow survey area may have affected a substantial portion of the Pacific Ocean floor. Various climatic and oceanographic processes are modified in response to glaciation, and these processes may interact to create conditions on the deep sea floor which favor increased sediment erosion and redistribution. These processes include the intensity of the atmospheric and surface water circulation, the rate of production of deep water in high latitudes, the rate of dissipation of tidal energy on the deep sea floor, and the intensity of chemical dissolution and biological activity at the sea floor. The conditions which apparently led to active sediment erosion in the central Pacific probably developed gradually during a time span of 10,000 to 100,000 years, in contrast to the episodic events of relatively short duration which are commonly characteristic of subaerial erosion processes.			

DD FORM 1 NOV 63 1473
0102-614-6000

1

UNCLASSIFIED

Security Classification

TABLE OF CONTENTS

	Page
LIST OF FIGURES	vii
LIST OF TABLES	x
LIST OF PLATES	xi
ACKNOWLEDGEMENTS	xii
ABSTRACT	xiv
INTRODUCTION	1
METHODS OF STUDY	4
Limitations of Previous Methods	4
Deep-towed Instrumentation	5
Sediment Coring	8
Bottom Current Measurement	9
Seismic Reflection Profiling	15
DESCRIPTION OF DEEP-TOW SURVEY AREA	16
Regional Setting	16
Bathymetry	22
Structure	26
Air gun profiles from surface ship	26
3.5 kHz profiles from deep-towed instrument	27
Sediment types	36
Biostratigraphy	40
Profile I	41
Profile II	44

	Page
Profiles III and IV	44
Profile V	45
Piston Cores	45
Sea Floor Environment	46
Activity of benthic organisms	46
Roughness	48
Bottom currents	55
Reflection profiling survey of surrounding region	56
INTERPRETATIONS OF RESULTS	63
Sediment Redistribution in Deep-tow Survey Area	63
Evidence for erosion	63
Time of erosion	64
Thickness of material eroded	65
Evidence for widespread erosion elsewhere in the central Pacific	67
Deep-tow survey of Area K	67
Detailed surveys in other abyssal hills regions	71
Proposed Mechanisms in Other Regions	72
Probable Mechanisms Influential in Deep-tow Area	75
Tectonic activity	75
Erosion by currents	77
Chemical dissolution	80
Activity of benthic organisms	82
Interaction of various mechanisms	83

	Page
PELAGIC SEDIMENTATION IN EQUATORIAL PACIFIC DURING THE PLEISTOCENE	86
Surface Circulation	86
Deep Circulation	38
Production of bottom water	88
Dissipation of tidal energy	90
Depositional Environment	93
Duration of Erosional Events	101
REFERENCES	102
APPENDIX I	127
APPENDIX II	147

LIST OF FIGURES

Figure		Page
1	Deep-towed instrumentation	6
2	Free vehicle current meter	10
3	Index map showing area of detailed study	17
4	Bottom water circulation in central Pacific	19
5	DSDP sites near study area; age of oceanic crust	21
6	Path of deep-towed instrument within survey area	23
7	Bathymetry of deep-tow survey area	24
8	Comparison of surface and near-bottom reflection profiles .	25
9	Locations of deep-tow reflection profiles (P records)	28
10	P records from west flank of plateau	29
11	P record showing an eroded synclinal structure	31
12	Line drawings based on P records from east flank of plateau	32
13	P records from north end of plateau	34
14	P records from region east of plateau	35
15	Locations of sediment cores	37
16	Unconformity in cores; porosity of major sediment types ..	38
17	Age of sediment cores: Profiles I and II	42
18	Age of sediment cores: Profiles III, IV and V	43
19	Locations of camera stations, bottom current meters, and side-scanning sonar profiles	47
20	Side-scanning sonar profiles	49
21	Bottom current measurements illustrating tidal effect	51

	Page
22 Original current meter records, showing uniform flow direction	52
23 Position plots for current meters #2, 3, and 4	53
24 Current meter records, showing agreement between instruments	54
25 Bathymetry of region surrounding area of detailed study .	57
26 Line drawings based on reflection profiles from region surrounding area of detailed study	58
27 Distribution of principal sediment types	60
28 Bathymetric profiles across floor of depositional basin .	61
29 Bathymetry of Area K	68
30 Reflection profiles from Area K	69
31 Causes of intensified ocean circulation during glaciation.	87
32 Effects of intensified ocean circulation upon deposition .	94
33 Line drawing of reflection profile from survey area	100
34 Hypothetical conditions of deposition during the Pleistocene	100
A1 Bottom photograph from Camera Run C	129
A2 Bottom photograph from Camera Run C	131
A3 Bottom photograph from Camera Run D	133
A4 Bottom photograph from Camera Run K	135
A5 Bottom photograph from Camera Run K	137
A6 Bottom photograph from Camera Run K	139
A7 Bottom photograph from Camera Run K	141

	Page
A8 Bottom photograph from Camera Run K	143
A9 Bottom photograph from Camera Run M	145

LIST OF TABLES

	Page
1a Radiolarian species used for age determinations	11
1b Radiolarian species used for age determinations	12
2a Stratigraphic ranges of Cenozoic radiolarian species	13
2b Stratigraphic ranges of Cenozoic radiolarian species	14
3 Physical properties of sediment cores	39
4 Summary of current meter data	50
5 Continuous Cenozoic sections drilled by DSDP in equatorial Pacific	98
6a Tabulation of current meter data	149
6b Tabulation of current meter data	151
6c Tabulation of current meter data	153

LIST OF PLATES

Plate	Page
1 Photographs of radiolarian species	112
2 Photographs of radiolarian species	114
3 Photographs of radiolarian species	116
4 Free-fall cores, Profile I	118
5 Free-fall cores, Profile II	119
6 Free-fall cores, Profile III	120
7 Free-fall cores, Profile IV	121
8 Free-fall cores, Profile V	122
9 Piston cores	123
10 Occurrence of foraminifera in Tertiary portion of cores .	124
11 Relative abundance of radiolaria in Tertiary portion of cores	125

ACKNOWLEDGEMENTS

Many individuals have provided assistance during this research project. I am especially grateful to Professor Fred B Phleger and Professor Fred N. Spiess for their thoughtful supervision and continuing encouragement.

I thank Professor F. N. Spiess and Professor J. D. Mudie for their leadership and support during the shipboard operations on expeditions EQUATOR and SEVENTOW. Many of the engineers and technicians of the Marine Physical Laboratory have contributed to the successful operation of the deep-tow instrumentation. Special thanks are due to those who participated in the work at sea, including M. S. McGehee, D. E. Boegeman, M. D. Benson, C. D. Lowenstein, F. W. Stone, J. T. Donovan, P. H. Rapp, and G. J. Miller. Bottom current measurements were obtained with the help of H. R. Kaye of the Marine Life Research Group at Scripps. I thank the officers and crew of the R/V THOMAS WASHINGTON and members of the scientific parties for their cooperation and assistance during the work at sea.

During the early phases of this research discussions with Tj. H. van Andel, G. R. Heath, T. C. Moore, Jr., and H. W. Menard were helpful in evaluating the difficulties involved in investigating ocean floor processes. W. R. Riedel assisted in the study and interpretation of sediment cores from the equatorial Pacific. Preliminary field observations were carried out on expedition STYX with the assistance of T. J. Walsh, T. C. Johnson, and J. M. McDonald. I thank W. R. Normark

for his early encouragement in applying the deep-tow instrumentation to the study of deep ocean sedimentation processes.

The sediment cores were analyzed with the help of several individuals. T. J. Walsh provided assistance in splitting and sampling the cores, and in photographing the cores and radiolarian specimens. W. R. Riedel, A. Sanfilippo, and T. C. Moore, Jr. assisted in the identification of several radiolarian specimens. Foraminifera were identified by F. L. Parker. E. L. Hamilton provided data on the physical properties of several of the cores.

Many of my colleagues at Scripps and at other institutions have provided helpful discussion during the course of this study. These individuals include G. Arrhenius, W. H. Berger, M. Hendershott, C. D. Hollister, H. W. Menard, W. Munk, J. L. Reid, Jr., W. B. F. Ryan, M. Wimbush, and E. L. Winterer. Students in the deep-tow group, including J. A. Grow, R. L. Larson, P. F. Lonsdale, B. P. Luyendyk, and W. R. Normark have provided continuing encouragement. Special thanks go to members of my doctoral committee for their continuing assistance, and for their patience in reviewing the manuscript.

Finally, I should like to thank Annette Pickens, Elaine Dunn, and my wife Diann for their assistance in typing and proofreading the manuscript.

This research was supported under grants from the National Science Foundation, the U. S. Office of Naval Research and the International Nickel Company.

STUDIES OF DEEP SEA EROSION¹
USING DEEP-TOWED INSTRUMENTATION

David A. Johnson

University of California, San Diego
Marine Physical Laboratory of the
Scripps Institution of Oceanography
San Diego, California 92152

ABSTRACT

Detailed geological and geophysical studies were conducted in a region of the equatorial Pacific (near 0°40'N, 124°00'W), using the deep-towed instrumentation of the Marine Physical Laboratory. Sediment cores and near-bottom reflection profiles show a sharp angular unconformity a few cm beneath the sea floor, which separates a thin upper layer of Holocene sediment from a chalk of Tertiary age. This unconformity is interpreted as a Pleistocene erosion surface which truncates sediments ranging in age from Upper Eocene to Middle Miocene. Bottom currents have evidently caused the erosion and redistribution of sediment tens to hundreds of meters in thickness. Much of the eroded material has been redeposited into a large (15 km x 25 km) topographic basin containing sediments which are considerably thicker than those in the surrounding region. Prominent channels feed into the basin from the areas where erosion has taken place. Significant

ocean floor erosion in the central Pacific did not begin until the late Tertiary, and was perhaps restricted to the glacial stages of the Pleistocene when bottom currents may have been considerably stronger than those present today. During successive episodes of high current speeds the erosion surface deepened and became increasingly irregular. The prominent unconformity which is observed today represents only the shape of the erosion surface when current speeds most recently decreased to the point where erosion could no longer take place. The results of this study are comparable with observations in other widely separated regions in the central Pacific, suggesting that some of the processes responsible for erosion in the deep-tow survey area may have affected a substantial portion of the Pacific Ocean floor.

Various climatic and oceanographic processes are modified in response to glaciation, and these processes may interact to create conditions on the deep sea floor which favor increased sediment erosion and redistribution. These processes include the intensity of the atmospheric and surface water circulation, the rate of production of deep water in high latitudes, the rate of dissipation of tidal energy on the deep sea floor, and the intensity of chemical dissolution and biological activity at the sea floor. The conditions which apparently led to active sediment erosion in the central Pacific probably developed gradually during a time span of 10,000 to 100,000 years, in contrast to the episodic events of relatively short duration which are commonly characteristic of subaerial erosion processes.

INTRODUCTION

The deep ocean is today the most remote and least understood environment on the surface of the earth. During recent years it has become increasingly evident that conditions on the deep sea floor are far from quiescent, and that sites of uniform, uninterrupted deposition may be rare. The utilization of techniques such as deep sea photography, continuous seismic reflection profiling, current meters, sediment coring, and deep drilling has identified features indicative of sediment redistribution in virtually every region where the sea floor has been examined in detail.

Early investigations of sediment transport in the deep ocean were undertaken along the continental margins and abyssal plains of the western North Atlantic (Ericson et al, 1952; 1961). The sediments in this region commonly contain graded bedding (Heezen et al, 1954) and displaced microfaunas (Phleger, 1951), features which indicate sediment redeposition. Apparently much of the sediment in this part of the deep ocean has been derived from shallower environments and transported hundreds of kilometers across the sea floor (Heezen, 1959). Wherever terrigenous sediment is in abundant supply, large-scale processes of erosion and redeposition such as turbidity currents (Heezen, 1963) and geostrophic contour currents (Heezen et al, 1966; Jones et al, 1970) have been suggested as the critical mechanisms controlling sedimentation.

In other areas of the sea floor, far removed from sources of large quantities of terrigenous material, the depositional record also

contains abundant evidence for reworking, but here the features indicative of redeposition are observed on a relatively small scale. The biogenous pelagic sediments of the equatorial Pacific, for example, have been studied extensively by sediment coring (Riedel, 1971; Hays et al, 1969) and most recently by deep drilling (Tracey et al, 1971; Hays et al, 1971). In this region the sedimentary record commonly contains hiatuses representing the nondeposition or erosion of tens of millions of years of material (Bramlette and Riedel, 1971). Faunal assemblages are often contaminated with microfossils of much greater age which have been reworked into younger material (Riedel and Funnell, 1964). Another characteristic aspect of the sedimentation pattern is its small-scale variability. Early investigations of closely spaced sediment cores revealed that there is significant variability over distances of kilometers or less (Arrhenius, 1963). Subsequent studies suggest that such small-scale irregularities are common, and may be characteristic of pelagic sedimentation throughout the central Pacific (Moore, 1970; Johnson and Johnson, 1970). This variability is puzzling, since the supply of pelagic material to the sea floor is probably uniform over relatively large distances. It appears that various processes are acting at or near the sea floor to create the irregular sediment distribution patterns which are observed.

This study was undertaken in order to gain a better understanding of the conditions which control sediment accumulation on the deep sea floor. During October of 1969 and February of 1970, a detailed investigation of the sea floor was carried out on board the

R/V THOMAS WASHINGTON, operating within a small region of the equatorial Pacific near 07°40'N, 134°00'W. The specific objectives of this study were: (a) to examine in detail a small portion of the ocean floor where substantial erosion and redeposition of sediment has taken place; (b) to establish the sediment distribution pattern on a small scale; (c) to determine the processes which were responsible for producing the depositional features observed; (d) to evaluate the extent in time and in space over which these processes have been influential; and (e) to attempt to predict the effects upon the depositional record in other regions if these processes prove to be of broad general applicability.

METHODS OF STUDY

Limitations of Previous Methods

Severe limitations have been encountered in attempting to study small-scale features and processes on the deep sea floor. One of these is the limited resolution of conventional shipboard echo sounders. During ordinary echo-sounding operations in deep water, a large area of the sea floor (several km^2) is insonified, and it is necessary to make significant corrections to the echo-sounding profiles in order to reconstruct the true sea floor topography (Krause, 1962). Features with dimensions of tens of meters or less may remain completely undetected by this method.

A second limitation is navigational precision. In order to survey and sample sea floor features with dimensions of a few kilometers, such as abyssal hills, one would need to know his relative position in the area of interest to an accuracy of perhaps several tens of meters or less. Satellite navigational techniques are adequate for obtaining an "absolute" position on the earth with an accuracy of tens to hundreds of meters, but the positions are not obtained with sufficient frequency or sufficient accuracy to detect small changes in one's position within a small area. Anchored radar buoys have been employed as navigational reference points (Moore and Heath, 1967; Emery and Ross, 1968; Johnson and Johnson, 1970), but this technique is not entirely satisfactory since changing wind and current conditions cause the buoys to wander considerably relative to the sea floor.

A third limitation is the restricted period of time during which observations of the sea floor can ordinarily be made. Manned submersibles are limited to a period of a few hours or a few days of continuous operation (Ballard and Emery, 1970), and surveys from surface ships are similarly restricted because of high operating costs. The use of free vehicles (Schick et al., 1968; Snodgrass, 1968) has extended the period of continuous operation to several weeks, but even this period of time may be insufficient for detecting the processes which are geologically significant. Geologic processes involving erosion are especially likely to be episodic in nature, and consequently the measurement of a set of parameters over a limited period of time may yield only a representation of "average" conditions. This limitation is difficult to overcome, and must be considered when interpreting short term observations.

Deep-towed instrumentation

The limitations of resolution and navigational precision in deep ocean surveys have been largely overcome through the recent development (by the Marine Physical Laboratory of the Scripps Institution of Oceanography) of a deep-towed instrument package (Spiess and Mudie, 1970). The instrument is towed at a height of 50-100 m above the sea floor (Fig. 1), and is capable of resolving sea floor features with relatively small dimensions which have been difficult to observe by other methods. Navigation of both the instrument and the towing ship is accomplished using an array of anchored acoustic transponders (Spiess et al., 1966; Lowenstein, 1968). Each

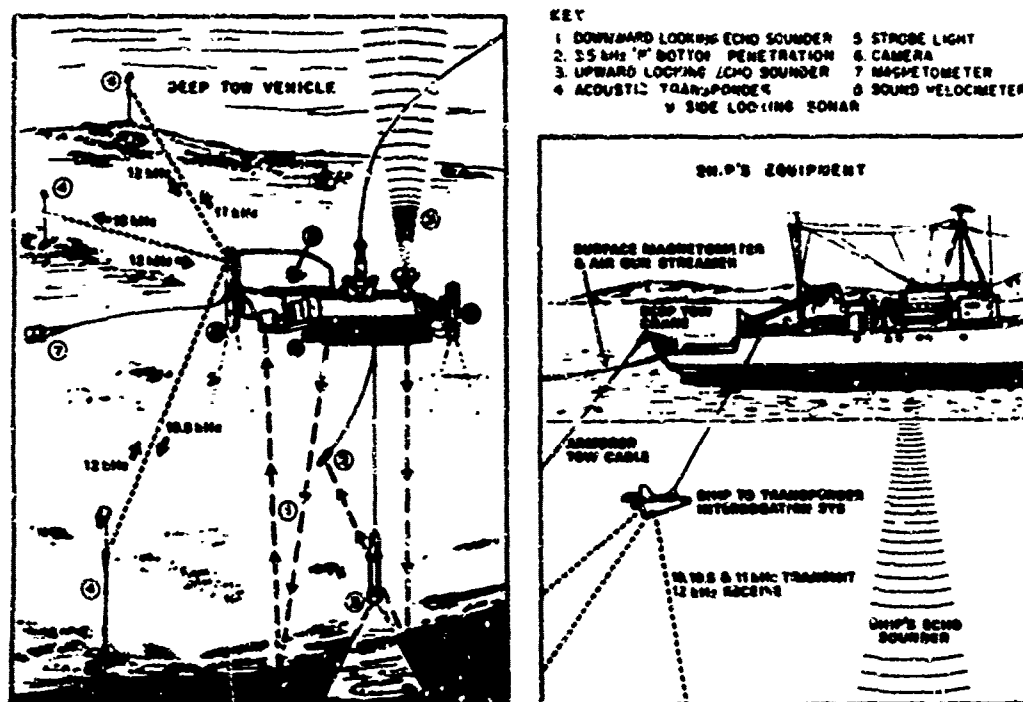


FIGURE 1 The deep-towed instrumentation of the Marine Physical Laboratory. A detailed discussion of the various systems is presented by Spiess and Mudie (1970).

transponder assembly contains a hydrophone positioned at a height of 100 m above the sea floor, which can be interrogated by the towed instrument at a distance of several kilometers. By selectively interrogating the transponders from the towed instrument and from the ship, a range (round trip travel time) to each transponder is determined. When two or more transponders "respond", a position is obtained; the position of the towed instrument relative to the transponder array can be determined to within several meters. The precise geographical coordinates and orientation of the transponder array are then determined by using an independent method of navigating the ship, such as satellite navigation.

Approximately 130 hours of towing within the study area yielded data along 200 km of survey track (Fig. 6). Instrumentation of particular importance during this survey included:

- a. Narrow-beam, 40 kHz down-looking echo sounder. This system, in conjunction with an up-looking echo sounder, provided detailed topographic profiles of the sea floor.
- b. Side-scanning sonar for observing sea floor roughness.
- c. Stereo cameras for photographing the sea floor from a height of about ten meters.
- d. Low frequency (3.5 kHz) sub-bottom penetration system for detecting shallow acoustic reflectors.

Echo soundings were corrected for the velocity of sound in sea water, using a calculated sound velocity profile for the survey area. Bathythermograph (XBT) data were used for the temperature

structure of the upper 500 m; the temperature and salinity of intermediate and deep water were estimated on the basis of recent hydrographic data (Reid, 1960).

Sediment Coring

Sediment samples were obtained using free-fall coring (Moore, 1961; Sachs and Raymond, 1965) and piston coring techniques. During all coring operations the ship was navigated relative to the anchored transponder array. The 42 free-fall cores were dropped in sequences, with five to ten cores along individual profiles. Four of the five profiles correspond to tracks along which deep-tow observations were previously obtained. The position of each free-fall core is known to within 50-100 m the uncertainty is due to small errors in determining the ship's position, and a possible horizontal drift of the cores while descending to the sea floor. During piston coring operations (Cores E-27 and E-28) a relay transponder (Boegeman et al, 1971) was attached to the wire above the tripping arm in order to navigate the core itself relative to the anchored transponder array.

The cores were split longitudinally, described and photographed, and sediment samples were taken for sedimentological and biostratigraphic studies (Plates 4-9). Because of the short length (<30 cm) of most of the cores, only a few samples from each core were required. The following physical properties of the sediment were determined: (a) median and mean grain diameters; (b) percent sand, silt and clay; (c) saturated bulk density; (d) grain density; (e)

porosity; and (f) compressional wave velocity.

The coarse fraction ($>62 \mu$) was separated from each sediment sample, and the radiolarian and foraminiferal assemblages were examined to determine the ages of the cores. Radiolaria of all ages were well preserved, whereas the foraminiferal assemblages showed considerable effects of dissolution, with only the more resistant species remaining. Therefore, the foraminifera were used principally to confirm the ages assigned on the basis of the radiolarian occurrences. Fifty-one Cenozoic radiolarian species (Table 1), all of which have been described previously, were used for assigning ages to the sediment. The ranges of these species are shown in Table 2, using as a basis the radiolarian zonation of Riedel and Sanfilippo (1971).

Bottom Current Measurement

Bottom currents were measured at four locations in the study area, using free-vehicle current meters (Fig. 2) developed by the Marine Life Research Group of the Scripps Institution of Oceanography (Isaacs et al, 1966; Schick et al, 1968). Each instrument was positioned several meters above the sea floor (Table 4), and recorded currents over a period of approximately four days. The direction and speed of the currents are recorded internally on a strip-chart recorder (Fig. 22). Current direction is monitored continuously, whereas the speed is commonly averaged over time increments of one hour. Current speed is designated by a sequence of tic marks along the record. The recorder is calibrated to produce a mark for a given

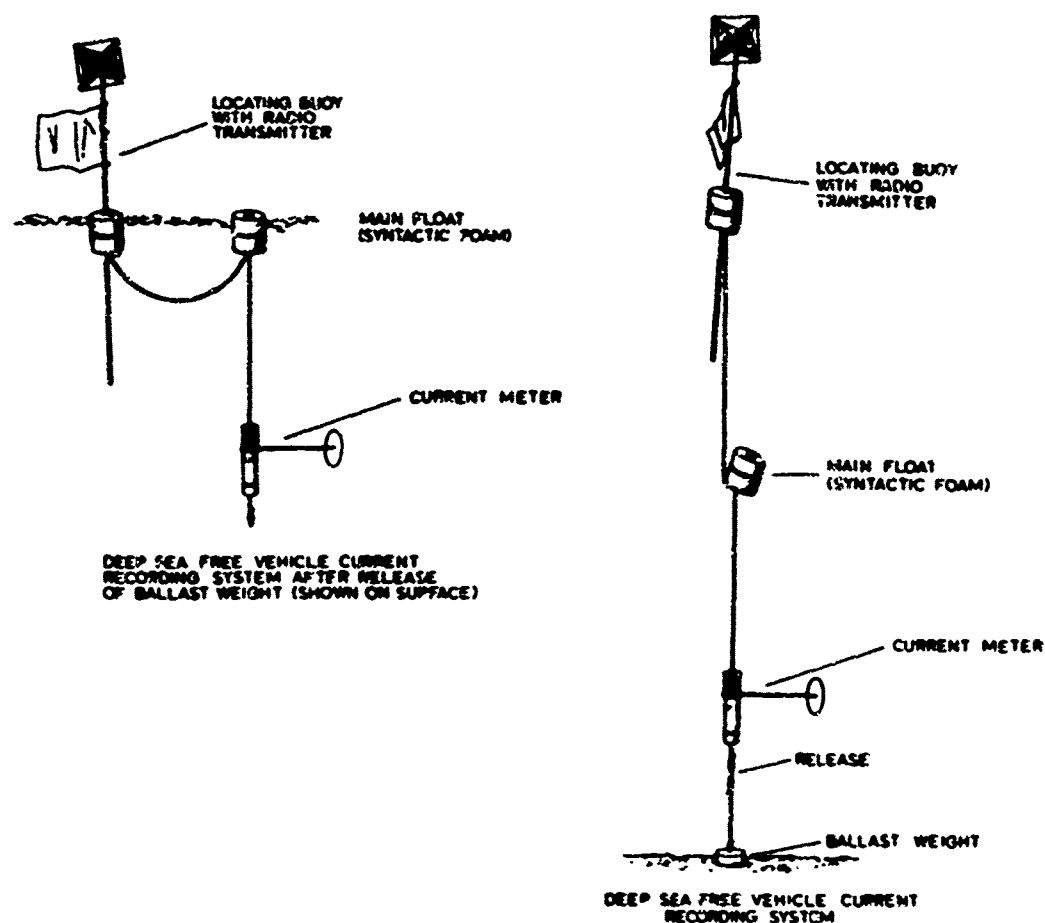


FIGURE 2 Schematic illustration of the free vehicle current meter assembly on the sea floor, and on the sea surface after release of the anchor. The instrumentation is described in detail by Schick *et al.* (1968).

TABLE 1a List of radiolarian species used for age determinations

<u>Species</u>	<u>Illustrations</u>
<u>Thyrsocyrtis triacantha</u> (Ehrenberg)	Plate 1, Fig. 1
<u>Thyrsocyrtis rhizodon</u> Ehrenberg	Plate 7, Fig. 7 in Riedel and Sanfilippo (1970)
<u>Cycladophora hispida</u> (Ehrenberg)	Plate 10, Fig. 7 in Riedel and Sanfilippo (1970)
<u>Thecampe mongolfieri</u> Ehrenberg	Plate 1, Fig. 8
<u>Sethocyrtis babylonis</u> (Clark and Campbell)	Plate 1, Fig. 3
<u>Lithocyclia ocellus</u> Ehrenberg group	Plate 5, Fig. 1 in Riedel and Sanfilippo (1970)
<u>Cycladophora turris</u> Ehrenberg	Plate 1, Fig. 4
<u>Thyrsocyrtis tetracantha</u> (Ehrenberg)	Plate 1, Fig. 2
<u>Lithocyclia aristotelis</u> (Ehrenberg) group	Plate 1, Figs. 13,15
<u>Artophormis barbadensis</u> (Ehrenberg)	Plate 1, Fig. 9
<u>Dorcadospyris triceros</u> (Ehrenberg)	Plate 1, Fig. 16
<u>Thyrsocyrtis bromia</u> Ehrenberg	Plate 1, Figs. 5,6
<u>Cyclampteryum milowi</u> Riedel and Sanfilippo	Plate 2, Fig. 7
<u>Theocyrtis tuberosa</u> Riedel	Plate 3, Fig. 1
<u>Artophormis gracilis</u> Riedel	Plate 1, Fig. 10
<u>Lithocyclia angustum</u> (Riedel)	Plate 1, Fig. 14
<u>Theocorys spongoconum</u> Kling	Plate 3C, Fig. 3 in Riedel and Sanfilippo (1971)
<u>Dorcadospyris quadripes</u> Moore	Plate 1, Fig. 11
<u>Theocyrtis annosa</u> (Riedel)	Plate 3, Fig. 2
<u>Dorcadospyris circulus</u> Moore	Plate 8, Figs. 4,5 in Moore (1971)
<u>Dorcadospyris ateuchus</u> (Ehrenberg)	Plate 2, Fig. 11
<u>Cannartus prismaticus</u> (Haeckel)	Plate 2, Fig. 1
<u>Dorcadospyris papilio</u> (Riedel)	Plate 2, Fig. 14
<u>Cyclampteryum pegetrum</u> Sanfilippo and Riedel	Plate 2, Fig. 8
<u>Dorcadospyris praeforcipata</u> Moore	Plate 9, Figs. 4,5 in Moore (1971)
<u>Calocyclella robusta</u> Moore	Plate 3, Fig. 3
<u>Lychnocanium bipes</u> Riedel	Plate 3, Fig. 5

TABLE 1b List of radiolarian species used for age determinations

<u>Species</u>	<u>Illustrations</u>
<u>Cyrtocapsella tetrapera</u> Haeckel	Plate 3, Fig. 11
<u>Calocycletta virginis</u> Haeckel	Plate 3, Figs. 6,7
<u>Cyrtocapsella cornuta</u> Haeckel	Plate 3, Fig. 10
<u>Dorcadospyrus simplex</u> (Riedel)	Plate 2, Fig. 12
<u>Stichocorys delmontensis</u> (Campbell and Clark)	Plate 3, Fig. 8
<u>Cannartus tubarius</u> (Haeckel)	Plate 2, Fig. 2
<u>Dorcadospyrus forcipata</u> (Haeckel)	Plate 10, Figs. 1,2 in Moore (1971)
<u>Cyclampterus leptetrum</u> Sanfilippo and Riedel	Plate 2, Fig. 9
<u>Stichocorys wolffii</u> Haeckel	Plate 3, Fig. 9
<u>Cannartus violina</u> Haeckel	Plate 2, Fig. 3
<u>Dorcadospyrus dentata</u> Haeckel	Plate 2, Fig. 15
<u>Calocycletta costata</u> (Riedel)	Plate 3, Fig. 4
<u>Lithopera renzae</u> Sanfilippo and Riedel	Plate 3, Fig. 14
<u>Dorcadospyrus alata</u> (Riedel)	Plate 2, Fig. 13
<u>Cyclampterus tanythorax</u> Sanfilippo and Riedel	Plate 2, Fig. 10
<u>Lithopera baueri</u> Sanfilippo and Riedel	Plate 2, Fig. 2 in Sanfilippo and Riedel (1970)
<u>Lithopera thornburgi</u> Sanfilippo and Riedel	Plate 2, Fig. 4 in Sanfilippo and Riedel (1970)
<u>Cannartus laticonus</u> Riedel	Plate 2, Fig. 4
<u>Cannartus petterssoni</u> Riedel and Sanfilippo	Plate 10, Fig. 19 in Riedel and Sanfilippo (1971)
<u>Cyclampterus brachythorax</u> Sanfilippo and Riedel	Plate 2, Fig. 15 in Sanfilippo and Riedel (1970)
<u>Lithopera neotera</u> Sanfilippo and Riedel	Plate 3, Fig. 15
<u>Lithopera bacca</u> Ehrenberg	Plate 1, Fig. 29 in Sanfilippo and Riedel (1970)
<u>Ommatartus antepenultimus</u> Riedel and Sanfilippo	Plate 2, Fig. 5
<u>Ommatartus hughesi</u> (Campbell and Clark)	Plate 2, Fig. 6
<u>Cyclampterus neatum</u> Sanfilippo and Riedel	Plate 2, Fig. 17 in Sanfilippo and Riedel (1970)

TABLE 2a

Stratigraphic ranges of Cenozoic radiolarian species. Radiolarian zonation is from Riedel and Sanfilippo (1971). Ranges of Eocene species are based on Figure 2 of Riedel and Sanfilippo (1970). Ranges of Oligocene and Miocene species are based on Figure 2 of Riedel and Sanfilippo (1971) and Table 1 of Moore (1971).

SPECIES	ZONES																									
		THYRSOCYRTIS TRIACANTHA	THYRSOCYRTIS RHIZODON	CYCLADOPHORA HISPIDA	THEOCAMPZ MONGOLIENSI	SETHOCYRTIS BABYLONIS	LITHOCYCLIA OCELLUM	CYCLADOPHORA TURBIS	THYRSOCYRTIS TETRACANTHA	LITHOCYCLIA ARISTOTELIS	ARTOPHYMIS ZABARDENIS	DORCADOSPYRIS TRICHROS	THYRSOCYRTIS BRODIA	CYCLAMPETRIUM HILGVI	THEOCYRTIS TURBOSA	ARTOPHYMIS GRACILIS	LITHOCYCLIA ANGUSTUM	THEOCYRTIS SPONGOCOMUM	DORCADOSPYRIS QUADRIPES	THEOCYRTIS ANNOSA	DORCADOSPYRIS CIRCULUS	DORCADOSPYRIS ATEUCHUS	CAMPARTUS PRISMATICUS	DORCADOSPYRIS PAPILLO	CYCLAMPETRIUM PACETRIUM	DORCADOSPYRIS PRANTOCISTRATA
CALOCYCLETIA	COSTATA																									
CALOCYCLETIA	VIRGINIS																									
LYCHNOCANIUM	BIPES																									
DORCADOSPYRIS	ATEUCHUS																									
THEOCYRTIS	TUBEROSA																									
THYRSOCYRTIS	BRODIA																									

number of revolutions of the Savonius rotor, and the spacing between these marks is inversely proportional to the current speed.

Seismic Reflection Profiling

An air gun reflection profiling system on board the survey ship was used to identify the acoustic basement and to determine the sediment thickness and sediment distribution pattern. Profiles were obtained within the deep-tow survey area, and in an extensive area (measuring approximately 50 km by 50 km) surrounding the site of detailed investigation. Approximately 700 km of continuous profiles were obtained.

DESCRIPTION OF DEEP-TOW SURVEY AREA

Regional Setting

The site chosen for detailed study (near 07°40'N, 134°00'W; Fig.3) lies within the equatorial zone of high primary productivity, and consequently the principal component of the sediment is biogenous (Arrhenius, 1963). Cores from previous expeditions (Riedel, 1971) recovered outcropping Oligocene sediment at the survey site, suggesting that considerable sediment erosion may have taken place.

The surface sediment distribution pattern in this region of the Pacific has been described by numerous investigators, including Arrhenius (1952), Hays et al (1969), and Riedel (1971). Carbonate sediment is confined to the relatively shallow regions to the south of the Clipperton Fracture Zone, and to depths less than about 4500 m on the East Pacific Rise (Parker and Berger, 1971). Apart from these shallow regions, sediment types are generally siliceous in low latitudes and increasingly nonbiogenous in higher latitudes. Quaternary sediment appears to be thickest at the equator (Tracey et al, 1971), although fossiliferous Quaternary ooze extends over a wide zone between latitudes 14°N and 7°S (Hays et al, 1969). The width of this zone can be attributed to seasonal fluctuations in the circulation pattern (Knauss, 1963), and the corresponding seasonal, latitudinal, and longitudinal variations in primary productivity (Owen and Zeitzschel, 1970). Reflection profiling (Ewing et al, 1968) and deep drilling (Tracey et al, 1971) have shown that the sediment pattern

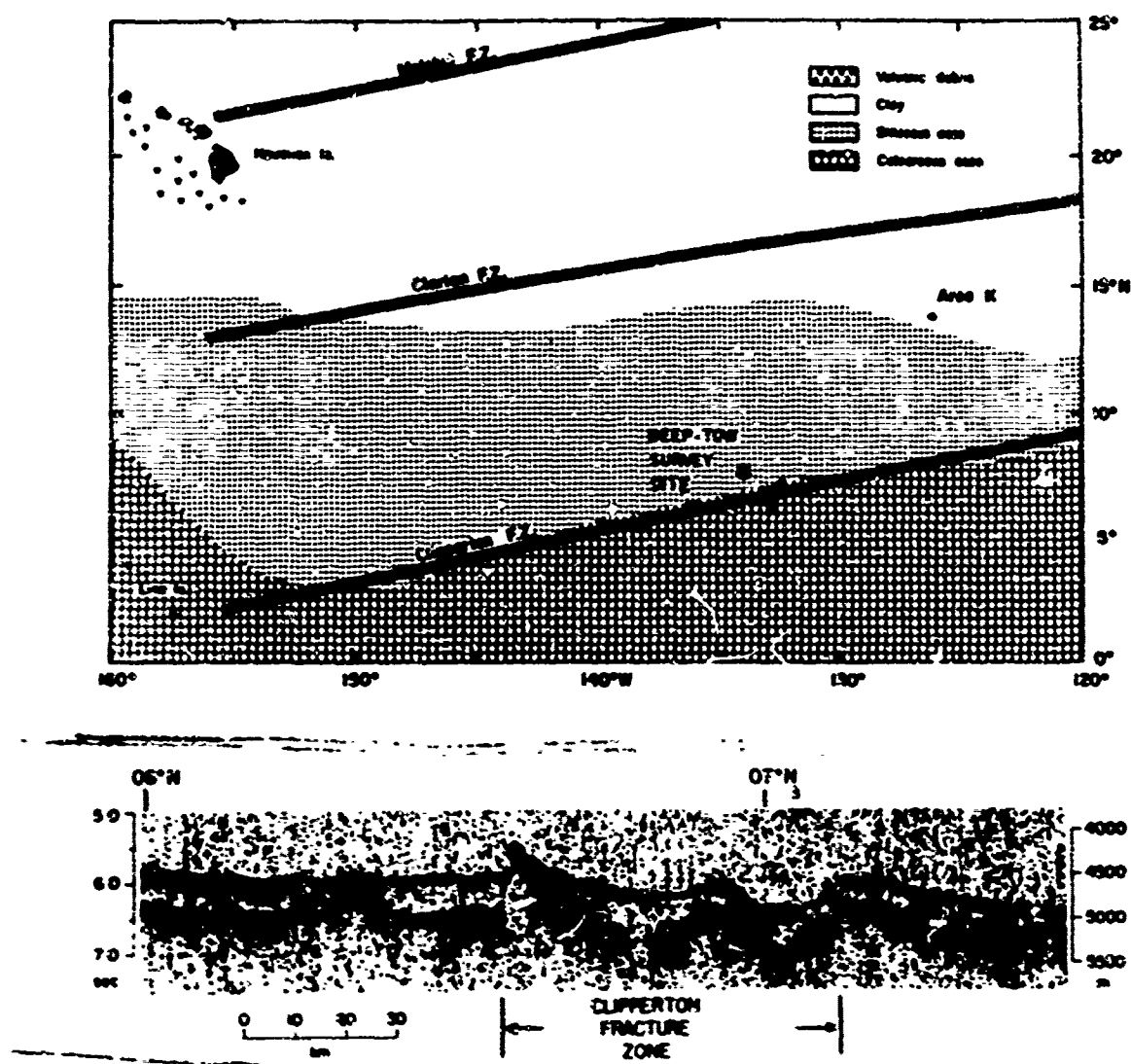


Figure 3 (top) Location of the deep-tow survey site in the equatorial Pacific. Distribution of sediment types is modified after data of Arrhenius (1963), Hays et al. (1969), and Riedel (1971). The solid line to the southeast of the deep-tow area shows the location of the seismic reflection profile across the Clipperton Fracture Zone, shown below. The location marked "Area K" was also surveyed using the deep-towed instrumentation. Some of the results from that survey are included in this report.

(bottom) Continuous seismic reflection profile across the Clipperton Fracture Zone. The relief of the acoustic basement within the fracture zone is quite irregular, and contrasts noticeably with the relatively smooth basement to the north and to the south. The sea floor to the south of the fracture zone is somewhat shallower than to the north, and the average sediment thickness increases from approximately 0.3-0.4 sec north of the fracture zone to 0.5 sec south of the zone.

has a pronounced north-south asymmetry, and that the sediment is thickest a few degrees north of the equator. This effect can be attributed, in part at least, to a northward component in the motion of the Pacific plate during the Tertiary relative to the biological equator.

The general features of the circulation of bottom water in the central Pacific are fairly well established as a result of hydrographic studies (Wooster and Volkmann, 1960; Reid et al, 1968; Edmond et al, 1971; Gordon and Gerard, 1971) and direct current measurements (Reid, 1969). Antarctic Bottom Water enters the Pacific Ocean south of New Zealand and flows northward along the western wall of the Tonga-Kermadec trench as an intensified western boundary current. The current enters the North Pacific through a narrow passage northeast of Samoa (Fig.4) and then apparently diverges. Major topographic features including the Hawaiian Ridge, Line Islands Ridge, and Mid-Pacific Mountains serve as barriers to bottom water flow within the North Pacific (Edmond et al, 1971). Bottom currents are apparently restricted to northwestward flow along the western side of the Line Islands Ridge (C of Fig. 4), and turn eastward across the ridge barrier at only two locations: Horizon passage (E of Fig. 4) and Clarion Passage (F of Fig. 4). To the east of the Line Islands Ridge and north of the Clipperton Fracture Zone the bottom water flow appears to be eastward to northeastward (G of Fig. 4; also Evans and White, 1971), but there are few direct current measurements in this region.

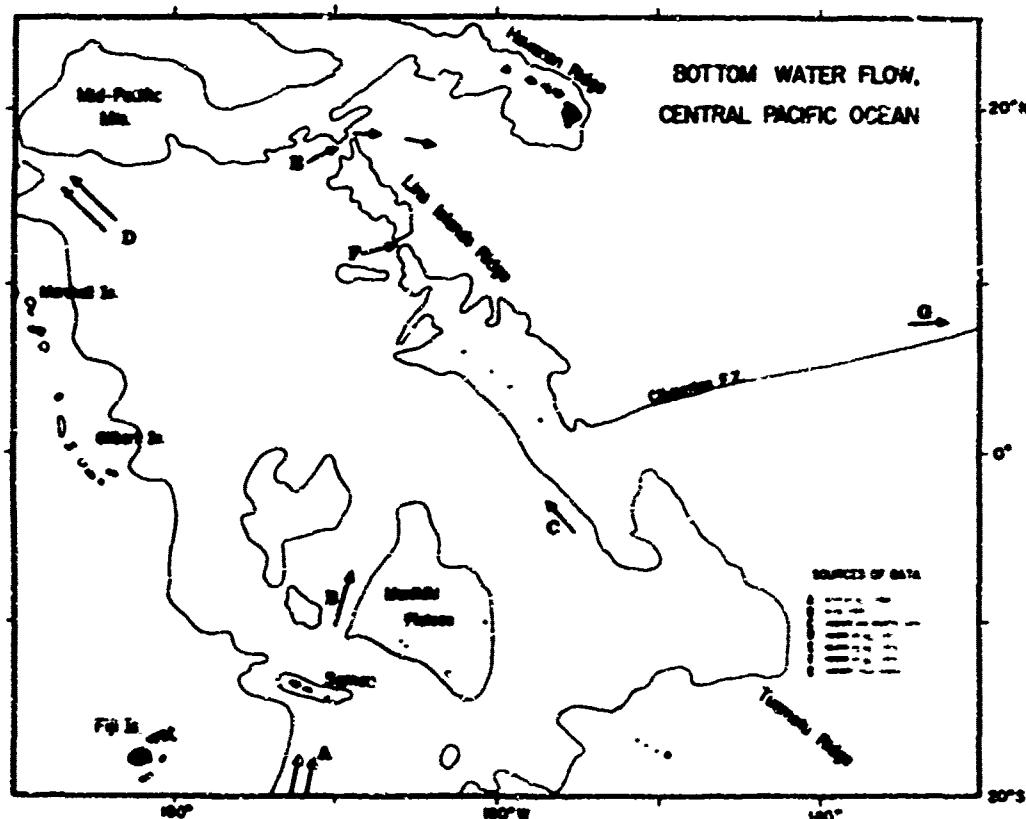


FIGURE 4 Direction of flow of bottom water in the central Pacific Ocean. The contour shown represents a depth of approximately 2500 fathoms (4700 meters). Arrows show the direction of flow of bottom water on the basis of hydrographic data and direct current measurements.

The Clipperton Fracture Zone (Menard and Fisher, 1958) is among the most prominent bathymetric and structural features in the eastern equatorial Pacific. The fracture zone is commonly a well defined north-facing escarpment (Heath and Moore, 1965; Ewing et al, 1968) with up to several hundred meters of relief. In the region nearest the study area the fracture zone is not an obvious topographic feature, but it can be identified by seismic reflection profiling (Fig.3).

Between the fracture zones of the northeast Pacific the principal topographic features are low abyssal hills up to several hundred meters in height (Chase et al, 1970). The hills are commonly elongated in a direction parallel to the trend of the magnetic anomalies, and appear to be both volcanic and tectonic in origin (Luyendyk, 1970). In low latitudes the magnetic lineations are difficult to identify (Atwater and Menard, 1970), and topographic lineations are obscured by the thick cover of pelagic sediment (Ewing et al, 1968).

The age of the oceanic crust at the deep-tow survey site can be estimated from the recent results of deep drilling. The Deep Sea Drilling Project Sites 155, 160, and 161, together with the deep-tow survey site, lie between the Clarion and Clipperton Fracture Zones (Fig. 5). Basalt was penetrated at each of these three DSDP sites (van Andel et al, 1971). If one assumes that (1) the age of the oldest sediment cored at these drilling sites is approximately the same as the crustal age, and (2) the rate of crustal formation was nearly uniform during the time interval

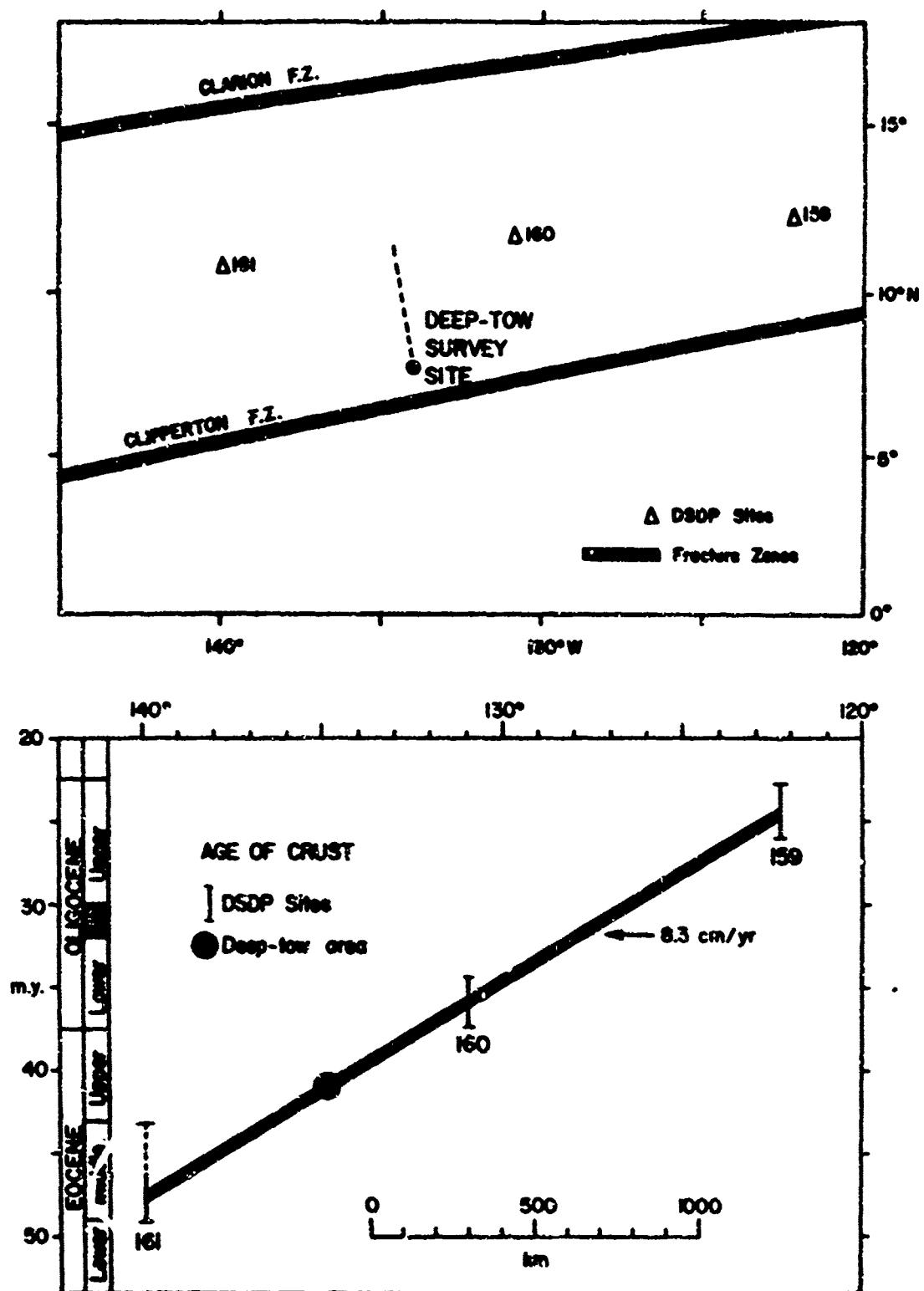


Figure 5 (top) Location of Deep Sea Drilling Project sites in the vicinity of the deep-tow survey area. Basalt was cored at each of these drilling locations. (bottom) Age of oldest sediment obtained at the drilling sites shown above (after Van Andel et al., 1971). The age of the oceanic crust at the deep-tow site can be estimated by interpolating from the drilling results. The half-spreading rate during this period of crustal formation was around 8.3 cm/yr.

represented by this portion of oceanic crust, then by interpolation one can estimate that the crustal age at the deep-tow survey site is approximately 41 million years, or within the Upper Eocene (Fig. 5). The average half-spreading rate during this interval of crustal formation was around 8 cm/yr, a rate which was predicted by Riedel (1967) on the basis of core data alone.

Bathymetry

The site of detailed study centers around a flat-topped plateau and an adjacent trough, both of which are elongated in a north-south direction (Fig. 7). The plateau is up to 5 km in width, and rises 200 to 300 m above the surrounding sea floor. The summit is bordered by a well defined break in slope, which deepens toward the northern end. The western flank of the plateau is smooth and gently sloping near the crest, with some escarpments 10-20 m in height near the base (Fig. 10). A topographic depression lies between the plateau and the surrounding sea floor to the west. The eastern flank is characterized by escarpments with slopes which locally are 60° or greater; some of these escarpments are up to 50 m in height (Fig. 12). The plateau narrows to the north until it is indistinguishable from the surrounding sea floor. To the south the plateau becomes part of a steep basement ridge.

A north-south trending trough lies to the east of the plateau (Figs. 7 and 8). The trough, which is 5 to 10 km in width, is apparently closed at the northern end of the survey area (Fig. 7). It deepens in a southward direction, and continues beyond the

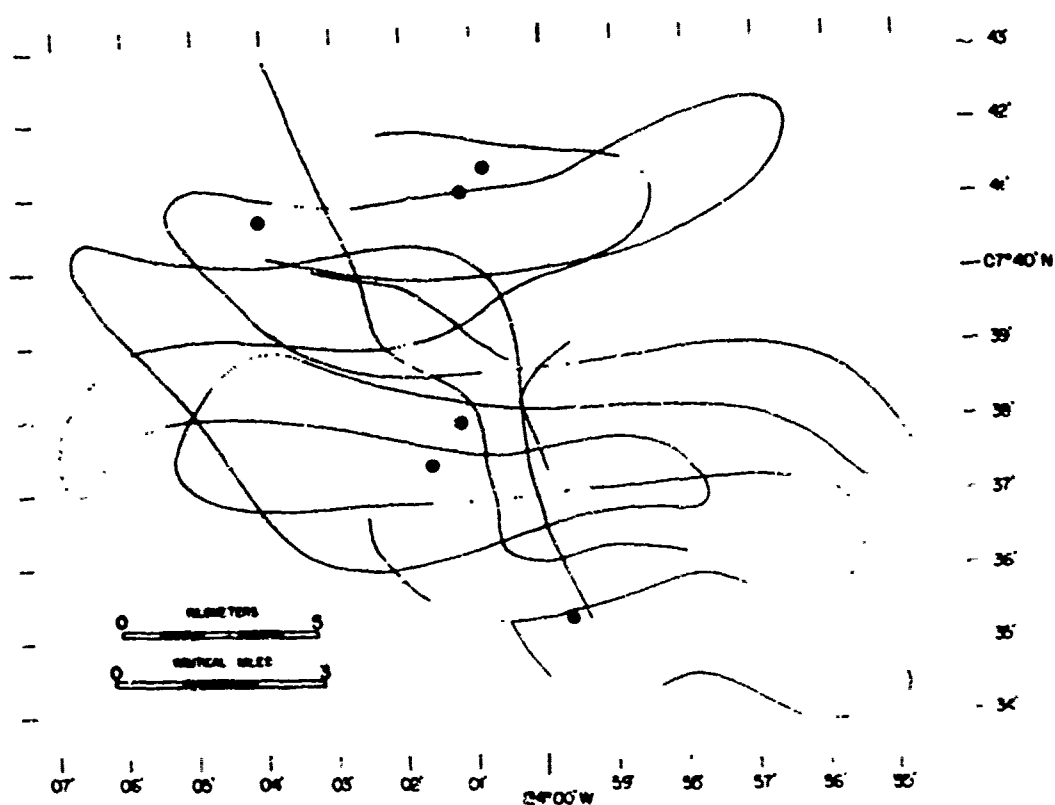


FIGURE 6 Path of the deep-towed instrument within the region of detailed study. Quartered circles show the location of anchored acoustic transponders. Ranges to two or more transponders were obtained along the portion of the track shown in solid lines.

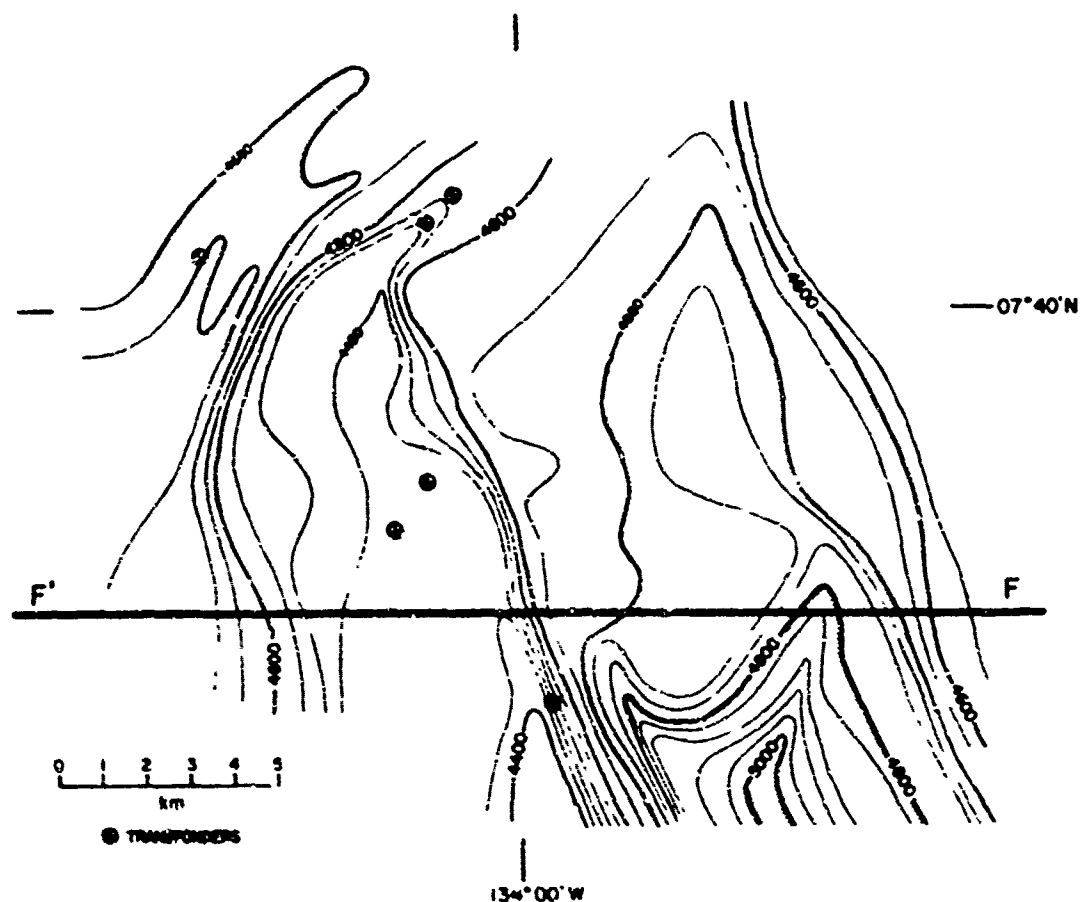


FIGURE 7 Bathymetry of the deep-tow survey area. Contour interval is 40 meters. Line F'F indicates the location of the seismic reflection profile shown at the top of Figure 8.

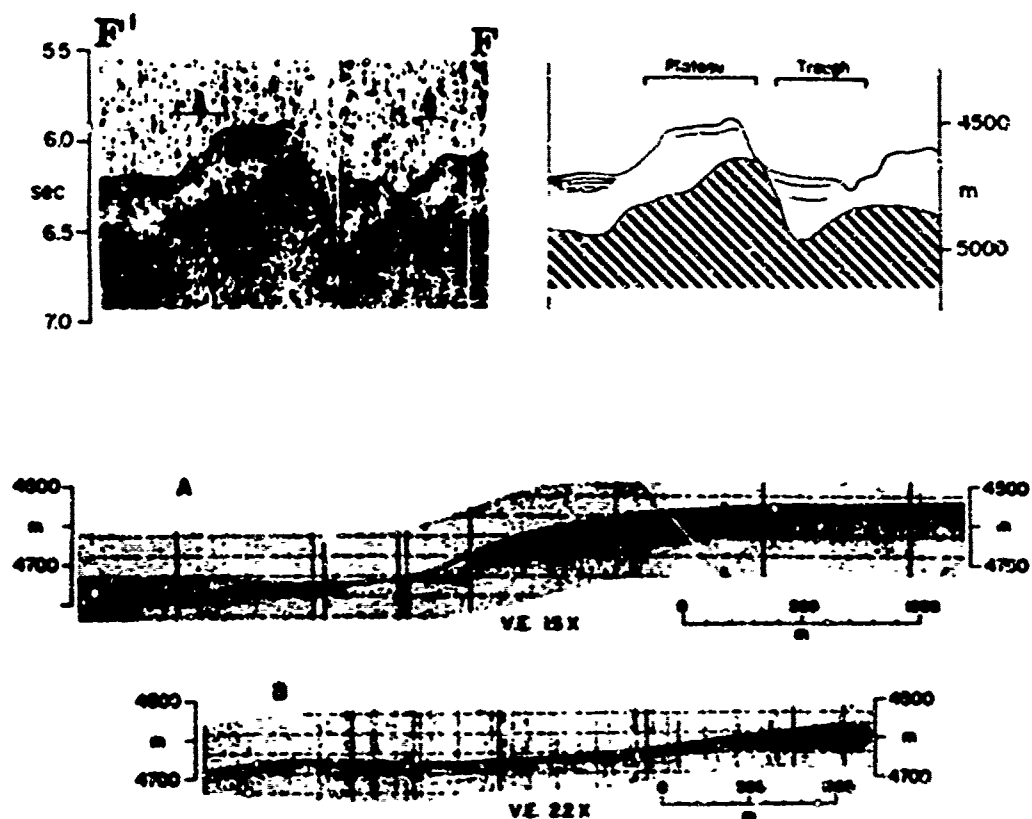


Figure 8 Comparison of surface and near-bottom reflection profiles. (upper left) East-west seismic reflection profile across the deep-tow survey area. Vertical exaggeration 16 X. (upper right) Line drawing of profile F'F'. The acoustic basement appears to outcrop at the base of the plateau's east flank. A prominent erosional channel can be seen on the floor of the trough. (bottom) Reflection profiles (3.5 kHz) obtained from the deep-towed instrument. The approximate locations of these profiles along F'F' are indicated. Profile A is from the west flank of the plateau, and profile B is from the east side of the trough. There is relatively little vertical exaggeration on the deep-tow profiles. The truncation of sub-bottom reflectors is clear on the deep-tow profiles, but cannot be resolved on the profile obtained from the sea surface.

southernmost limit of the area of detailed study. A major channel extends southward along the axis of the trough, with at least one secondary channel entering from the plateau to the west. The principal channel is bordered by broad, smooth terraces, several km in width, which parallel the channel along the floor of the trough.

Structure

Air gun profiles from surface ship

Seismic reflection profiling techniques from the surface ship were utilized to estimate the sediment thickness and distribution pattern within the deep-tow survey area and in the surrounding region. The plateau in the area of detailed study is composed of 0.3 to 0.4 sec of sediment which overlies an irregular acoustic basement (Fig. 8). On the plateau's eastern flank the basement appears to outcrop locally. In the trough, to the east of the plateau, sediments are 0.2 to 0.3 sec in thickness. The relief of the sea floor bears some relation to that of the acoustic basement, but the total sediment thickness is highly variable over distances of a few kilometers or less.

The air gun profiles obtained by the ship are insufficient for resolving the sedimentation pattern around small features and for detecting fine-scale layering within the sedimentary unit. These profiles commonly show few or no internal reflectors within the sedimentary material. Considerably more detail appears when low frequency profiling techniques are used from the towed instrument operating near the sea floor (see Fig. 8 for comparison of surface

and near-bottom reflection profiles). Continuous reflection profiles obtained by the 3.5 kHz system on the deep-towed instrument show stratification within the sediment which could not be resolved by the air gun profiling techniques. These near-bottom profiles are the basis for identifying the relative ages of outcropping strata, and determining the fine-scale sediment distribution pattern within the survey area.

3.5 kHz profiles from deep-towed instrument

Near-bottom reflection profiling shows that the plateau is underlain by horizontal to gently dipping sedimentary layers which outcrop on both the east and west flanks. The relief on the plateau's west flank is characteristically smooth near the crest, and profiles from these regions (Fig. 10) clearly show outcropping strata which appear to be progressively older down the flank. The layers which outcrop near the base appear to be 100 to 200 m stratigraphically beneath those which outcrop near the crest (Profile 2). There is evidence on Profile 1 (Fig. 10) that folding of the sediments has taken place; this interpretation is supported by results of sediment coring along this profile (Fig. 17, Profile II).

A topographic depression separates the plateau from the surrounding sea floor to the west. In this region the relief is often irregular (Fig. 10, Profiles 3 and 4), and identification of sub-bottom reflectors is more difficult. The profiles suggest that this depression is an erosional channel. Locally the channel is bordered by escarpments up to 50 m in height with near-horizontal

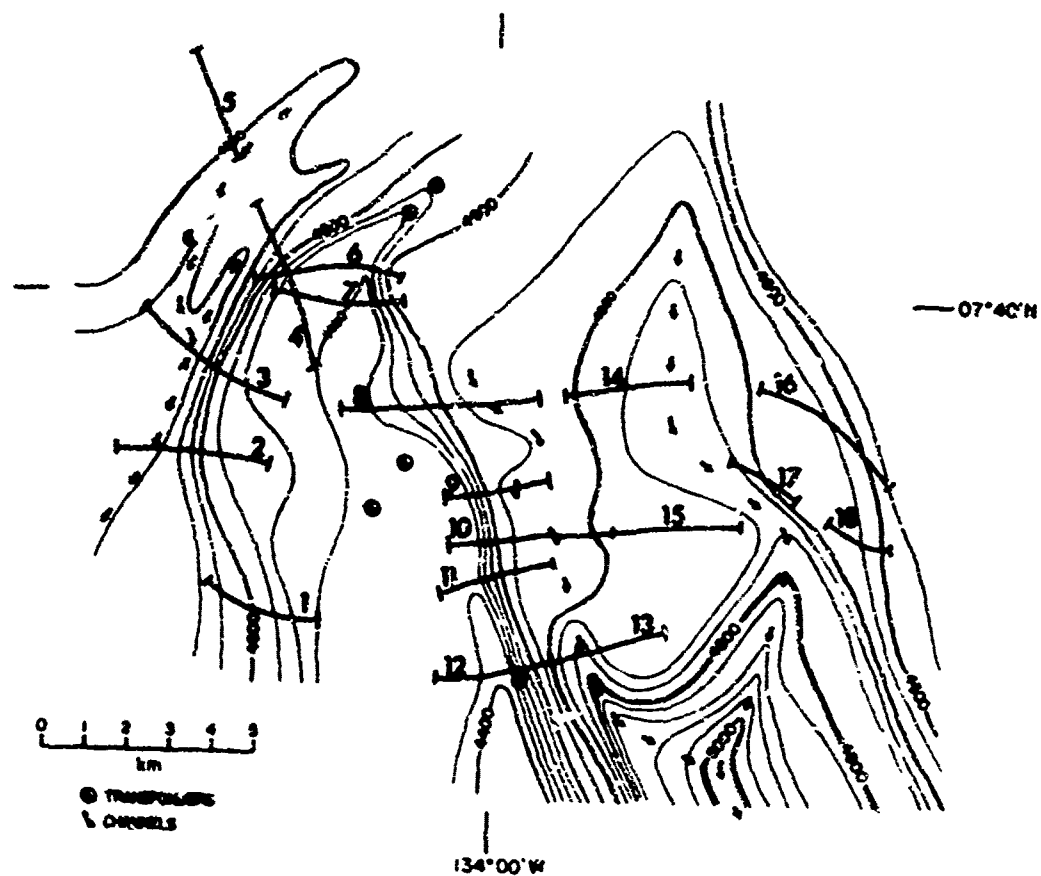


FIGURE 9 Locations of near-bottom reflection profiles shown in Figures 10 through 14. Arrows indicate erosional channels which appear on the profiles.

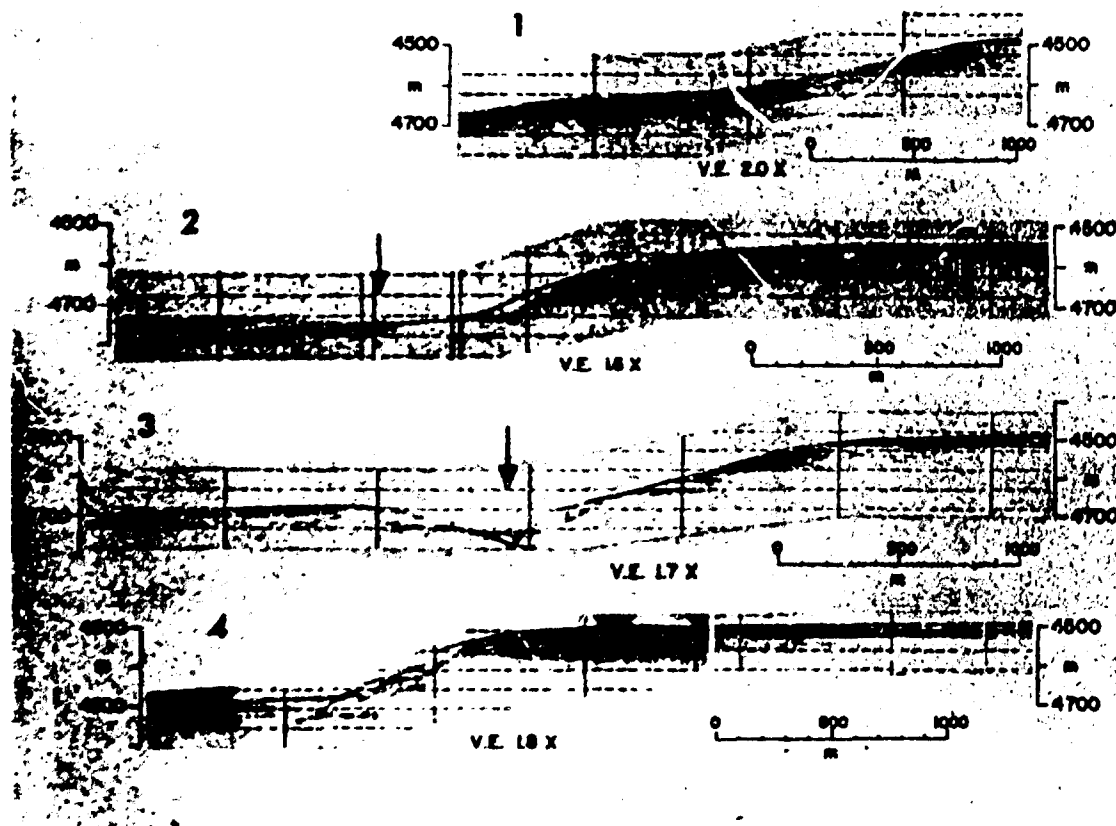


Figure 10 Near bottom reflection profiles from the west flank of the plateau. Outcropping horizontal strata can be seen on the upper flank. Topographic and structural details at the base of the slope on profile 3 are obscure because of the height of the instrument at this point. Arrows indicate the location of a principal erosional channel which extends southward along the base of the slope.

sedimentary strata outcropping at the walls on both sides (Fig. 10, Profile 3; Fig. 17, Profile 1). Elsewhere the relief at the base of the plateau is relatively smooth (Fig. 10, Profile 2).

The sea floor to the west of the plateau is characterized by gently dipping strata which are abruptly truncated at the sea floor interface. Fig. 11 shows an eroded synclinal structure in which layers that are 100-200 m apart stratigraphically appear to outcrop within a distance of one or two kilometers. This sharp angular unconformity is widespread throughout the surveyed area and results in outcropping strata of markedly different ages over a small area. Beneath the sea floor, however, the strata appear to be conformable, with no evidence of similar unconformities at depth.

The topography on the east flank of the plateau is irregular, with steep ($>60^\circ$) escarpments 20 to 100 m in height in some regions (Fig. 12, Profiles 8, 9, and 11), and smooth slopes elsewhere (Profiles 10, 12). Near the crest the strata dip gently toward the west, and in the trough beyond the base of the plateau the layers dip eastward, suggesting an eroded anticlinal structure (Profiles 8, 9, and 10). On the intervening lower slopes the topography is irregular and the sea floor is acoustically opaque to the 3.5 kHz profiler, commonly obscuring the details of the subsurface structure. Near the southern end of the survey area a strong acoustic reflector outcrops at the sea floor (Fig. 12), which probably corresponds to the acoustic basement identified by reflection profiling from the ship (Fig. 8).

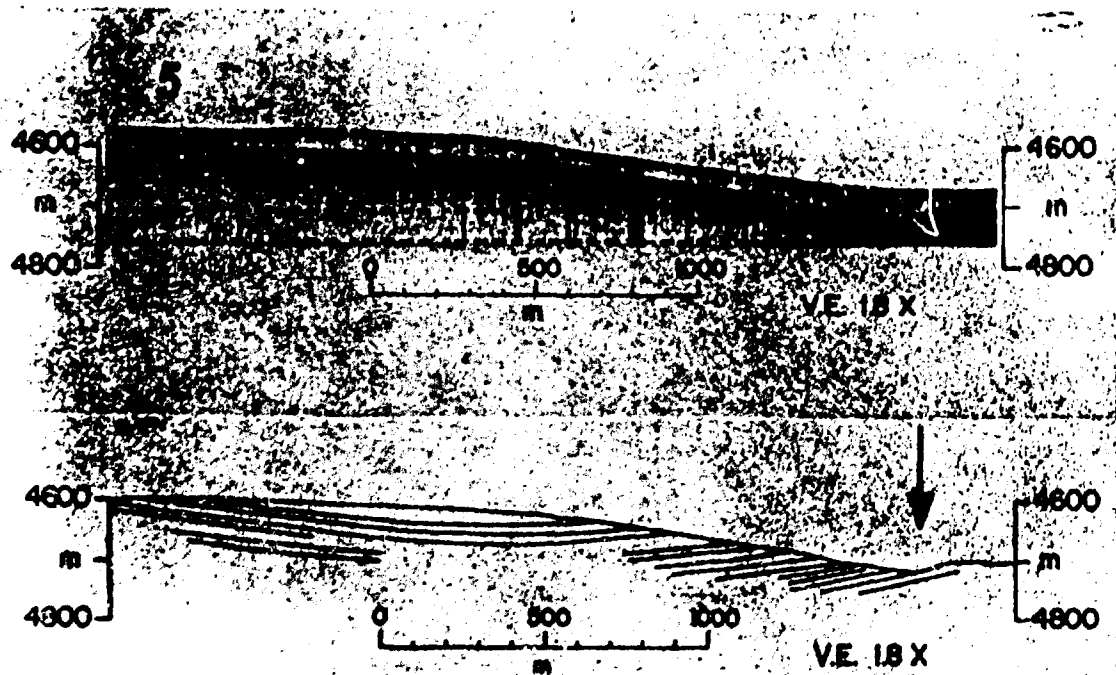


FIGURE 11 (top) Near-bottom reflection profile showing an eroded synclinal structure.
(bottom) Line drawing interpretation of Profile 5 shown above. The arrow marks the axis of an erosional channel.

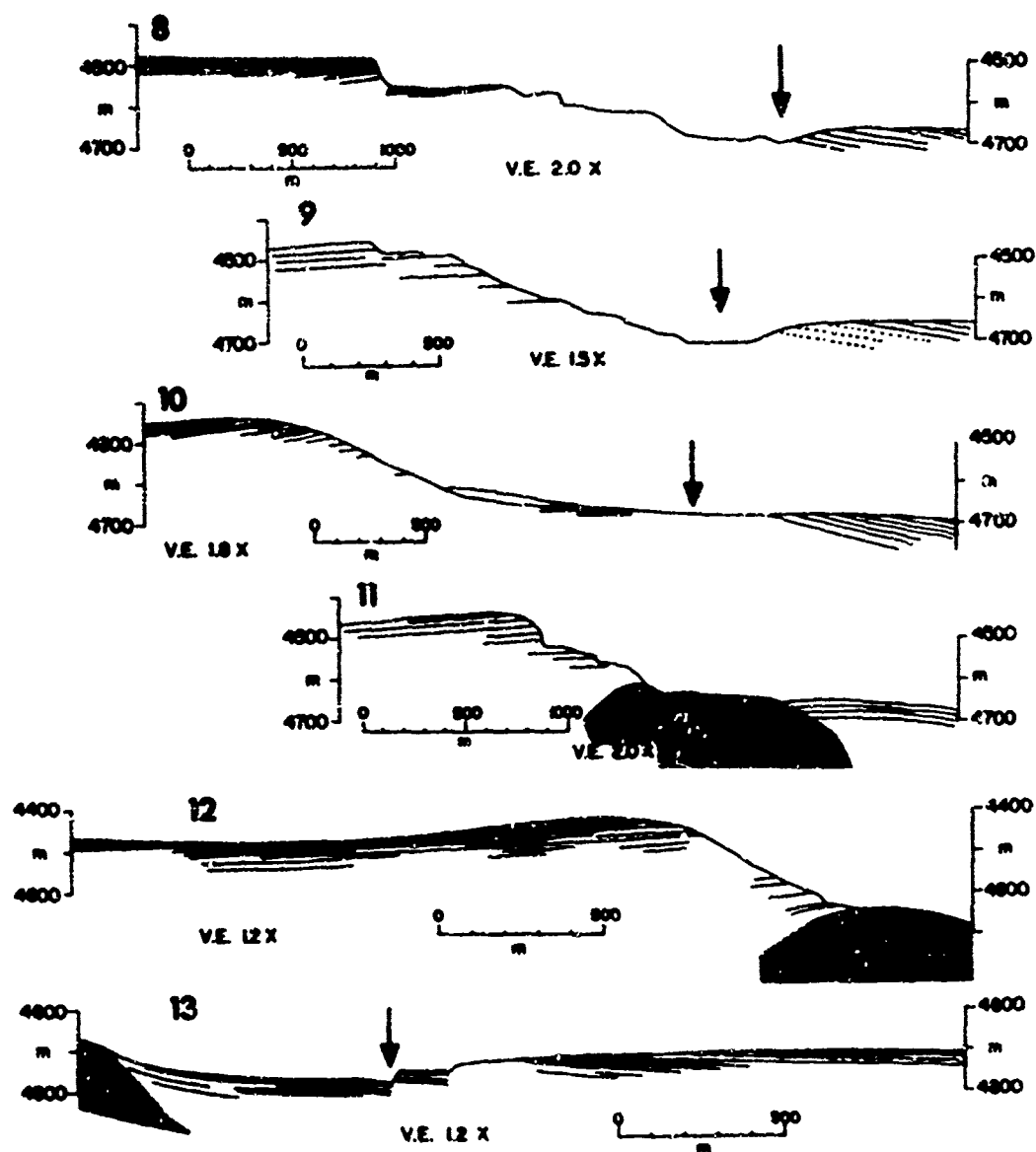


FIGURE 12 Line drawings based on near-bottom reflection profiles from the east flank of the plateau. Apparent outcrops of the acoustic basement are shown on the southernmost profiles. The arrows indicate the axis of a channel at the base of the plateau.

A channel extends southward along the base of the plateau's east flank (see arrows on profiles in Fig. 12). The oldest sediment recovered from the area was cored at two locations within the axis of the channel (Fig. 18, Cores E-10 and E-19). Near the southern end of the deep-tow survey area this channel joins a larger one which extends down the axis of the trough to the east (Fig. 9).

The plateau becomes increasingly narrow toward its northern end until it is indistinguishable from the surrounding sea floor. Profiles across the northern end (Fig. 13) show that the strata beneath the plateau are synclinal, and that the depth is shallower at the plateau's edges than in the center. The relief on the plateau's flanks in this region is steep and irregular, and the towed instrument was not sufficiently close to the bottom to delineate the fine-scale topographic features.

The trough to the east of the plateau has gentle relief, with no steep escarpments except locally along the axis of the channel. Broad smooth terraces border the channel on either side (Fig. 14). Beneath the surface of the terraces the layers are horizontal to gently dipping. Here, as elsewhere within the study area, the sea floor topography bears little relation to the structure of the underlying strata. On the terraces to the west of the channel the strata are near horizontal, and increasingly older layers are outcropping in the direction of the channel axis (arrow on Profile 14). East of the channel the strata are gently dipping and show evidence of compressional folding (Profiles 16-18). The structures have been

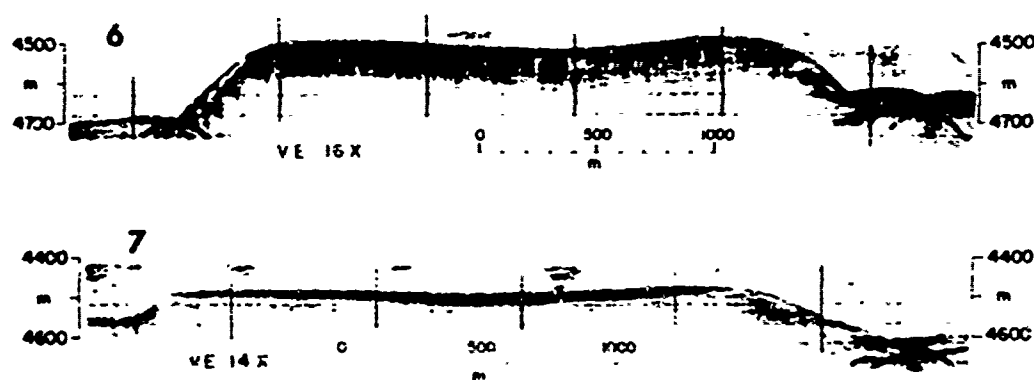


FIGURE 13 Near-bottom reflection profiles across the northern end of the plateau. Horizontal strata can be seen beneath the plateau's surface. Topographic details on the slopes are obscure because of the height of the instrument on these crossings.

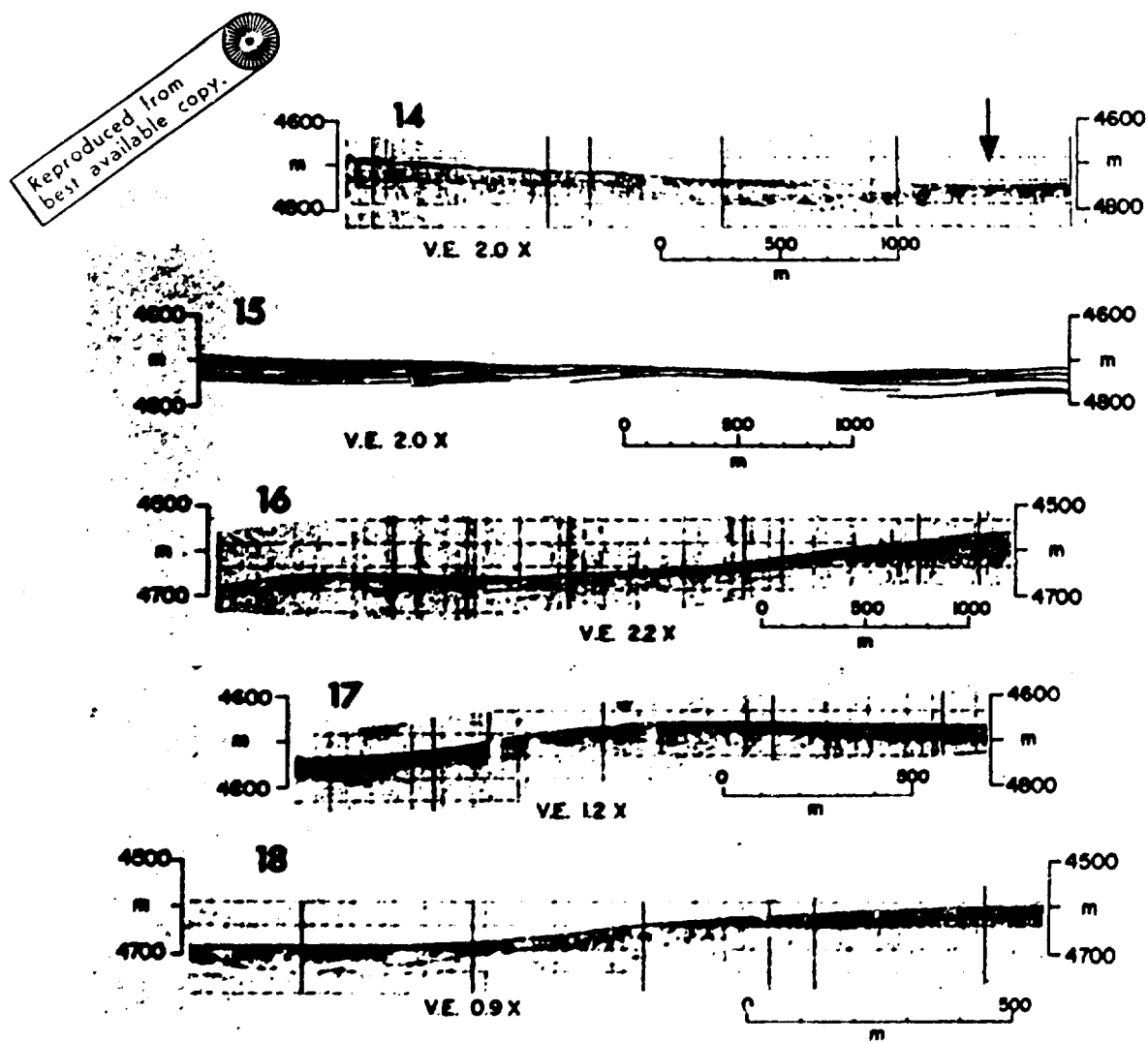


FIGURE 14 Near-bottom reflection profiles from the gently undulating region east of the plateau. All profiles show strata which are truncated at the sea floor interface. The arrow on profile 14 indicates the axis of the channel which extends southward along the floor of the trough.

sharply truncated at the sea floor by erosion, both on the slopes and on the relatively level terraces themselves. As elsewhere there is no indication of similar unconformities at depth.

Sediment Types

Forty-two free-fall cores and two piston cores were obtained within the survey area (Fig. 15). The principal objective of the coring was to determine the age of the outcropping sediment layers which were identified by reflection profiling from the towed instrument. All except one of the cores (Core E-22, Fig. 18) penetrated through a thin covering of Holocene sediment and recovered significantly older material corresponding to the outcropping acoustic reflectors.

There are two distinct sediment types represented in the cores; these major units are separated by a marked unconformity (Fig. 16; Plates 4-9):

a. The upper unit is a dark brown (10 YR 4/3) siliceous calcareous ooze, consisting largely of biogenous skeletal debris, but with a small amount (<15%) of clay-size nonbiogenous material. The ooze has a high water content (Fig. 16; Table 3), and is markedly different in texture from the underlying material. The upper unit is up to a few centimeters thick in most of the cores, but in a few cores the unit is missing entirely.

b. The lower unit is a white (N9) to yellowish brown (10 YR 5/6) chalk, consisting almost entirely (>98%) of biogenous skeletal debris. The chalk has a stiff texture and a significantly

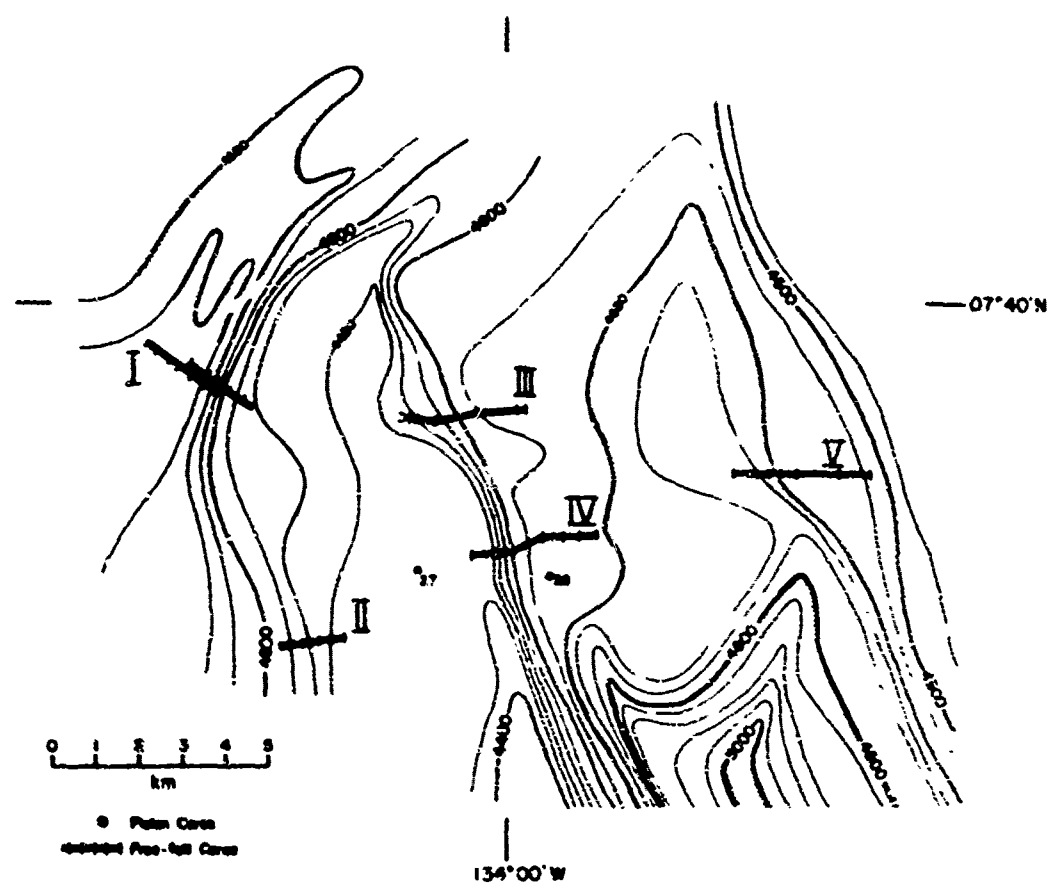


FIGURE 15 Locations of sediment cores from the area of detailed study. The circles labeled "27" and "28" indicate the locations of piston cores E-27 and E-28, respectively. Coring procedures are discussed in the text.

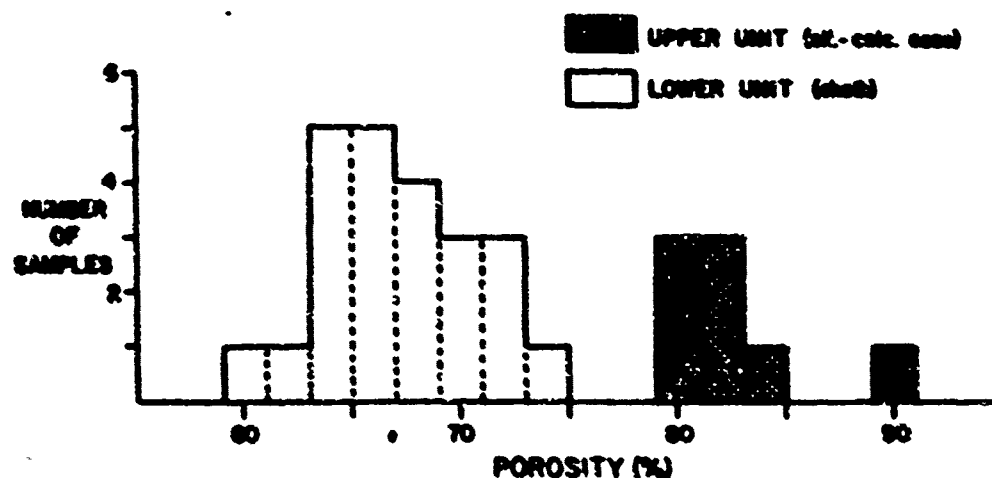
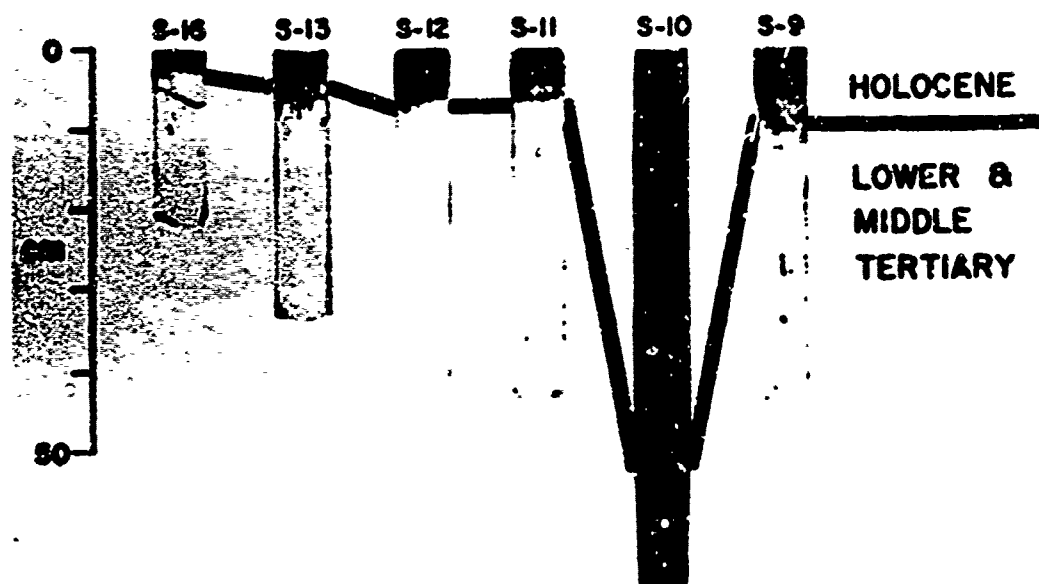


Figure 16 (top) Free-fall cores from Profile II, showing the sharp unconformity between Holocene ooze and the chalk of Tertiary age. This unconformity was penetrated in 43 of the 44 cores obtained. (bottom) Histogram summarizing results of porosity determinations. The chalk beneath the unconformity has a significantly lower porosity and water content than the overlying Holocene sediment. The stiff texture of the chalk prevented deeper penetration of the cores.

TABLE 3 Physical properties of several of the cores

Core No.	Level (cm)	Mean diam. (mm)	Percent:			Saturated bulk density	Grain density	Porosity (%)	V. (m/sec)
			Sand	Silt	Clay				
E-4	0-8	.0050	6.6	49.3	44.1	1.299	2.597	82.5	----
E-6	25-33	.0122	0.9	72.3	26.8	1.610	2.731	65.7	1523
E-11	12-20	.0043	0.7	56.1	43.2	1.530	2.702	63.9	1542
E-16	0-5	.0092	11.3	56.4	22.3	1.235	2.635	80.7	----
E-16	36-44	.0043	1.0	56.8	42.2	1.536	2.751	70.4	1537
E-17	11-19	.0137	1.4	71.9	26.7	1.541	2.687	68.9	1527
E-19	18-26	.0052	1.0	65.5	33.5	1.295	2.748	84.3	1519
E-20	18-26	.0051	2.4	57.2	40.4	1.575	2.680	66.7	1523
E-21	14-22	.0051	4.7	62.0	33.3	1.487	2.668	71.8	1526
E-22	4-12	.0043	14.4	32.6	53.0	1.313	2.666	82.4	1527
E-23	3-11	.0053	2.5	57.2	40.3	1.496	2.681	71.5	1519
E-26	13-21	.0052	2.4	60.1	37.5	1.516	2.660	69.9	1524
E-27	0-9	.0052	13.2	39.8	47.0	1.319	2.631	81.6	----
E-27	9-13	.0057	17.0	35.2	47.8	1.368	2.680	79.2	1533
E-27	94-102	.0045	2.8	53.2	44.0	1.171	2.489	90.0	1527
E-27	230-238	.0028	1.5	36.1	62.4	1.683	2.685	60.3	1546
E-27	363-371	.0027	2.3	35.2	62.5	1.627	2.700	64.0	1532
E-28	36-44	.0052	1.2	58.8	40.0	1.597	2.706	65.9	1527
E-28	118-126	.0048	1.0	59.6	39.4	1.604	2.685	65.1	1526
S-2	10-18	.0053	7.2	50.1	42.7	1.615	2.647	63.6	1572
S-4	3-11	.0092	3.0	48.1	48.9	1.556	2.688	68.0	1540
S-6	2-10	.0199	2.6	72.0	25.4	1.589	2.683	65.9	1538
S-8	12-20	.0100	2.1	69.7	28.2	1.651	2.693	62.4	1536
S-9	28-36	.0040	2.0	56.2	41.8	1.554	2.695	68.3	1526
S-10	26-34	.0126	3.8	70.2	26.0	1.352	2.620	79.4	1520
S-11	31-39	.0106	1.4	67.5	31.1	1.570	2.700	67.5	1537
S-12	30-38	.0055	2.0	63.7	34.3	1.618	2.662	63.7	1538
S-13	22-30	.0059	2.1	67.6	30.3	1.623	2.665	63.5	1550
S-17	0-8	.0039	1.2	49.7	49.1	1.506	2.690	71.1	1518
S-19	0-8	.0041	1.2	55.7	43.1	1.552	2.651	69.4	1530
S-21	0-8	.0069	1.4	48.4	50.2	1.416	2.646	75.8	1512

lower water content than the overlying ooze. The chalk appears to be partially lithified, but microscopic examination indicated that very little recrystallization had taken place. The stiffness of the chalk prevented the free-fall core barrels from penetrating deeper than a few tens of centimeters (Plates 4-8).

There has been significant vertical mixing of material across the boundary between these two layers. The lower unit in cores E-4 and S-21 contains burrows several cm in length (Plates 6 and 8), and these burrows have been filled with sediment from the upper unit. There is a significant amount of contamination by microfossils from the underlying chalk into the Holocene sediment.

Biostratigraphy

The upper unit in the cores contains abundant Quaternary radiolaria, including Ommatartus tetrathalamus, Sponaster tetras, Euchitonia elegans, Pterocanium praetexum, and Theocorythium trachelium. The radiolarian assemblage in this unit contains a considerable proportion of reworked Tertiary species, some of which have been vertically mixed from the underlying chalk, whereas others must have been eroded from nearby outcrops and laterally transported to the site of deposition. The foraminifera present in this unit include Globorotalia tumida, G. cultrata, Globoquadrina dutertrei, and Pulleniatina obliquiloculata. The species which are present show considerable effects of dissolution; the original assemblage may have included additional species which are more easily dissolved (Berger, 1958a). All of these species are present day low latitude forms

(Bradshaw, 1959; Parker, 1971), and are interpreted as Holocene in age.

The age of the outcropping chalk ranges from Upper Eocene to Middle Miocene within the study area (Figs. 17 and 18). The radiolarian and foraminiferal assemblages within this unit consist of species of uniform age, with no evidence of reworking. The apparent lack of reworking and the excellent preservation of the radiolarian specimens enabled precise age assignments to be made. The foraminiferal assemblages showed considerable effects of dissolution with only the more resistant species remaining. A tabulation of the abundances of radiolaria and occurrences of foraminifera within the lower unit of the cores is shown in Plates 10 and 11.

Profile 1

Fifteen free-fall cores were obtained along this profile, which extends from the crest of the plateau down the west flank, across the slope-base depression, and on to the surrounding sea floor. The nine cores from the plateau's flank are progressively older toward the base (Fig. 17), confirming the evidence from reflection profiling which suggests outcropping layers of near horizontal strata. Within the topographic depression at the base, however, the chalk layers are significantly younger than those on either side (Fig. 17, Profile 1), suggesting that the depression and the adjacent escarpments may be in part a result of post depositional normal faulting. Late Tertiary and Quaternary sediment is virtually absent within the axis of the depression, indicating that erosional processes

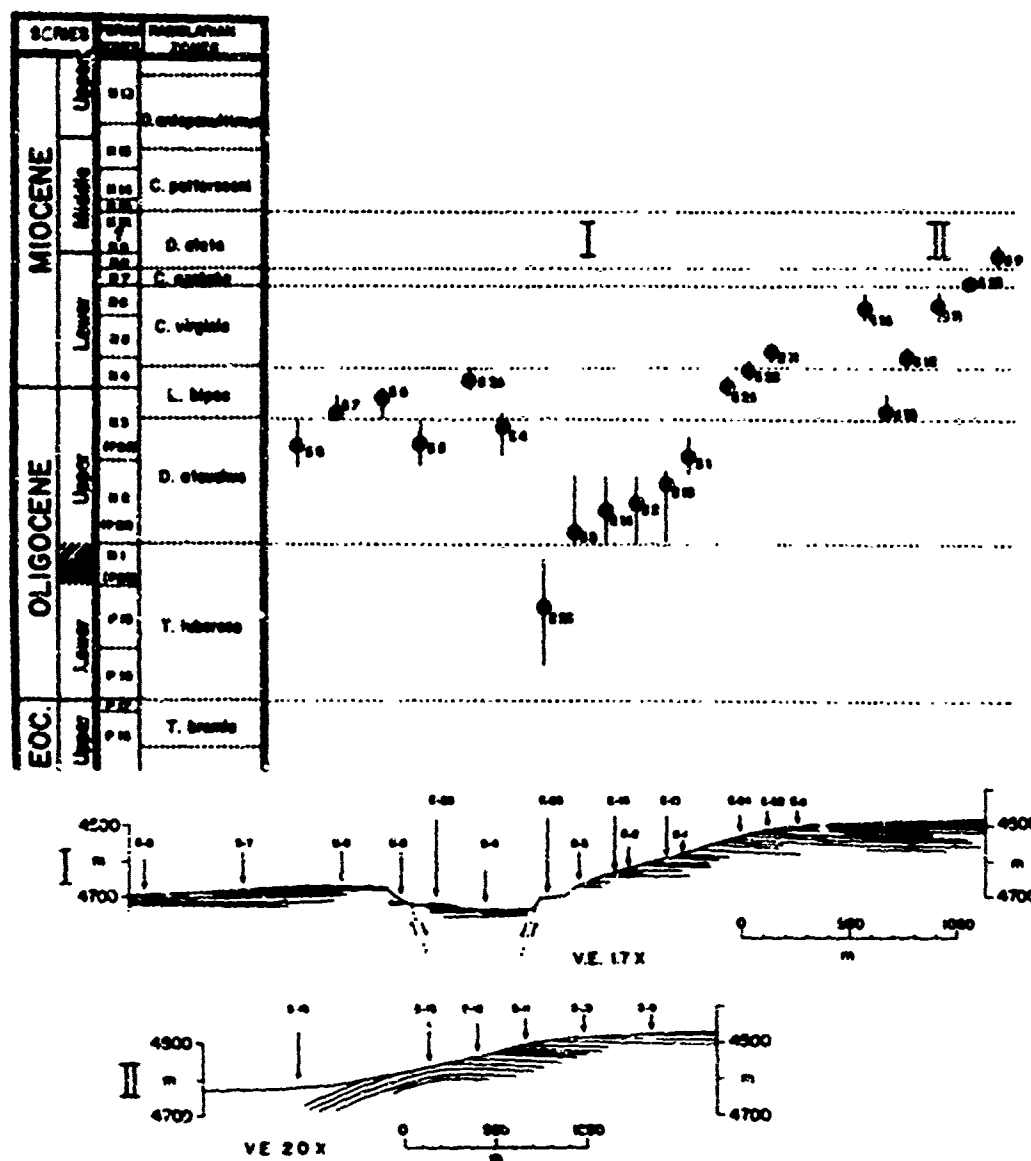


Figure 17 Age of lowermost material in sediment cores from Profiles I and II. The sub-bottom reflectors shown on the profiles are traced from 3.5 kHz continuous reflection profiles obtained by the deep-towed instrument package operating close to the sea floor. Age assignments are based on radiolarian assemblages, and are shown relative to the radiolarian zones of Riedel and Sanfilippo (1971). Vertical lines indicate the uncertainty in age determinations. The radiolarian zones are correlated with foraminiferal zones and time-stratigraphic units after Berggren (1971).

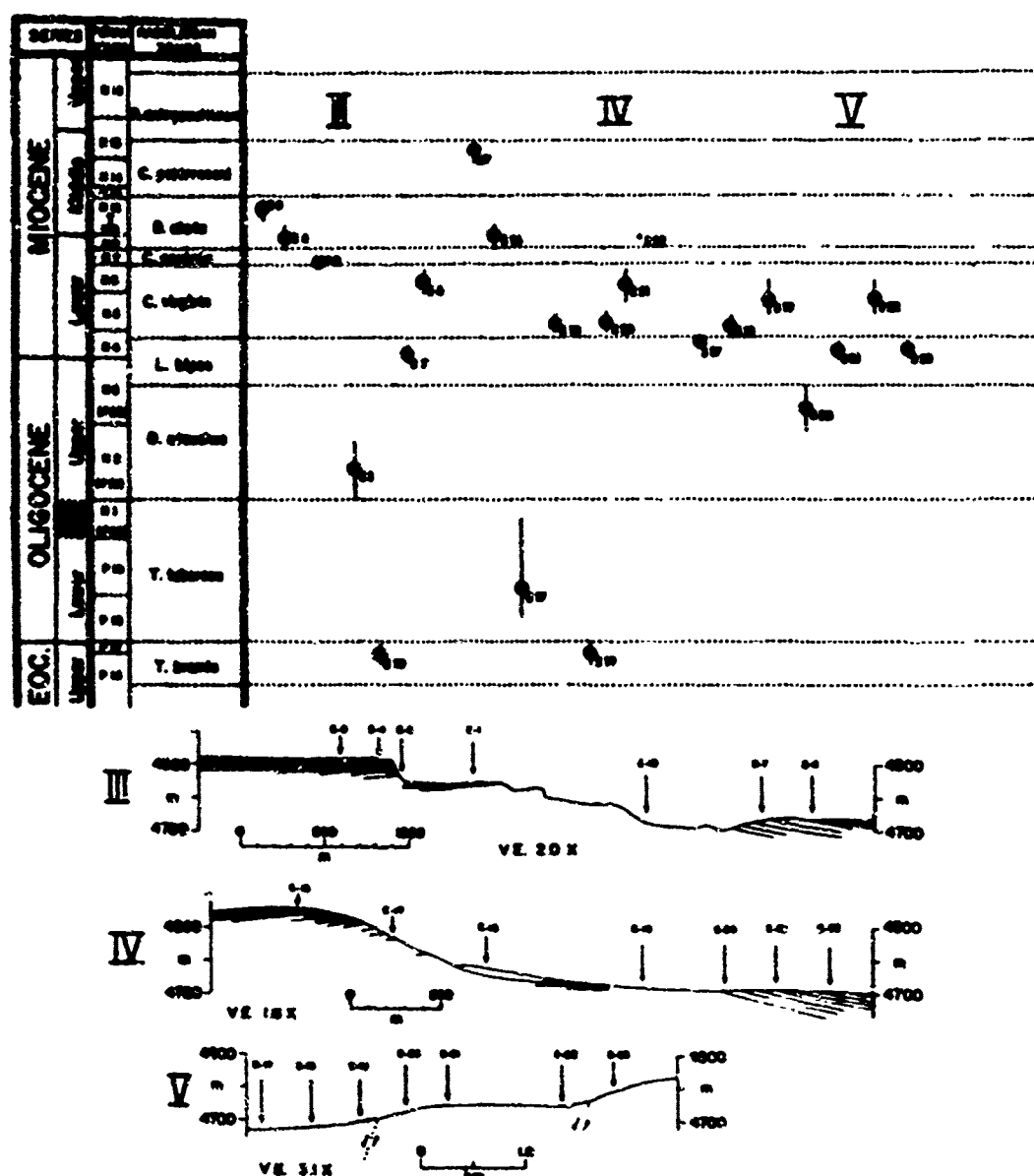


Figure 18 Age of lowermost material in sediment cores from Profiles III, IV, and V. Profiles III and IV are traced from 3.5 kHz records obtained by the deep-towed instrumentation. Profile V is from the ship's echo sounding record. Age assignments are based on radiolarian assemblages (see Plate 11), with vertical lines indicating the uncertainty in age determinations. Core E-27 is grouped with those of Profile IV. *Core E-22 is Quaternary throughout its entire length, and consequently the age of the chalk at this locality is not known.

subsequent to faulting have been influential in shaping and modifying the channel topography.

Profile II

Six cores are from the west flank of the plateau near the crest, at a site where reflection profiling suggested that the sedimentary strata had been folded and subsequently truncated at the sea floor (Fig. 10, Profile 1). The ages of the cores confirm this interpretation (Fig. 17).

Profiles III and IV

Cores along these profiles were taken on the irregular east flank of the plateau. The outcropping strata dip gently to the west near the crest, and are increasingly older at greater depths. Radiolarian ooze of Upper Eocene age outcrops in the channel at the base of the slope (Cores E-10, E-19) in a region where the sea floor is acoustically opaque to the 3.5 kHz profiler. To the east the layered strata reappear, dipping eastward. The presence of escarpments on the east flank is suggestive of faulting. The evidence from the limited number of cores, however, suggests that if faulting occurred, there were no substantial vertical displacements involved.

One of the cores from Profile IV (Core E-18) sampled an irregular mass of sedimentary material which appears to be out of place. Reflection profiling suggests that the mass is lens shaped with no internal bedding structures. The lens is surrounded by substantially older material (Cores E-17, E-19), and may therefore have slumped to its present position at the foot of the slope from a higher

elevation on the flank.

Profile V

The seven cores in this sequence were taken in the trough to the east of the plateau. The profile begins in the axis of the channel and extends eastward onto the adjacent terrace and slope. Near-bottom reflection profiles were not taken at the site of Profile V, hence the dips of the strata along the profile are not known. The age relationships of the cores (Fig. 18), however, suggest that post depositional faulting has been influential to some degree in creating the channel.

Piston cores

One piston core (E-27) was obtained within the topographic depression at the center of the plateau, about 1 km west of Profile IV; the second core (E-28) is from the east flank in a region where the sea floor is acoustically opaque to the 3.5 kHz profiler.

Core E-27 recovered a chalk and siliceous ooze of Miocene age, and approximately 35 cm of Holocene siliceous calcareous ooze (Plate 9). The lowermost two meters of the core is a nannofossil chalk identical in physical properties to that obtained in the free-fall cores (Table 3). The age of the chalk is within the Cannartus petterssoni zone, and is shown in Fig. 18 along with the cores of Profile IV. At a depth of about 150 cm in the core, the chalk grades upward into a siliceous ooze whose age is within the lower Ommatartus antepenultimus zone. The siliceous ooze is unconformably overlain by Holocene sediment at a depth of about 35 cm. The Holocene section

is thicker in this core than in most of the free-fall cores, perhaps because this site is relatively protected from the effects of erosion.

Core E-28 recovered an outcropping chalk of Lower Miocene age with no overlying Holocene material present. The age of the chalk is within the lower Calocycletta virginis zone and is identical to that of core E-20 of Profile IV.

Sea Floor Environment

Activity of benthic organisms

Sea floor photographs and sediment cores from the survey area (Fig. 19) indicate that the present sediment surface is a zone of intense biological activity. Burrowing and mottling structures are common within cores from locations where Holocene sediment is thickest (Cores E-22, E-27). In all cores there has been considerable vertical mixing of material across the Holocene-Middle Tertiary unconformity. A substantial proportion of the microfossils within the Holocene sediment are older specimens which have been reworked from the underlying chalk. In a few cores (E-4, S-21) there is evidence of burrowing into the chalk with Holocene sediment filling the burrows. Most of the vertical mixing, however, is upward rather than downward; reworked microfossils are generally absent from the chalk.

Photographs of the sea floor in the study area (see Appendix I) confirm that organisms are presently active in homogenizing the upper few centimeters of sediment. Only two of the more than 250 photographs obtained show individual organisms (e.g., Fig. A-3), but most of the remaining ones contain tracks, trails, mounds, and

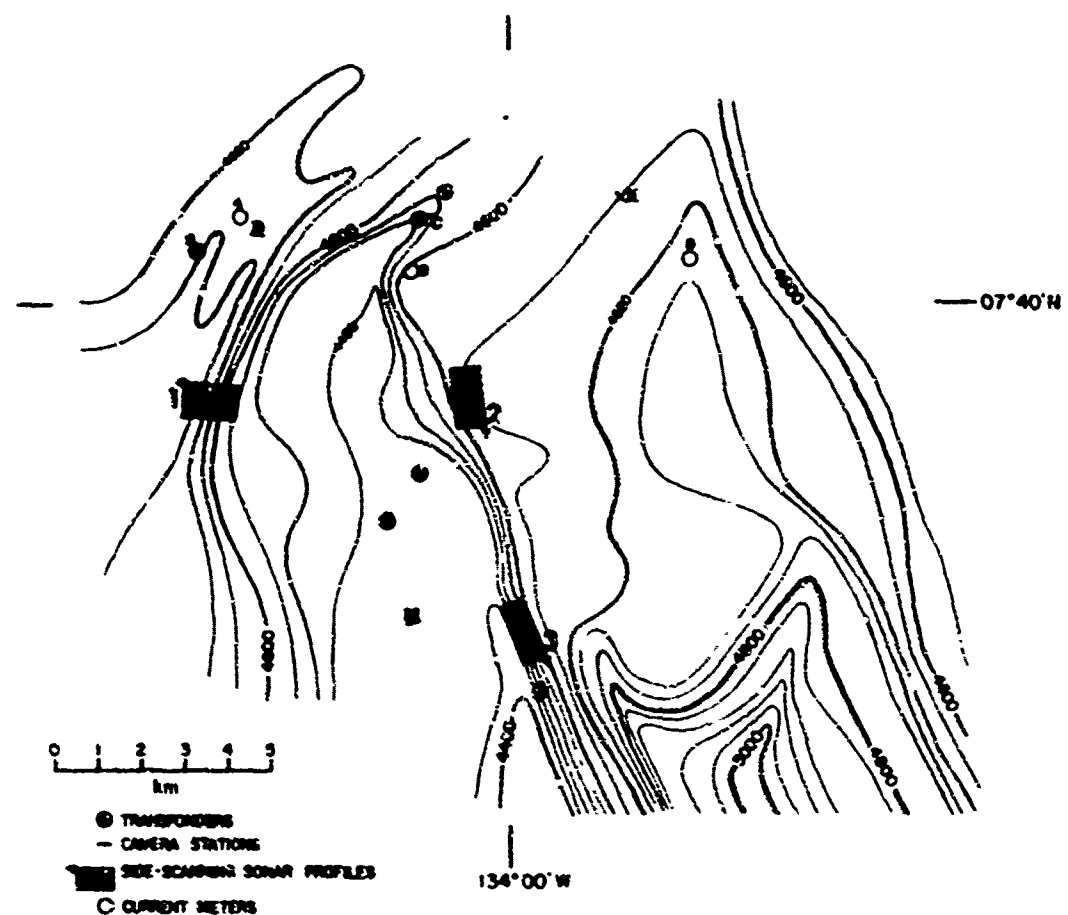


FIGURE 19 Location of camera stations, side-scanning sonar profiles, and bottom current meters.

other features indicative of the activity of benthic organisms. Small trails and mounds are closely spaced in some photographs (Fig. A-5), and some of the larger mounds (Fig. A-1) and Lebensspuren (Figs. A-6 and A-9) appear to have vertical dimensions of several centimeters. The presence of the unconformity just beneath the sea floor (Fig. 16) apparently serves as an effective barrier to deeper burrowing and mixing, and hence the activity is intense within the relatively thin layer of Holocene material.

Roughness

The use of side-scanning sonar techniques (Mudie et al, 1970) in addition to sea floor photography indicates that the relief is smooth over most of the surveyed area. A few photographs showed what appeared to be rock outcrops (Figs. A-2, A-8), but the acoustic return is at least 0.2 sec beneath the sea floor at these sites.

None of the rocky material was present in any of the sediment cores, hence the nature of this material is unknown.

Side-scanning sonar profiles show indications of steep local relief at some points on the flanks of the plateau and in the vicinity of erosional channels. The west flank of the plateau is generally smooth, but the channel at the base has prominent relief (Fig. 20a). Similar features are observed on side-scanning sonar profiles across other channels within the area. The east flank is generally rough (Fig. 20b), although there are some locations where smoothing has created a surface with no prominent features (Fig. 20c).

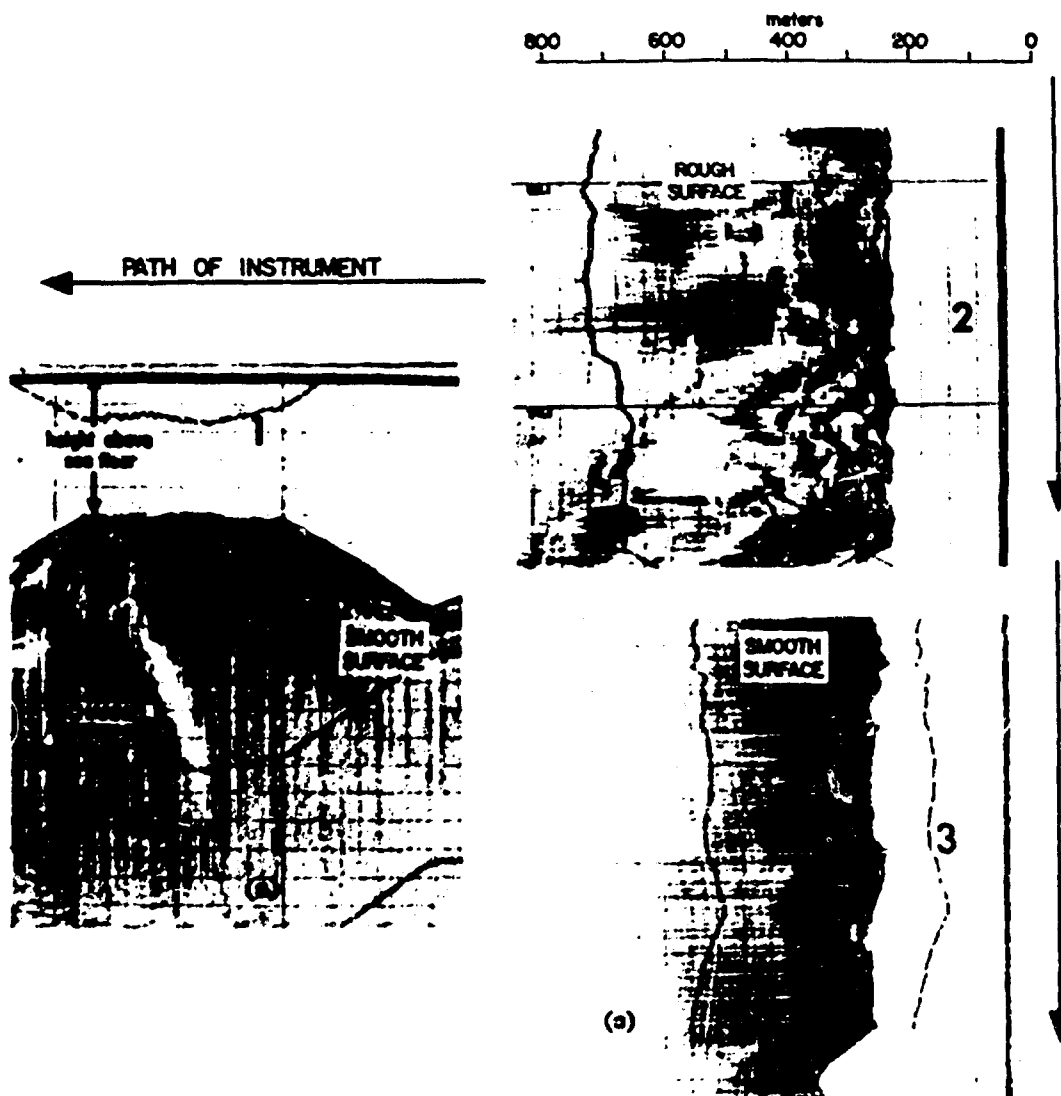


Figure 20 Side-scanning sonar profiles from the west and east flanks of the plateau, illustrating the contrasting types of sea floor micro-relief within the surveyed area. Locations of the profiles are shown on Figure 19. The arrows indicate the direction of travel of the towed instrument package. In each of the profiles the instrument is operating at a height of approximately 200 meters above the sea floor.

TABLE 4 Summary of current meter data

Instrument Number	Height Above Bottom	Mean Direction	Mean Speed (cm/sec)	Maximum Speed (cm/sec)
2	25 m	056°	4.8	8.3
3	19 m	099°	5.4	9.6
4	5 m	063°	4.5	8.1
5	5 m	102°	---	---

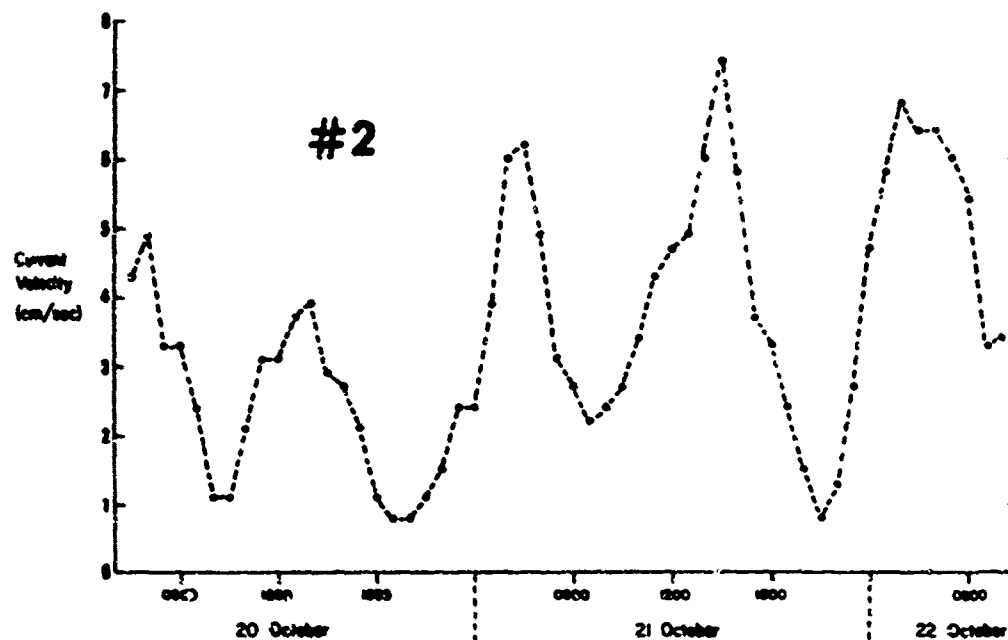


FIGURE 21 Bottom current measurements obtained by instrument #2 over a period of approximately two days, illustrating the pronounced tidal effect upon deep ocean current velocities. Similar tidal variations in speed were recorded by the other instruments.

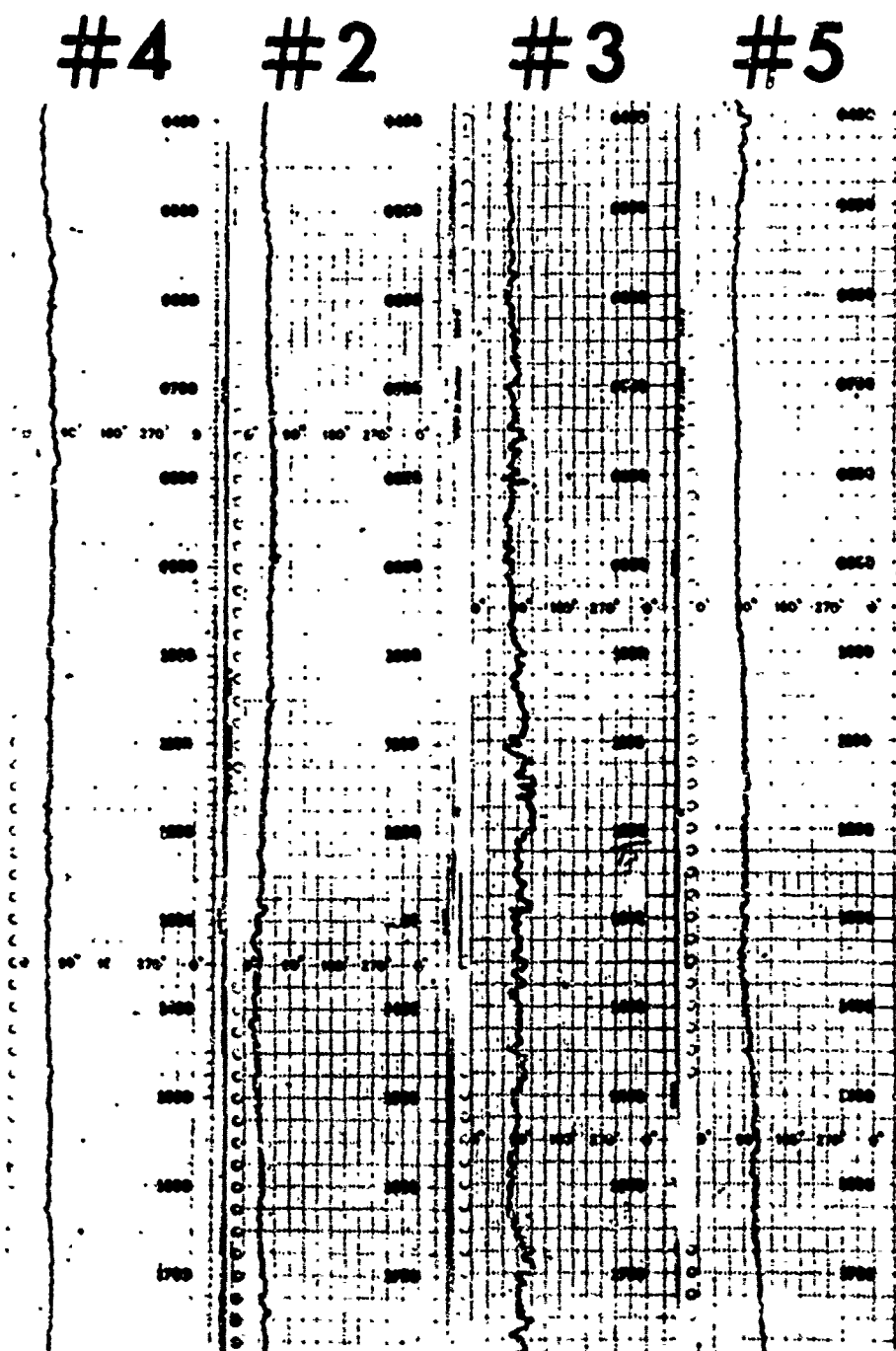


Figure 22 Original current meter records, illustrating the relative uniformity in flow direction at each site. Eastward-flowing currents were recorded at instruments #3 and #5, whereas the flow direction was generally northeastward at instruments #2 and #4.

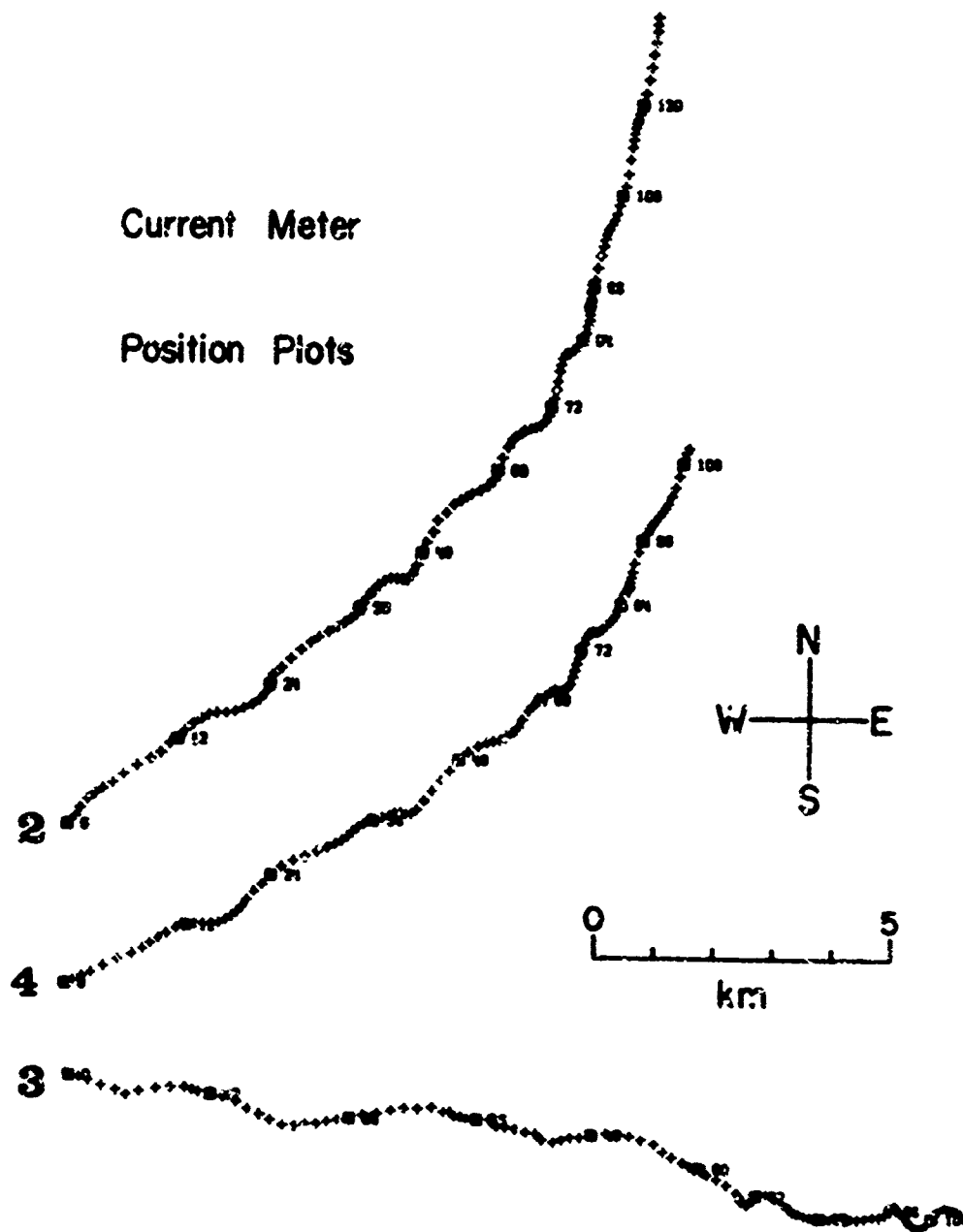


FIGURE 23 Position plots from current meters #2, #3 and #4, obtained by vectorially adding consecutive current velocities which have been averaged over one-hour increments.

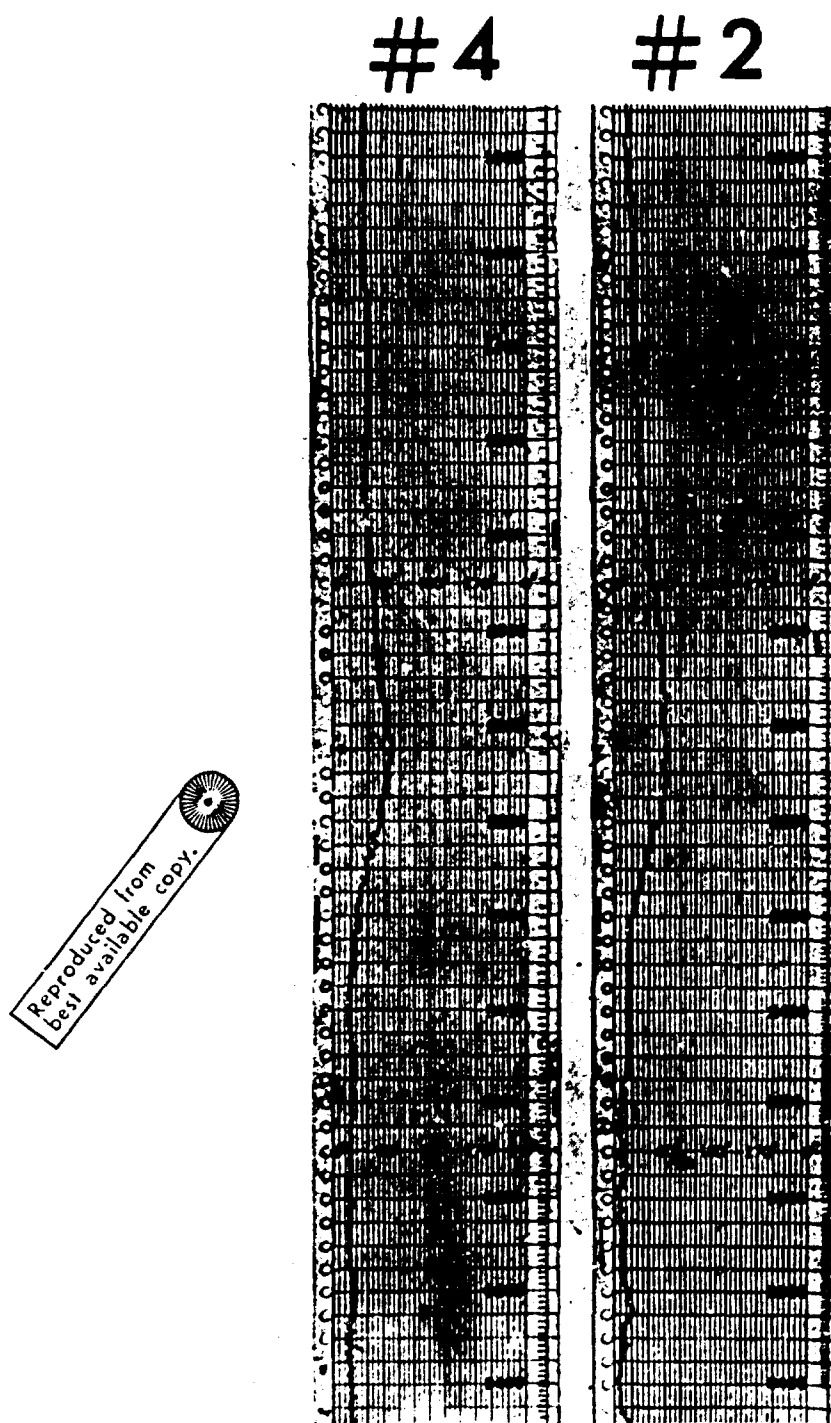


Figure 24 Portions of the original records from current meters #2 and #4, illustrating the close agreement between the two instruments. During the period between 2000 and 2300 the flow changes in direction from northeastward to eastward, and there is a corresponding decrease in current speed.

Bottom currents

Bottom currents were measured at four locations within the survey area (Fig. 19; Table 4). Two of the instruments (#2 and #4) were located in the depression to the west of the plateau. A third instrument (#3) was located near the northern end of the plateau, and a fourth (#5) was located in the trough to the east. Current speed and direction were measured for a period of four days by each instrument except #5, which recorded direction only. Data obtained from the current meters are listed in Table 6.

The observed current speeds were generally low (<10 cm/sec), but fluctuated significantly because of tidal effects. Figure 21 shows the strong semidiurnal tidal component present in the current, as recorded by one of the instruments; similar fluctuations in speed were observed at each of the other instrument locations.

In spite of the fluctuations in speed, the direction of flow at each location was remarkably uniform during the period of observation (Fig. 22). Eastward flowing currents were recorded at instruments #3 and #5, whereas in the depression to the west of the plateau, instruments #2 and #4 recorded a northeastward flow (Figs. 22 and 23). The data suggest that the regional flow of bottom water is toward the east, with local modifications in direction due to topographic effects. The nearby Clipperton Fracture Zone (Fig. 4) may be influential in controlling the direction of flow of bottom water in this part of the Pacific.

There appears to be a correspondence between minor changes

in flow direction and changes in current speed. Figure 24 shows a change in current direction which was recorded by both of the instruments in the channel west of the plateau (#2 and #4). During the period of northeastward flow the current speed was strongest, whereas the speed dropped markedly when the flow direction changed to eastward. The data support the interpretation of a relatively slow eastward flowing bottom current in the region, which at some localities (e.g., at the base of sea floor topographic irregularities) is accelerated in response to tidal influences, and changes direction to conform to the local topography.

Reflection Profiling Survey of Surrounding Area

The region surrounding the site of detailed study was surveyed using continuous seismic reflection profiling techniques from the surface ship. The survey included twelve east-west crossings within an area measuring approximately 50 km by 50 km (Fig. 25). Line drawings of some of the profiles are shown in Fig. 26.

The relief of both the sea floor and the acoustic basement is relatively smooth at the northern end of the area (Fig. 26, Profile I'I), and becomes increasingly irregular toward the south. The plateau within the area of detailed study (Profiles F'F, G'G) terminates to the south against a steep basement ridge, and the trough to the east of the plateau extends southward into an elongated depositional basin approximately 15 km in width and at least 25 km in length (Fig. 25). In the vicinity of this basin the acoustic basement has in excess of 1 km of relief, and basement outcrops

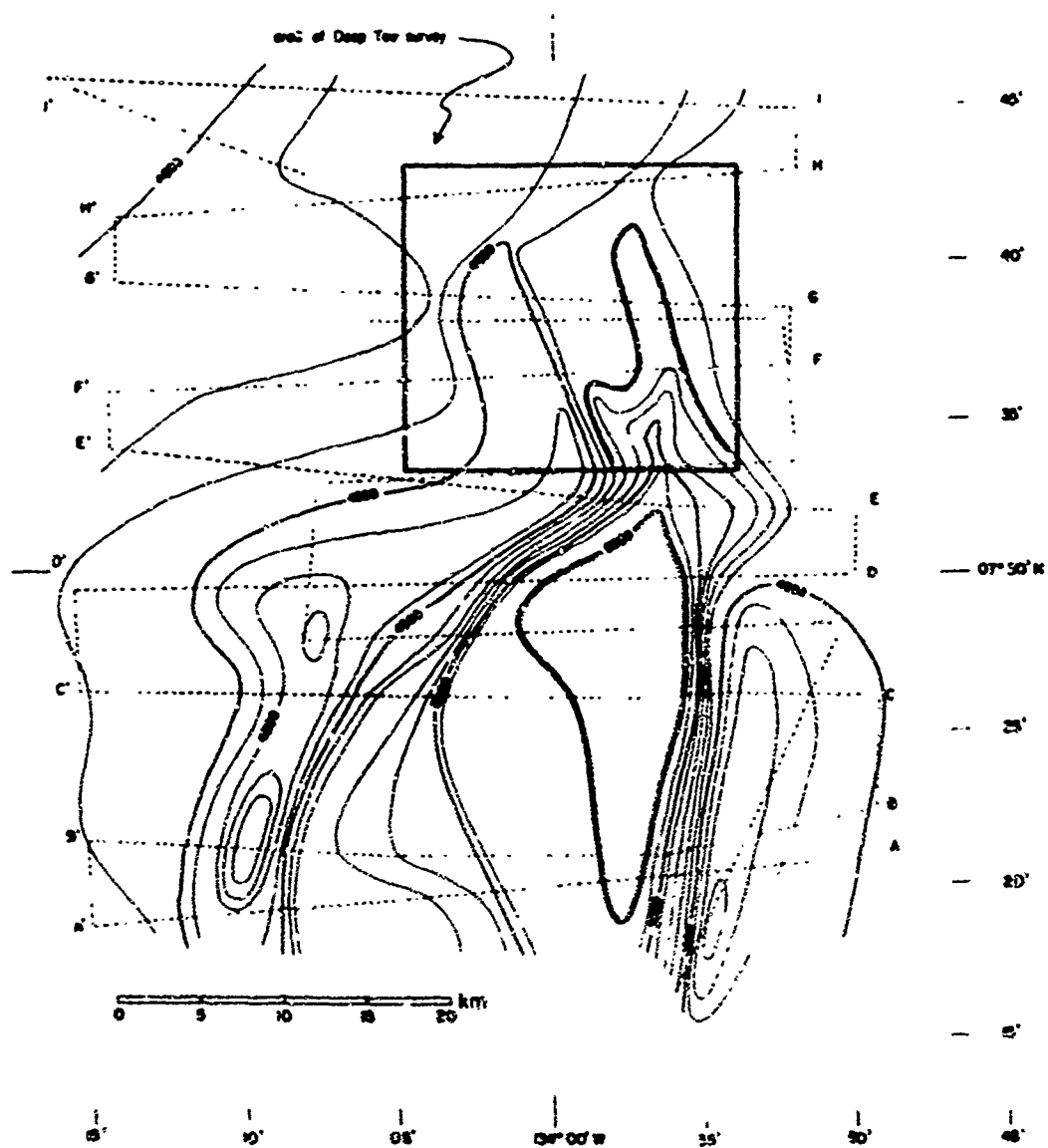


Figure 25 Bathymetry of extended area surrounding the region of detailed study. Dotted lines show ship's tracks through the area. Reflection profiles from some of these tracks are shown in Figure 26.

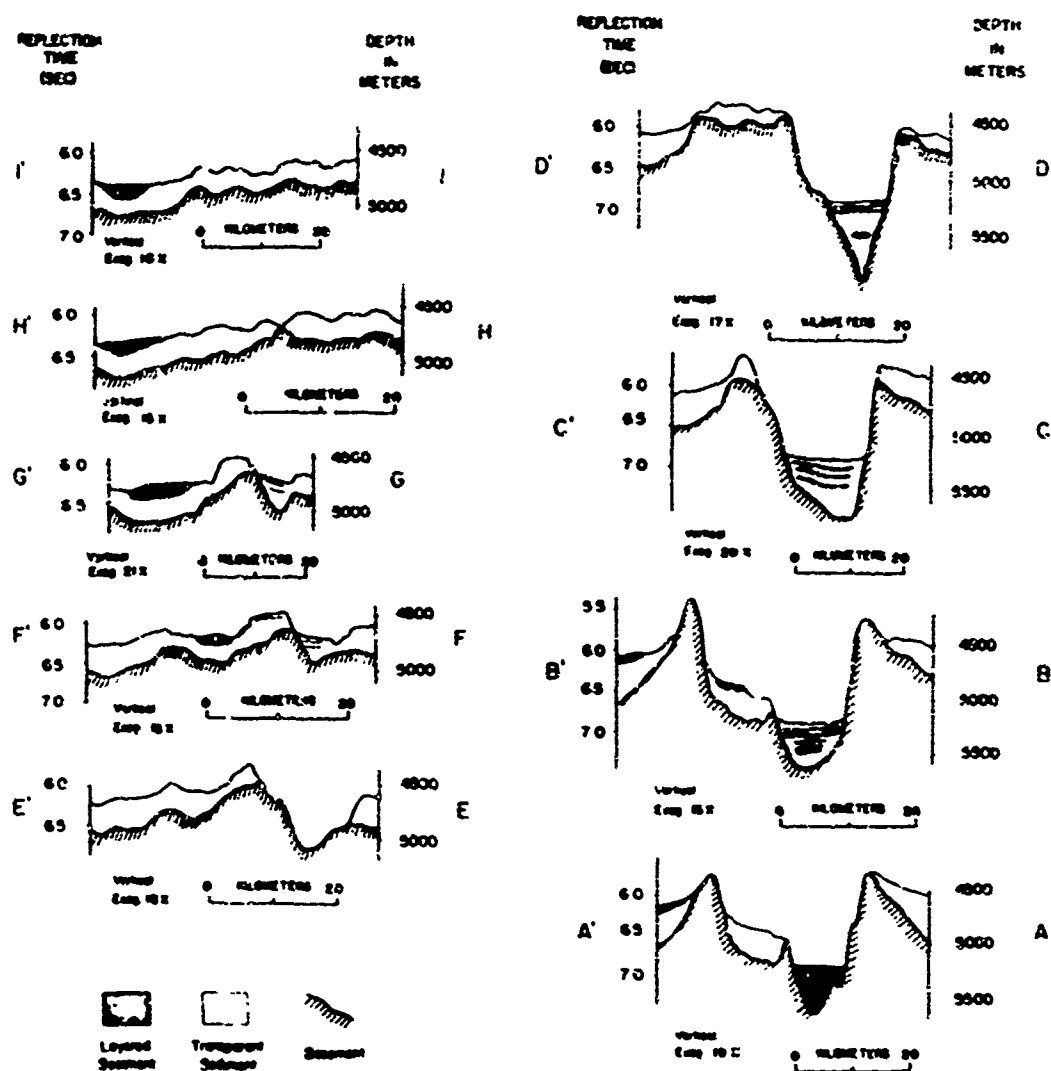


FIGURE 26 Line drawings based on continuous seismic reflection profiles within the extended survey area. See text for discussion.

surround the basin and extend northward up the east flank of the plateau (Fig. 27).

Air gun reflection profiles suggest that two contrasting types of sedimentary material are distributed over the study area (Fig. 27):

- (1) Acoustically transparent sediment covers most of the area. This "transparent" material shows few or no internal reflectors on the air gun profiles, although layering within this unit is commonly observed on near-bottom profiles (Figs. 19-14). The thickness of this unit varies between 0.3 and 0.4 sec (Fig. 26), and in the northern part of the area (Profiles H'H and I'I) it is generally conformable with the relief of the acoustic basement. Toward the south, where the relief becomes much greater, outcrops of the acoustic basement are common and the transparent sediment is irregularly distributed.
- (2) Relatively thick accumulations of stratified sediment (or layered sediment) occur elsewhere in the survey area. On the air gun profiles this material commonly contains near horizontal internal reflectors. It is generally restricted to relatively deep regions, and is significantly thicker than the "transparent" sedimentary material which is present on the surrounding topographic elevation. A broad area containing stratified sediment overlying relatively transparent sediment extends northwestward from the deep-tow survey area (Fig. 27). The elongated basin to the south of the deep-tow area also contains relatively stratified sediment, perhaps several hundred meters in thickness. No samples of this "stratified" unit were obtained, and therefore its composition is unknown. The profiles suggest, however,

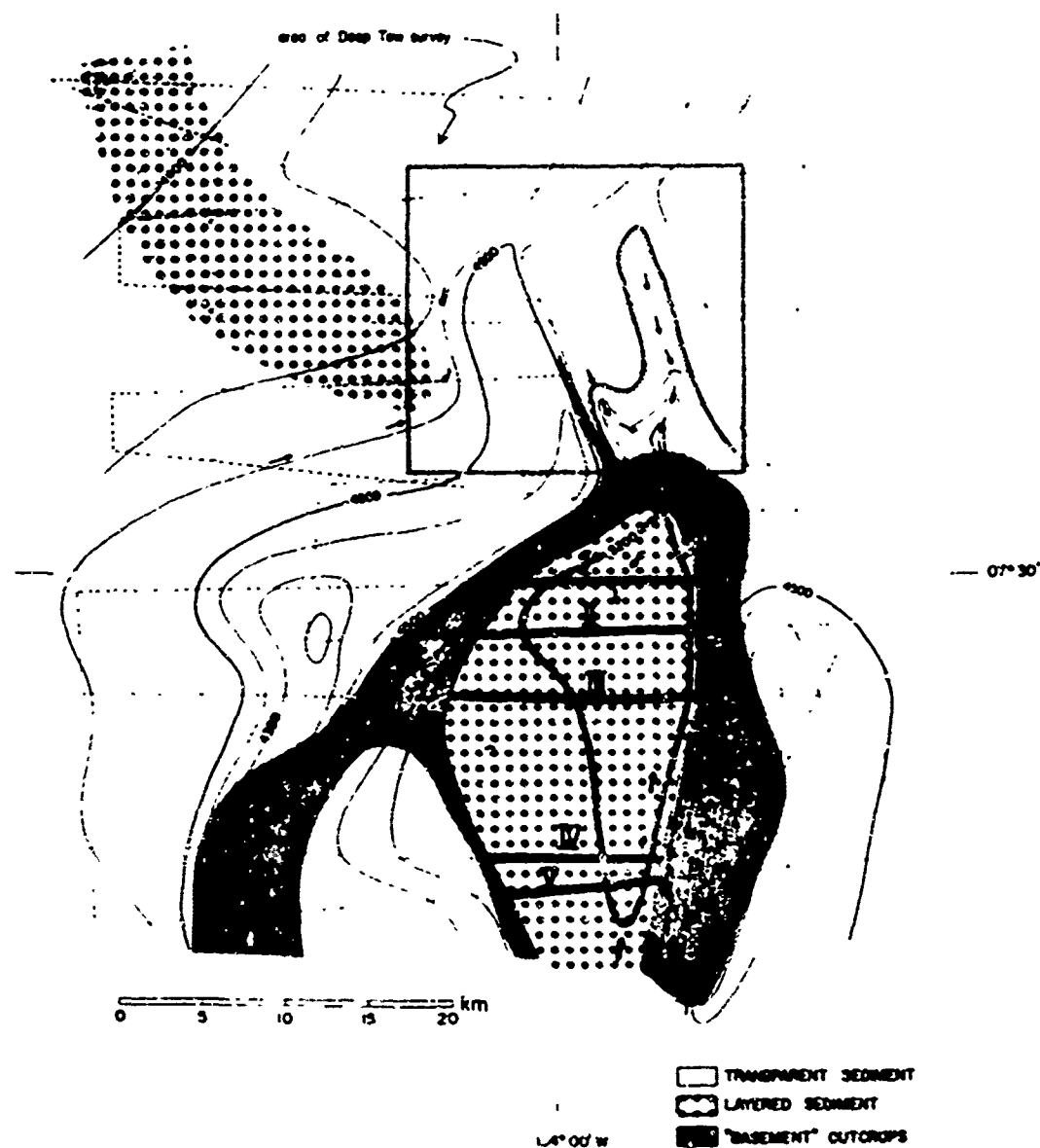


Figure 27 Distribution of major sediment types within the extended area. "Transparent" sediment contains no internal reflectors on air gun profiles, but generally shows stratification on near-bottom profiles. "Stratified" (or layered) sediment commonly contains sequences of near-horizontal internal reflectors on air gun profiles.

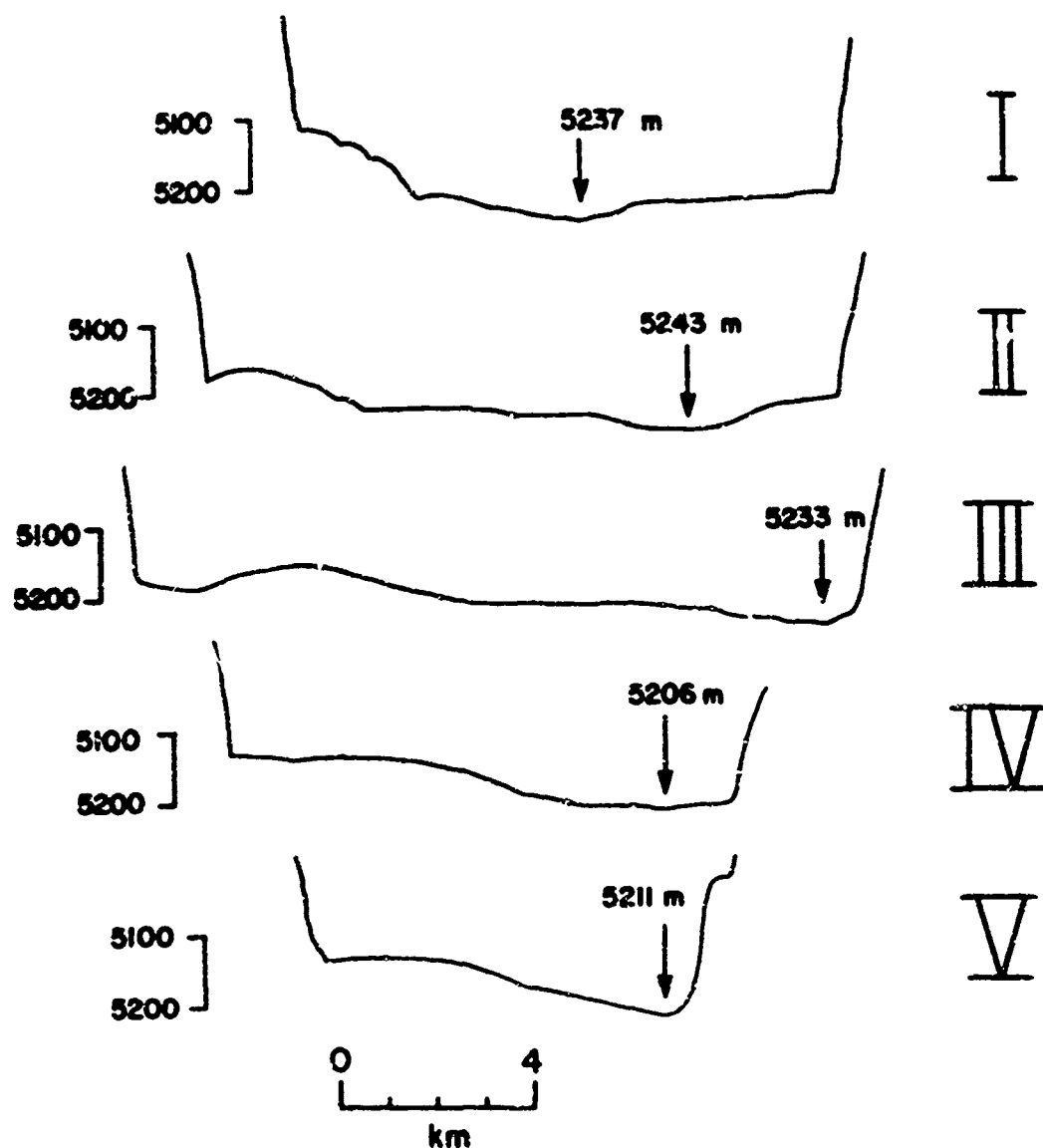


FIGURE 28 Bathymetric profiles across the floor of the basin to the south of the deep-tow survey area. The basin is fed by major channels from both the northern and southern ends. Profile locations are shown in Figure 27.

that much of the sediment which appears stratified on the air gun profiles has been redeposited from surrounding regions.

INTERPRETATIONS OF RESULTS

Sediment Redistribution in Deep-tow Survey Area

Evidence for erosion

Continuous seismic reflection profiling from the surface ship gives clear evidence for sediment erosion and redeposition within the extended survey area (Fig. 27). Each of the two principal regions where "stratified" sediment is present appears to be a site where significant volumes of reworked material have accumulated. The large basin south of the deep-tow area is fed from the north by two principal channels which join before entering the basin. Within the deep-tow area (Fig. 9; Fig. 26, Profiles F'F and G'G) these channels are as much as several tens of meters in depth, and have eroded deeply into Tertiary chalk. At some locations (Fig. 18, Cores E-10 and E-19) the channels have exposed Upper Eocene sediments, whose age is only a few million years younger than the presumed age of the oceanic crust at this site (Fig. 4). At the southern end of the deep-tow area these channels join, and substantially more material is eroded exposing outcrops of the acoustic basement along the channel axis (Fig. 26, Profile E'E). South of this point the basement deepens abruptly and the region of deposition begins, marked by the thick accumulation of stratified sediment. The channel appears to continue meandering southward through the basin itself until it reaches the deepest part of the basin (Profile II, Fig. 28). A separate channel enters the basin from the southern end (Fig. 27).

The "fan" of stratified sediment west of the deep-tow area

(Fig. 27) is fed by a major channel which extends southward along the base of the west flank of the plateau (Fig. 9). A secondary channel enters the head of the fan from the opposite direction, and supplies sediment from the region to the southwest of the deep-tow area. This "fan" overlies 0.2 to 0.3 sec of acoustically transparent sediment, and appears to have filled a previously existing topographic depression.

Near-bottom reflection profiles and sediment cores confirm that significant erosion has taken place, and indicate that erosion has affected virtually the entire deep-tow survey area (Fig. 27). Reflection profiles from throughout the area (Figs. 10-14) show an abrupt truncation of acoustic reflectors at the sea floor interface, but there is no indication of similar unconformities at depth. Forty-three of the forty-four cores penetrated an unconformity between Holocene ooze and Lower to Middle Tertiary chalk, and in most cores this unconformity is within a few centimeters of the sea floor (Plates 4-9).

Time of erosion

The presence of the unconformity near the sea floor interface indicates that erosion processes have occurred relatively recently in geologic time. The presence of a thin layer of Holocene material above the unconformity (Fig. 16), however, suggests that substantial erosion is not taking place today. Bottom current speeds were low (<10 cm/sec) during the period of observation (Tables 4 and 6), and bottom photographs showed well preserved sedimentary structures resulting from the activity of benthic organisms. It is therefore

likely that condition on the sea floor today are relatively quiescent compared to the conditions which must have existed during the recent past. During the Pleistocene the circulation patterns of the atmosphere and oceanic surface waters are presumed to have undergone periods of marked intensification in response to the extreme climatic fluctuations (Arrhenius, 1950; 1966). It may be that the deep circulation was subjected to corresponding pulsations with intensified current speeds during the glacial stages.

Thickness of material eroded

The minimum quantity of material which has been eroded can be estimated from the near-bottom reflection profiles (Figs. 10-14). Profile 5 (Fig. 11) shows a synclinal sedimentary structure which has been truncated by erosion on both sides of the synclinal axis. The resulting sea floor relief exposes layers covering a stratigraphic thickness of 100-200 m within a distance of one kilometer. Similarly, Profile 15 (Fig. 14) reveals that at least several tens to hundreds of meters of cover has been removed from a gently folded sequence of strata.

Coring and near-bottom profiling indicate that the region to the east of the plateau may be an eroded anticlinal structure (Fig. 12; Fig. 18). On the plateau's east flank the strata dip westward, whereas in the trough to the east the layers dip eastward (Fig. 18, Profiles III and IV). In the intermediate region, near the channel at the base of the plateau, Eocene sediments outcrop. If the strata which now outcrop on the east flank of the plateau were formerly

continuous with strata to the east of the channel, then perhaps several hundred meters of material has been eroded in the vicinity of the channel (see arrows on profiles in Fig. 12).

The depositional history at the survey site can be reconstructed by noting the ages of sediment cores in relation to their outcrop pattern, and estimating the amount of material which is missing. Cores from Profile I on the west flank of the plateau (Fig. 17) sampled a continuous sequence of outcropping strata ranging in age from lowermost Oligocene to Middle Miocene. The average accumulation rate for this sequence of strata is approximately 12 to 15 m per million years, or 12 to 15 mm per thousand years. If this accumulation rate were extrapolated from the Middle Miocene to the present, however, it would almost certainly be too high. Rates of supply of sediment to this portion of oceanic crust have varied considerably during the Cenozoic as a result of a northward component in the motion of the Pacific plate (Francheteau et al, 1970; Tracey et al, 1971). Maximum rates of deposition occurred when this region was beneath the biological equator; this may have occurred during the Oligocene (approximately 25 to 30 million years ago) on the basis of recent drilling results which suggest that the Pacific plate has had a northward component of motion of approximately 3 cm/yr during the late Cenozoic (E. L. Winterer, personal communication). Since that time, as the Pacific plate has moved northward, the rate of sediment supply has decreased. Today, sediment is supplied at a significantly lower rate, perhaps 3 to 5 m per million years. Using these figures,

several tens of meters of sediment (representing the Middle Miocene through Pleistocene) is missing from the deep-tow survey area, and presumably has been redeposited elsewhere.

The stiff texture and relatively low water content of the outcropping chalk layers (Fig. 16) suggest that the chalk was formerly under a higher overburden pressure. Modern deep sea sediments commonly have porosities of 75% to 85% (Hamilton, 1971), and recent deep drilling into continuous sections of pelagic carbonate has encountered low porosity (60%) material only at depths of several tens of meters or more (Hays et al, 1971). The physical properties of pelagic sediments, however, are dependent not only upon former overburden pressures, but upon the entire set of conditions to which the material has been subjected since original deposition (E. L. Hamilton, personal communication). Quantitative estimates of former overburden thicknesses within the deep-tow area on the basis of porosity alone, therefore, are not justified.

Evidence for Erosion Elsewhere in the Central Pacific

Deep-tow survey of Area k

Another small area in the central Pacific, which will be designated Area K, was recently surveyed using the deep-towed instrumentation (Mudie et al, 1971). This site is located several hundred kilometers to the northeast of the primary deep-tow survey area described above (Fig. 2), and lies within the zone of red clay sedimentation where rates of accumulation are relatively slow. The topography at Area K is characterized by lineated abyssal hills and

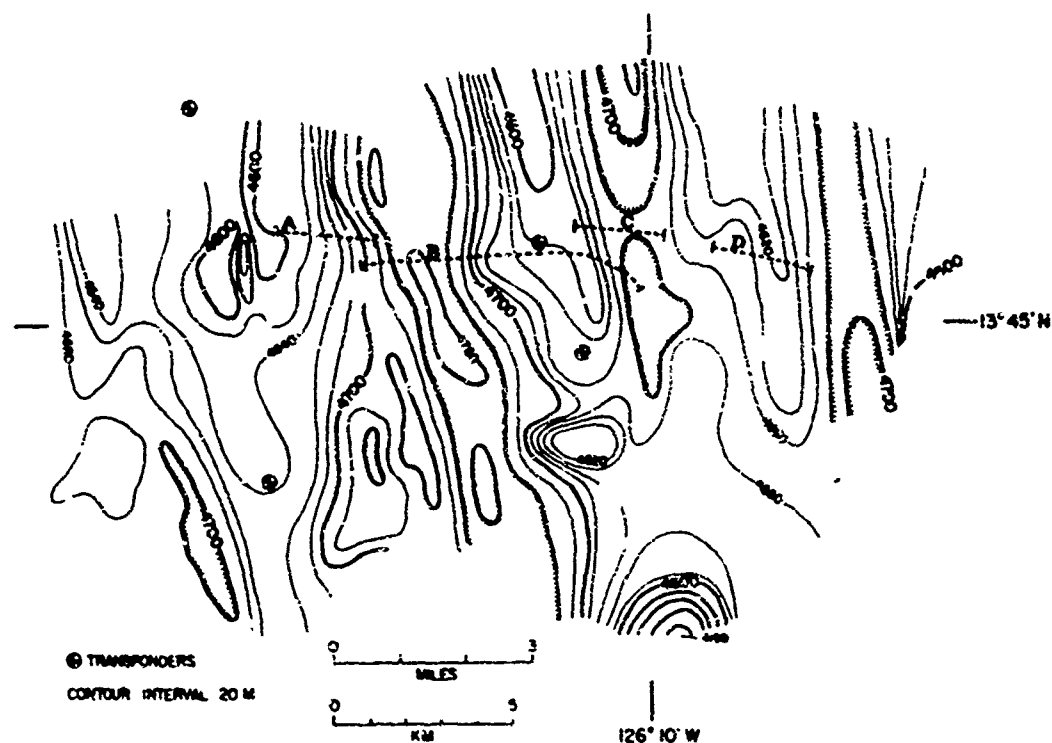


FIGURE 29

Bathymetry of "Area K", after Mudie *et al.* (1971). Lineated abyssal hills and troughs are characteristic of this area. Dotted lines indicate the locations of near-bottom reflection profiles shown in Figure 30.

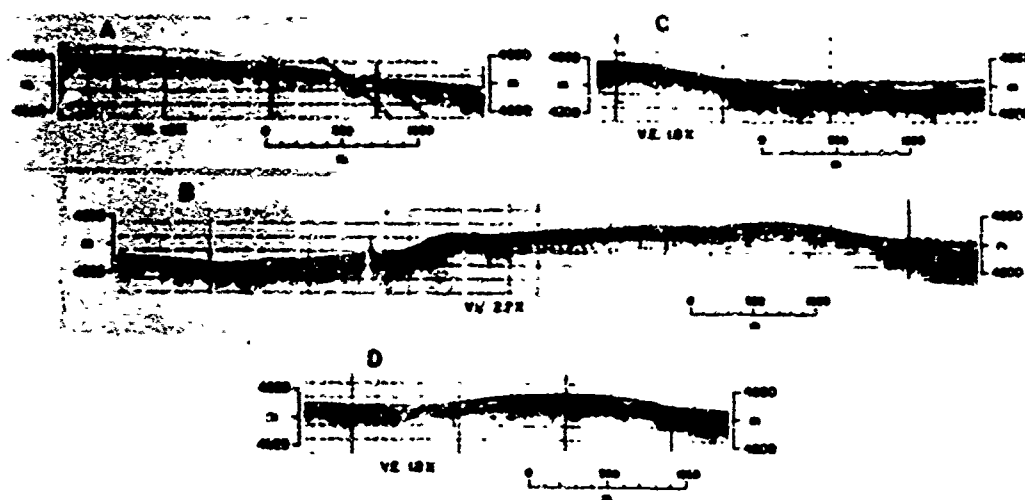


Figure 30 Near bottom reflector profiles from Area K. The structural and erosional features in this area are remarkably similar to those observed in the primary area studied. See text for discussion.

troughs (Fig. 29). A large circular abyssal hill is present in the southern part of the area, and a small trough surrounded by steep escarpments occurs to the southwest of Profile A. Elsewhere within the area the relief is smooth with no evidence of faulting.

Continuous seismic reflection profiles were obtained within the area using the 3.5 kHz system on the deep-tow vehicle. Many of the profiles from Area K are remarkably similar to those obtained in the primary deep-tow area in the equatorial region.

Profile A (Fig. 30), which crosses the eastern limb of one of the abyssal hills, shows sedimentary strata which have been gently folded into anticlinal and synclinal forms, and subsequently truncated at the sea floor interface. It is difficult to determine whether the layering is a reflection of the basement topography or whether compressional folding of the strata has taken place.

Profile B (Fig. 30) crosses one of the abyssal hills, and includes the troughs on either side. The structure of the hill itself is remarkably similar to that of the plateau within the primary survey area. The hill in Profile B is underlain by near horizontal strata which outcrop on both the east and west flanks. The sediments in the trough to the west are also truncated by erosion at the sea floor, and it appears that these outcropping layers at the deepest part of the trough are stratigraphically at least 100 m beneath those which outcrop at the crest of the hill.

Profile C shows in more detail the trough to the east of the hill shown in Profile B. As before the strata underlying the hill outcrop along the hill slope. Within the trough, however,

the sea floor is horizontal and smooth, and the relatively transparent sediment is ponded around the acoustic basement. The smoothness of the floor of the trough and the ponded nature of the sediment suggest that the sediment within the trough has been reworked from surrounding areas, perhaps from the adjacent hill slopes.

Profile D crosses another of the elongated abyssal hills, where essentially horizontal strata underlying the hill are outcropping on the slopes. A line of ten free-fall cores was dropped along the east flank of the hill shown in Profile B in an attempt to determine the age of the outcropping sediment layers. All of the material within the cores was unfossiliferous, hence the ages of the strata cannot be determined. The reflection profiles, however, indicate that substantial erosion has occurred, and the presence of the unconformity at the sea floor suggests that the erosion occurred relatively recently. The evidence for erosion at Area K is remarkably similar to that observed in the primary survey area.

Detailed surveys in other abyssal hills regions

Detailed investigations recently have been carried out in two other small areas in the central Pacific, and at each of these sites there is evidence for recent ocean floor erosion. Moore and Heath (1967) surveyed an abyssal hills region south of Hawaii (near 08°20'N, 153°00'W), and used closely spaced free-fall cores to determine the small-scale sediment distribution pattern. They found that, in each of the cores that penetrated through Quaternary sediment, an unconformity separated the Quaternary section from underlying

sediment of Middle Miocene age or older (Moore, 1970). Johnson and Johnson (1970) used similar surveying and coring techniques in an abyssal hills area west of the Line Islands (near $03^{\circ}50'S$, $155^{\circ}45'W$), and found a similar outcropping or near-outcropping of Lower and Middle Miocene sediments. The two deep-tow survey areas (Fig. 3) and the areas surveyed by Moore (1970) and by Johnson and Johnson (1970) are widely separated (hundreds of kilometers), and evidence for recent erosion was present in each of the four areas. The presence of similar features indicative of recent erosion over such a widespread area suggests that the erosion processes may have occurred on a large scale, and not merely in response to local conditions.

Proposed Mechanisms in Other Regions

Several attempts have been made to explain the irregularities which are commonly observed in deep sea sedimentation patterns. Arrhenius (1963, p. 721) noted the abnormal thinness of Quaternary strata on the crest and slopes of a hill, and proposed that there is a "continuous process of resuspension and transport downhill ... probably caused by the churning action of benthic animals, some of which have been observed forming a suspension cloud which may be displaced by any horizontal movement of the near-bottom water." Luyendy' (1969) has recently attempted to express quantitatively the relation between differential sediment accumulation patterns and the degree of activity of benthic organisms.

Tareyev (1965) proposed that topographic irregularities at the sea floor can create standing internal waves, and that the

resulting differences in vertical velocity components in the water column lead to differential sedimentation rates on a small scale. In a region of ascending currents, such as hill slopes which face "upstream", only particles with a settling velocity which is greater than the vertical component of current velocity are capable of reaching the sea floor. Conversely, sediment deposition will be intensified in areas where descending currents are maintained.

Moore (1970) suggested that tectonic activity during the Tertiary created normal fault structures on the sea floor, exposing Tertiary sediments to erosion by bottom currents and benthic organisms. Johnson and Johnson (1970), in a study of a small area to the south and west of the Line Islands Ridge, found that bottom currents have played an important role in shaping the sea floor topography and in redistributing sediments. Berger (1967, 1970) and others have demonstrated that the bottom waters of the Pacific are markedly undersaturated with respect to CaCO_3 , and that consequently chemical dissolution is important in removing the carbonate fraction of the sediment in abyssal depths. van Andel and Kumar (1969), in a detailed study of sediment cores from the crest of the mid-Atlantic Ridge, suggest that turbidity currents have ponded pelagic sediments into topographic valleys near the ridge crest. There is a similar ponding of sediment into lineated valleys near the crest of the East Pacific Rise (Larson, 1971).

Even in the absence of lateral transport, intensive vertical mixing is commonly present in the upper few tens of centimeters of

sediment. Glass (1969) has demonstrated that thin microtektite layers are vertically displaced over distances of tens of centimeters, perhaps as a result of the activity of benthic organisms. Berger and Heath (1968) have attempted to predict quantitatively the effects of vertical mixing as a function of the rate of sedimentation and the depth of the "mixed" layer at the sea floor interface.

Some of the depositional irregularities have been attributed to changing conditions on a global scale through geologic time. Arrhenius (1963; 1966) suggested that fluctuating climatic conditions during the Quaternary have caused highly variable rates of primary productivity and chemical dissolution in the equatorial Pacific yielding variable net rates of sediment accumulation. Rates of supply of terrigenous debris to the deep sea floor have also varied considerably during the Quaternary as a result of variable rates of subaerial erosion and migrating shorelines (Broecker et al, 1958). This effect commonly obscures the depositional history of pelagic materials (Ruddiman, 1971). The outcropping pre-Pliocene sediments of the equatorial Pacific appear to show increasing age northward from the equator (Hays et al, 1969); this effect has been attributed to a wider zone of high productivity during pre-Pliocene time. Rates of chemical dissolution at the sea floor interface may have increased during the Tertiary in response to decreasing bottom water temperatures and increasing rates of production of bottom water in high latitudes (Heath, 1969). Large-scale motions of crustal plates (McKenzie and Parker, 1967; Morgan, 1968) across biogeographic

boundaries produce further complications, such as the north-south asymmetry of sediment accumulation in the equatorial Pacific (Tracey et al, 1971).

Probable Mechanisms Influential in Deep-tow Area

Tectonic activity

Significant horizontal and vertical crustal displacements appear to have taken place in the vicinity of the study area. The basement relief to the south of the site of detailed study is remarkably steep (Fig. 26), and may be a result of tectonic activity along the Clipperton Fracture Zone lying 50 to 100 km to the south (Fig. 3). The north-south trending basement ridge which outcrops along the east flank of the plateau (Fig. 12) appears to have been displaced 10 to 20 km in a right-lateral direction at the south end of the deep-tow survey area (Fig. 25). The elongated depositional basin to the south of the deep-tow area (Fig. 27) may be a result of crustal extension which provided a site for thick sediment accumulation.

There is evidence that tectonism and vulcanism have occurred in the vicinity of other fracture zones in the northeast Pacific. Andrews (1971) suggests that differential crustal spreading rates across fracture zones are important in producing secondary topographic features which may be lineated at an oblique angle to the lineated hills which are created near spreading centers. It may be that the steep, irregular topography south of the deep-tow area is a consequence of differential crustal motion along the Clipperton

Fracture Zone.

The eroded anticlinal structure on the east side of the plateau (Fig. 12) coincides in position with that of a basement ridge (Fig. 8; Fig. 12). This elevation in the acoustic basement may represent a post depositional intrusive which deformed the overlying sediments. There is evidence for deep ocean volcanism at locations which are far from active spreading centers (Spiess et al, 1969), and basaltic material obtained by deep drilling has been dated and determined to be significantly younger than the probable age of the underlying oceanic crust (Macdougall, 1971). It may be that volcanic and intrusive activity is common at great distances from plate boundaries, and that the "basement" at some places within the surveyed area represents a relatively recent igneous event.

Vertical crustal displacements of several tens of meters have occurred within the survey area. Bathymetric profiles obtained with the towed instrument show that small regions of the sea floor with slopes in excess of 60° are widespread (Figs. 10 and 12), and closely spaced sediment cores demonstrate that at least some of these relatively steep slopes must have been formed by post depositional normal faulting (Fig. 17, Profile I). At one location (Fig. 18, Profile V) an active erosional channel was initially created by normal faulting, and subsequent erosional processes apparently have reshaped the topography so that prominent escarpments are no longer present.

There is no evidence that reworked sediment has accumulated

at the base of topographic escarpments on the plateau's flanks, or that sediment movement was initiated by tectonic processes. If gravitational slumping did occur as a result of tectonic activity, then the slumped material must have been removed subsequently by bottom currents. One possible exception is the lens of sediment at the site of core E-18 which appears to be stratigraphically out of place (Fig. 18, Profile IV), and may have slumped to its present position from a higher elevation on the plateau's flank.

Tectonic processes, therefore, have facilitated sediment erosion and redeposition within the area studied. Sediments have been deformed by post depositional vulcanism and perhaps by lateral compression as well. Normal faulting on a small scale has created channels within which eroded sediment can be preferentially transported. Transcurrent faulting and perhaps igneous activity has created topographic depressions within which eroded sediment can accumulate.

Erosion by currents

There is considerable evidence that bottom currents which are now present in the deep ocean may be capable of eroding and transporting modern sea floor sediments (Hollister and Heezen, 1966). Bottom photographs commonly show features indicative of sediment transport (Laughton, 1963; 1968; Heezen and Hollister, 1964; Hollister and Elder, 1969), and direct measurements have detected bottom currents with appreciable speeds (McCoy, 1969; Reid, 1969; Schwartzlose and Isaacs, 1969).

It is difficult to determine precisely the critical erosion velocities for the sediment types present at the deep-tow survey site. Numerous observations have been made of the flow conditions required to move various types of sediment (e.g., Rubey, 1938; Hjulstrom, 1939), but relatively few experiments have been performed on pelagic deep sea sediment. Generally the sediment types used in laboratory flumes have a relatively simple geometry, such as quartz grains of uniform size or artificial glass beads (Vanoni, 1964). The components of deep ocean sediments, however, are highly complex in morphology; this is especially true of biogenous skeletal debris. Therefore it is hazardous to estimate erosion velocities for pelagic sediments on the basis of studies performed upon other types of material.

An additional source of uncertainty in determining critical erosion velocities for deep ocean sediment is the differing boundary layer conditions which are present during different experiments and observations. A smooth deposit of fine-grained sediment which remains unaffected in the presence of moderate current speeds might be readily eroded if, due to the activity of benthic organisms, small perturbations were created along the sediment surface. The effects of small-scale topographic irregularities and an active benthic fauna are no doubt of great importance in facilitating sediment transport. These effects, however, are difficult to observe directly, and consequently there is considerable uncertainty in studying quantitatively the effect of perturbations within the boundary layer.

Southard et al, (1971) have recently performed laboratory

flume experiments on an argillaceous carbonate silt from the deep ocean, composed principally of foraminiferal tests and coccolithophorid debris. The critical erosion velocity for this material was determined for flow conditions in a shallow (6 cm depth) channel using sea water at room temperature. They observed that velocities for erosion are 7 to 10 cm/sec for a bed which has been recently stirred (simulating conditions of recent deposition), and 15 to 20 cm/sec for a bed which has been allowed to settle for several tens of hours. These experimental velocities should be multiplied by a correction factor of ~ 1.8 in order to obtain erosion velocities for the same material if measured 1 m above the ocean bottom (Southard et al, 1971). Thus the critical erosion velocities for this sediment in deep ocean conditions would range from about 15 to 35 cm/sec.

Maximum current velocities recorded in the deep-tow survey area were approximately 10 cm/sec (Appendix II). These current speeds apparently are insufficient for eroding the Holocene sediment, since this thin layer appears to be widespread throughout the survey area (Plates 4-9). The Holocene material is not of uniform thickness, however, and in some cores it is missing entirely. There may be local intensification of currents at these locations, and here the currents may attain speeds substantially greater than those recorded by current meters. Alternatively, the uneven distribution of Holocene material may be due to a relatively recent event of intensified current flow, perhaps a monthly or a seasonal effect, which was not detected due to the relatively limited duration of the survey.

Critical erosion velocities for fine-grained sediment (i.e., constituent particles smaller than about 0.05 mm) are strongly dependent upon the degree of consolidation of the material. The layer of Holocene ooze within the survey area has a high water content (80% to 90%), and is apparently not eroded in the presence of current speeds up to 10 cm/sec. This observation is consistent with experimentally determined erosion velocities of 15 to 30 cm/sec for fine silts and clays with water contents of 80% to 90% (Postma, 1967, Figs. 1 and 2). As sediment becomes more consolidated the critical erosion velocity increases significantly. Current speeds on the order of 100 cm/sec are required to erode fine silt and clay with a water content of 60% to 70% (Postma, op. cit.). It therefore appears that, if the erosion into the Tertiary chalk were accomplished by means of current action alone, current speeds much greater than those present today must have been required.

Chemical dissolution

The sediment types and their net rate of accumulation in much of the deep ocean are determined primarily by the rate of corrosion of skeletal debris at the sea floor interface. Dissolution in the deep ocean affects primarily the calcareous microfossils, and foraminiferal species are particularly susceptible (Berger, 1967). Calcareous nanofossils, by contrast, are relatively protected from corrosion by a thin proteinaceous outer layer (E. D. Milow, personal communication). There is evidence that significant dissolution of siliceous material also can take place (Berger, 1968b). Radiolarian

species have become increasingly more fragile during the Cenozoic, and relatively recent species are preferentially corroded within mixed assemblages (Riedel and Funnell, 1964; Moore, 1969).

Sediments of all ages within the survey area show substantial effects of dissolution; only the more resistant foraminiferal species have been preserved, and the specimens present are highly corroded. The depth where rapid carbonate solution begins (the lysocline) corresponds to the top of the Antarctic Bottom Water (Berger, 1970; Edmond et al, 1971). There is evidence that in the Atlantic, the lysocline was several hundred meters shallower during the glacial stages than it is now (Berger, 1968a), suggesting that during this time bottom water was being formed more rapidly. One might anticipate increased solution of both siliceous and calcareous debris during periods of rapid formation of bottom water. The CO_2 -rich and SiO_2 -deficient surface water would be supplied to the sea floor interface at a faster rate, and the increased respiration of benthic animals would furnish additional CO_2 to the sea floor interface (Arrhenius, 1963).

Chemical dissolution alone, however, is not a sufficient explanation to account for all of the erosional features observed. If dissolution alone were initiated in a region of low relief and near horizontal strata, one would anticipate that it should proceed downward at a relatively uniform rate within a small area. At the deep-tow site, however, material has been preferentially removed on a small scale, creating a sharp angular unconformity at the

sea floor. Perhaps differential erosion and dissolution on a small scale has occurred in response to local intensification of the flow of bottom water within the area

Activity of benthic organisms

Intensive reworking of the upper few centimeters of sediment by deposit-feeding benthic organisms produces significant changes in the physical stability of the sediment surface. The water content and the roughness of the sediment surface are increased, and the critical erosion velocity for the sediment is lowered. Rhoads and Young (1970) recently conducted experiments on shallow water muds to determine the effects that deposit-feeding organisms have on the sediment stability. Equal volumes of sieved mud were introduced into two halves of a wave tank, and specimens of a deposit-feeding bivalve (Nucula proxima) were introduced into one half of the tank and allowed to rework the sediment surface until it developed a granular, burrowed texture. Then the water above the sediment surface in both tanks was oscillated at velocities ranging up to 13 cm/sec, and differential resuspension was determined by noting the turbidity in each half of the tank:

Little turbidity was developed in either tank at velocities up to 3 and 4 cm/sec. But at velocities greater than 4 cm/sec, there was greater resuspension of sediment and greater turbidity above the burrowed sediment than over the unburrowed sediment. Fecal pellets and mud clasts in the burrowed sediment were preferentially eroded and suspended at velocities greater than 4 cm/sec. These particles soon disintegrated into silt-size and clay-size grains, producing high turbidity. During erosion of the loose granular sediment, the roughness of the sediment surface was increased, producing turbulence, which accelerated the erosion process. (Rhoads and Young, 1970, pp. 166-168).

Bottom photographs from the deep-tow area (Appendix I) demonstrate that the upper few tens of centimeters of sediment is a zone of intense biological activity. Any sedimentary material which is put into suspension will be transported laterally if any current whatsoever is present. Under conditions of intense biological activity and relatively low rates of sediment supply, a sedimentary particle might travel great distances as a result of repeated resuspension and lateral drift. Within the deep-tow area, rates of supply of material are relatively low (several mm per thousand years), and some species of benthic organisms are evidently capable of burrowing several centimeters beneath the sea floor. A sedimentary particle need be resuspended only once every few thousand years in order to remain within the "mixed layer" and thereby subject to continual lateral movement.

Interaction of various mechanisms

It appears that erosion has been accomplished by all of the mechanisms discussed above. Tectonic processes have created various topographic features which facilitated sediment redistribution, including: (a) steep, irregular basement relief; (b) faults within the strata along which channels could develop for the subsequent transport of eroded sediment; and (c) wide, deep depressions to serve as sites for sediment redeposition. The activity of benthic organisms has undoubtedly served to disturb the boundary layer at the sea floor, and thereby provide for the lateral transport of sedimentary material which, in the presence of low currents, would have been

otherwise buried and unaffected by erosion.

The principal mechanisms responsible appear to be (a) erosion by intensified bottom currents, together with (b) differential chemical solution in response to these currents. Either of these two processes alone is probably insufficient to explain the features observed. Chemical dissolution has occurred during the entire depositional history of the area, and probably at increased rates during the late Tertiary and the Pleistocene glacial stages. Solution alone, however, would be unlikely to produce the widespread angular unconformity and the irregular outcrop pattern which is observed. Erosion by currents alone is a possible explanation, but unreasonably high current speeds might be required in order to erode into the chalk because of the chalk's stiff texture and high cohesiveness. In the presence of solution processes, however, individual fragments within the chalk would become disaggregated at the sea floor interface, and erosion would be accomplished more easily.

The form which the erosion surface assumes may have been controlled by former topographic irregularities which became accentuated during the erosional episodes. It is suggested that small-scale topographic features served to create regions where the current flow became intensified locally, and that in these regions both chemical solution and mechanical erosion could proceed more rapidly than in more protected regions nearby. For example, a minor depression initially created by faulting may have become eroded preferentially, and gradually became a channel which grew as eroded material

was transported along it. There were probably numerous episodes of intensified current flow and ocean floor erosion during the Pleistocene, and during successive stages the erosion surface became increasingly complex. The prominent unconformity which is observed today (Fig. 16) represents only the shape of the erosion surface when the current speeds most recently decreased to the point where erosion could no longer take place.

The extensive areas of outcropping Tertiary strata in the central Pacific (Hays et al, 1969; Riedel, 1971) may be explained most satisfactorily in terms of regional erosion and redeposition. Nondeposition or local erosional events appear to be inadequate explanations.

PELAGIC SEDIMENTATION IN THE EQUATORIAL PACIFIC DURING THE PLEISTOCENE

It has been suggested here and elsewhere (e.g., Arrhenius, 1952; Olausson, 1969) that the extreme climatic fluctuations during the Pleistocene had a profound effect upon the deep ocean circulation, and upon depositional conditions on the sea floor. In particular, it has been proposed that substantial ocean floor erosion occurred during the glacial stages in response to intensified bottom currents. The following discussion attempts to predict how various oceanographic processes would change in response to glaciation, and how these processes might interact to create conditions favoring increased sediment redistribution on the sea floor (Figs. 31 and 32).

Surface Circulation

The intensity of the atmospheric circulation and the wind-driven oceanic circulation is controlled by the rate of heat exchange between low and high latitudes (Fairbridge, 1962; Arrhenius, 1966). When the major climatic belts migrate toward the equator or toward the poles, there are corresponding increases and decreases in the north-south temperature gradient, and in the intensity of the surface circulation. During the Tertiary, for example, there was a steady climatic deterioration in middle and high latitudes as a result of the migration of the geographic poles to regions of thermal isolation (Donn and Ewing, 1966). Consequently the circulation intensified, and upwelling and productivity were increased in the equatorial

EFFECTS OF GLACIATION UPON OCEANIC CIRCULATION

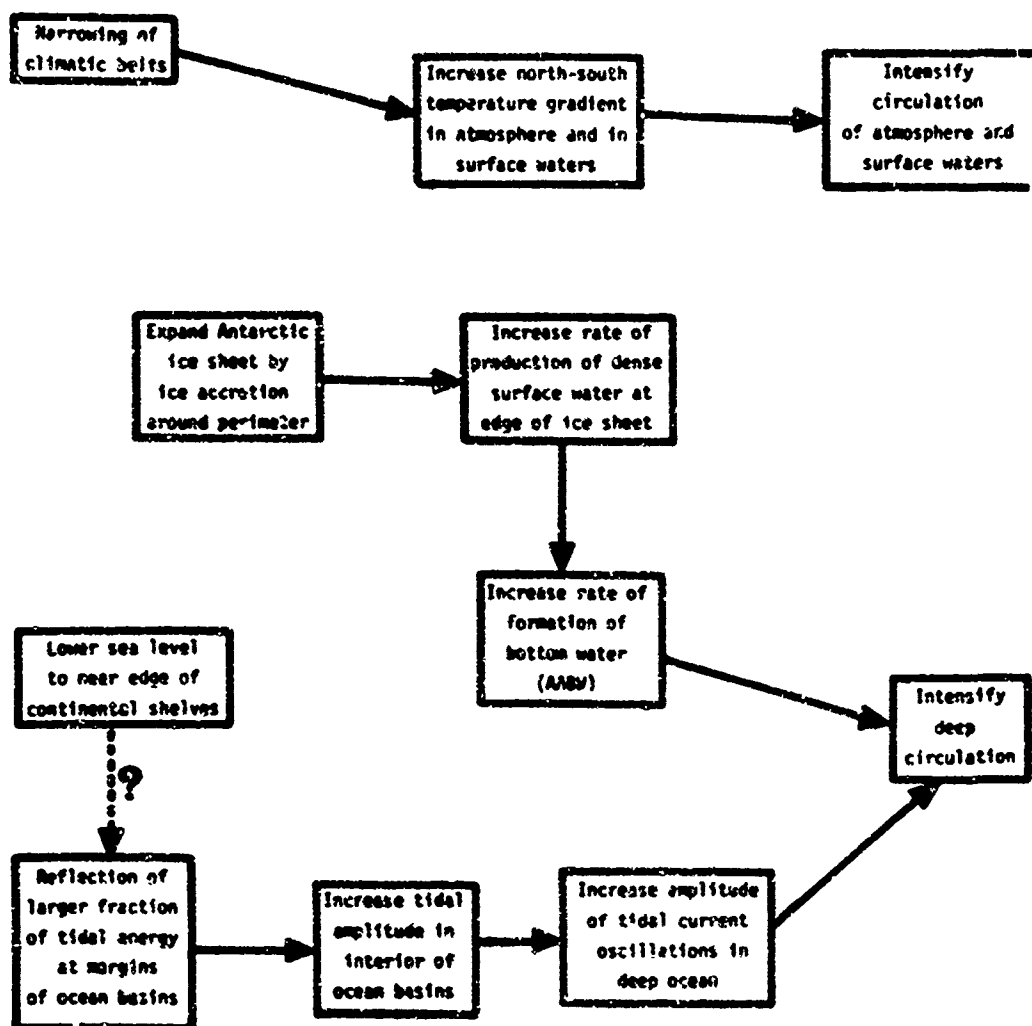


Figure 31 A schematic representation of how various climatic and oceanographic factors might interact to produce intensified oceanic circulation during the glacial stages of the Pleistocene. See text for discussion.

zone (Arrhenius, 1950).

With the onset of extensive glaciation at the end of the Tertiary, the climatic conditions began to undergo major oscillations. The climatic fluctuations which characterize the Pleistocene are probably best explained in terms of a variability in the moisture supply for glacial growth (Donn and Ewing, 1966). Since glaciation was probably synchronous in the northern and southern hemispheres (Epstein et al, 1970), the earth's climatic belts expanded during the interglacials and contracted during the glacials (Fairbridge, 1962; Lamb and Woodroffe, 1970). There were corresponding increases (glacials) and decreases (interglacials) in the intensity of the trade winds, and in the rates of upwelling and primary productivity (Arrhenius, 1966). These migrations of climatic belts and the accompanying variations in rates of circulation and primary productivity are commonly observed in the depositional record (e.g. Emiliani, 1966; Ericson and Wollin, 1968; Hays et al, 1969; McManus, 1970).

Deep Circulation

Production of bottom water

The deep ocean circulation as well as the surface circulation may have been affected substantially by glacial conditions. For example, the rate of production of bottom water in high latitudes may have increased. Today the deep water of the Pacific Ocean (Antarctic Bottom Water) originates in the shallow seas surrounding the Antarctic continent, principally the Weddell Sea and the Ross Sea (Jacobs et al, 1970; Seabrooke et al, 1971). The formation of

Antarctic Bottom Water occurs when relatively cold surface water mixes with warmer intermediate water near the shelf edge. These two parent water masses have approximately the same density, but significantly different temperatures and salinities (Seabrooke et al, 1971). Because of the nonlinear equations of state of sea water the resulting mixture is denser than either of the two original water masses (Fofonoff, 1956), and a cabbeling instability develops to transport the Antarctic Bottom Water which is produced downward to the deep ocean floor (Foster, 1971).

Several attempts have been made to explain how the cold surface water is brought to a condition which allows mixing with warmer intermediate water to produce bottom water (AABW). Seabrooke et al, (1971) have proposed that the surface water of the westward flowing Antarctic Coastal Current is modified in temperature and salinity as it flows beneath the wide shelves of the Weddell Sea, and that it eventually reaches a state (-1.9°C ; $34.60 \text{ }^{\circ}/_{\text{oo}}$) where it is sufficiently dense to form an appropriate mixture with warmer intermediate water. Theoretical studies by Foster (1971), however, suggest that the cooling and freezing of sea water on the underside of an ice shelf occurs at too slow a rate to produce any significant modification of the shelf water. He suggests that the required changes in the properties of the surface water which are necessary for bottom water production are provided by haline convection induced by the direct freezing of sea water. In spite of considerable uncertainty in determining the mechanism by which the surface water is modified,

it appears likely that the process is seasonal, and that consequently the maximum production of AABW occurs during the southern winter during the accretion of ice around the perimeter of the Antarctic ice cap (Foster, 1971).

During the glacial stages of the Pleistocene conditions favoring the formation of cold, saline surface water around the Antarctic ice cap were extended in time and space beyond the normal seasonal expansions and contractions. As ice accretion proceeded during the glacial stages, there was an increasingly greater area of ice cover around which cold and relatively saline surface water could form. The subsequent production of bottom water was probably directly proportional to the rate of ice formation. Munk (1966) has attempted to approach quantitatively the problem of bottom water production rates, and estimates that 43 grams of bottom water are formed for each gram of ice that freezes. It therefore appears likely that conditions of an expanding ice cap around the Antarctic continent favor a steadily increasing rate of production of bottom water.

Dissipation of tidal energy

The velocities of deep ocean currents are characteristically periodic. Semidiurnal tidal components are commonly recorded during measurements of several days' duration (Nowroozi et al, 1968; Doeblner, 1967; Winbush and Munk, 1970; Lonsdale et al, 1971), and monthly variations also have been reported (Schmitz et al, 1970). It is likely, therefore, that deep ocean currents in some localities are

a reflection of the dissipation of tidal energy as well as a net transport of bottom water from one region of the ocean basin to another.

Tidal energy in the ocean basins is dissipated at a rate of 2.7×10^{19} ergs/sec, a rate which is determined from precise observations of the moon's acceleration (Munk, 1968). This dissipation rate is quite high, and is such that all of the energy stored in the tides at any instant is dissipated in several days (Hendershott, personal communication). A substantial fraction of this total dissipation, between 1.4 and 1.7×10^{19} ergs/sec, takes place along the continental margins and in shallow seas (Miller, 1966).

Frictional dissipation in shallow seas is not the only possible mechanism to serve as a sink for tidal energy. Cox and Sandstrom (1962) show that tidal energy flowing over a rough ocean bottom is converted to internal waves, and that the subsequent dissipation of these waves may be important in accounting for the total rate of dissipation of tidal energy. Miller (1966) attempted to estimate the frictional dissipation in the deep ocean using an empirical expression for the rate of energy loss per unit area (γu^3 where $\gamma = .002$ and u = current speed). He estimated that for the entire area of the deep oceans the dissipation is on the order of 10^{16} ergs/sec, or three order of magnitude less than the total dissipation rate required. He assumed, however, that tidal current speeds in the deep ocean are on the order of 1 cm/sec. By assuming tidal current oscillations on the order of 10 cm/sec, which is

consistent with recent observations, the deep ocean dissipation is on the order of 10^{19} ergs/sec. This value compares favorably with the energy dissipated in shallow seas and with the total dissipation rate required.

One might consider the possibility that the pattern of tidal energy dissipation was substantially different during the glacial stages. Sea level was approximately 130 m lower than at present during the most recent glacial advance (Curry, 1965), and consequently many of the world's continental shelves and shallow seas were subaerial and no longer available for the dissipation of tidal energy. One possible consequence of lowering sea level to near the shelf edge is a greater reflection of tidal energy at the oceanic boundaries. This condition would result in higher tidal amplitudes at the sea surface in the interior of the ocean basins, and a corresponding increase in the amplitude of tidal oscillations on the deep sea floor (Hendershott, personal communication).

It is by no means clear, however, that the oceanic boundaries would become less dissipative to tidal energy as the shore line migrates seaward across the continental shelves. The continental slopes of the world vary considerably in steepness, but in many extensive regions the slopes average no more than two or three degrees (Shepard, 1963). In these regions the slopes may be insufficiently steep to reflect significant tidal energy. The energy which is absorbed at the continental margins during interglacial times may continue to be absorbed at the shelf edges during glacial stages,

resulting perhaps in intensified erosion of sediment on the continental slopes. The mechanisms controlling tidal currents in the deep ocean today are poorly understood; consequently there is much uncertainty in attempting to predict the tidal oscillations on the ocean floor during periods of markedly different geographic and climatic conditions.

Depositional Environment

Assuming that both the surface circulation and deep circulation were intensified during glacial stages, one can then predict the effect of these changes upon depositional conditions on the ocean floor (Fig. 32). First of all, there was more material supplied to the sea floor from the overlying waters. Large quantities of terrigenous sediment were transported to the deep ocean as a result of the effects of lower sea level. Apart from this effect, there remained a substantial increase in the rate of supply of pelagic sediment as well. Some of this material was derived from arid or semi-arid continental regions (Damuth and Fairbridge, 1970; Frenzel, 1968) and transported to the open ocean by intensified wind systems (Bonatti and Arrhenius, 1965). In addition, the rate of supply of biogenous skeletal material was increased as a result of increased primary productivity (Arrhenius, 1963). This increase in productivity occurred primarily in regions where productivity is high today, such as the equatorial zone and certain coastal regions. Productivity may have been increased in the central water masses as well. Today the production of bottom water in high latitudes is compensated

EFFECTS OF GLACIATION UPON DEPOSITIONAL CONDITIONS

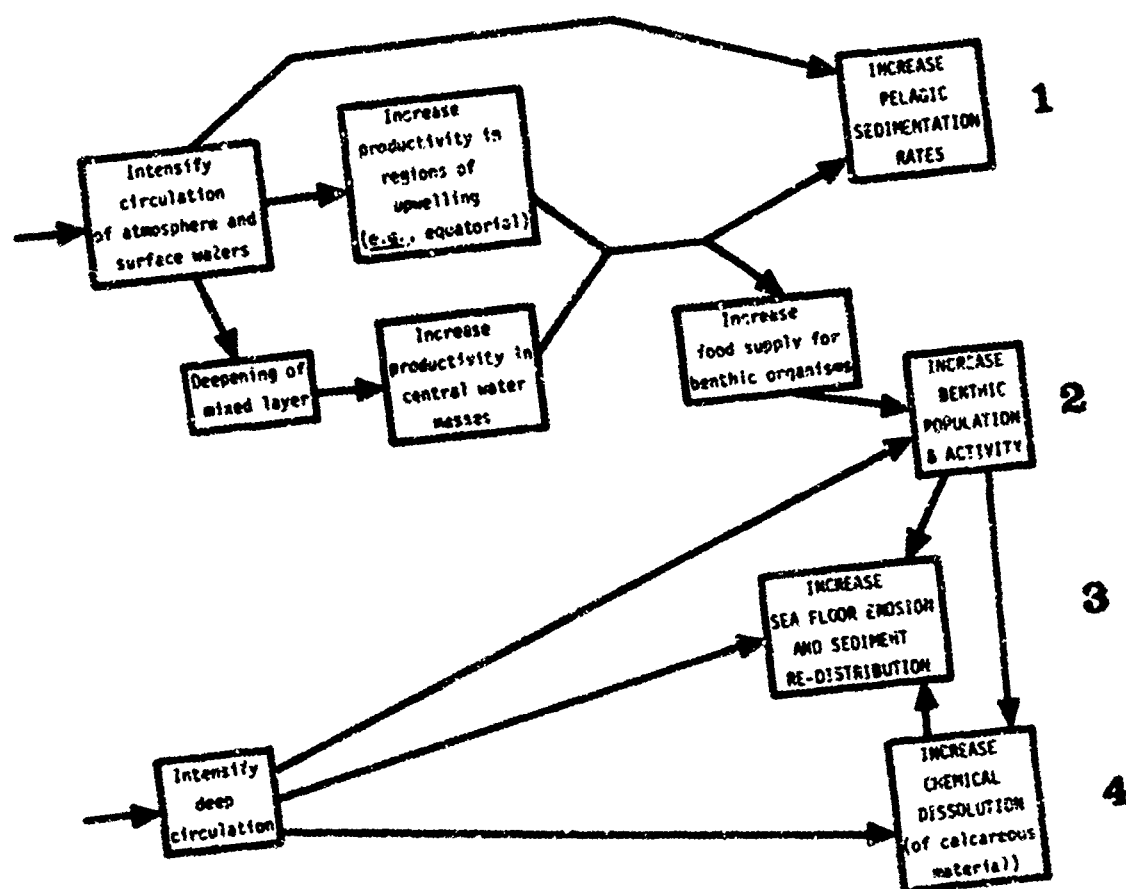


Figure 32 Effects of intensified oceanic circulation upon environmental conditions at the sea floor. The four principal effects are of varying degrees of importance, depending upon the topographic features in the area of interest.

quantitatively by vertical upwelling within the Pacific at a rate averaging 1.2 cm/day (Munk, 1966). An increased rate of production of deep water during glacial stages would then be accompanied by a compensating increased rate of upwelling throughout the Pacific basin.

A second change which might be anticipated is a more abundant population of benthic organisms, particularly in protected regions where deposition rates are highest. Since the size of a benthic population is limited principally by food supply (Sanders and Hessler, 1969; Griggs et al., 1969), a higher planktonic population in the surface waters should support a more abundant benthic population on the sea floor beneath. If oxygen supply were an additional limiting factor to benthic activity, glacial conditions should provide oxygenated surface waters to the sea floor at a higher rate, and thereby allow a more active benthic fauna. In addition, the deposit-feeding and suspension-feeding organisms might show a marked spatial separation. Experiments and observations in shallow water (Rhoads and Young, 1970, Figs. 6 and 7) suggest that the sea floor in relatively protected environments is abundantly populated by deposit feeders which produce a granular, burrowed sediment surface. At nearby sites which are relatively exposed, deposit feeders are less abundant, and the sediment surface is less disturbed by burrowing. The frequent resuspension of sediment where deposit-feeders are present produces sediment instability and water turbidity, and thereby serves as a limiting factor for most suspension-feeders at these locations (Rhoads and Young, 1970). Third, glacial conditions should facilitate

the dissolution of calcareous skeletal material at the sea floor. The presence of an active benthic population would favor rapid solution by providing more CO_2 to the waters near the sea floor interface (Arrhenius, 1963; Berger, 1968a). In addition, the sediment components might be mechanically disintegrated during the feeding activities of benthic organisms, thereby facilitating both chemical solution and erosion by currents. The most profound solution effects, however, would be due to the increased rates of production of bottom water in high latitudes. Extensive studies (Berger, 1970; Parker and Berger, 1971) have shown that there is a continuous destruction of almost all calcareous sediment exposed on the Pacific Ocean floor, and that the regions where solution is most intense are in contact with Antarctic Bottom Water. Olausson (1969) indicates that dissolution of carbonate sediment in the North Atlantic was intensified during the glacial stages, and suggests that the bottom waters were more corrosive as a result of either a lower temperature or a more rapid rate of flow. Kennett (1970) has found evidence of intense solution of glacial-age carbonate sediments in the sub-Antarctic region, probably a result of increased production of bottom water. Kaye (1957) performed laboratory experiments on calcite crystals and limestone blocks, and determined that fluid motion is of considerable importance in controlling the rate of solution of carbonate materials. Edmond (1971) has reinterpreted the results of the buoy experiment in which the rates of solution of calcite spheres (Peterson, 1966) and foraminiferal tests (Berger, 1967) were determined at several depths in the

water column. He demonstrates that the variable rate of solution of CaCO_3 is not a reflection of the carbonate chemistry of the water, but rather is a consequence of the water's flow rate. This correspondence supports the interpretation that more intense solution during glacial stages was due to stronger bottom currents, in response to increased rates of production of bottom water in high latitudes.

Finally, physical erosion and redistribution of sediment should increase during glacial stages. There is evidence that sediment reworking increased progressively during the Tertiary, and may have been particularly intense during the glacial stages. Heath (1969) has pointed out that the early and middle Tertiary sediments of the equatorial Pacific are much more uniform and better sorted than the late Tertiary and Quaternary sediment, and suggests that intensified bottom currents and benthic activity would be expected as increasing volumes of bottom water are formed beneath the growing Antarctic ice cap. Studies of sediment cores (Riedel and Funnell, 1964; Riedel, 1971) show that Quaternary sediments generally contain a substantial proportion of reworked material, but the outcropping or near-outcropping Tertiary sediments often contain relatively homogeneous faunal assemblages, indicating very little mixing. Recent deep drilling at several sites in the equatorial Pacific (Table 6) has recovered tens to hundreds of meters of Tertiary sediment containing no apparent unconformities and little evidence of reworking. The evidence supports the interpretation that substantial ocean floor

TABLE 5 Continuous Cenozoic sections recovered by Deep Sea
Drilling Project in equatorial Pacific

<u>DSDP Site</u>	<u>Location</u>	<u>Age of Sediments</u>	<u>Depth below Sea Floor</u>
69	06°00'N 152°52'W	L. Mioc. - U. Eoc.	52 m to 162 m
70	06°20'N 140°22'W	U. Mioc. - L. Olig.	8 m to 325 m
71	04°28'N 140°19'W	L. Pleist. - M. Olig.	0 m to 436 m
77	00°29'N 133°14'W	U. Pleist. - L. Olig.	0 m to 470 m
78	07°57'N 127°21'W	M. Mioc. - L. Olig.	0 m to 315 m

erosion in the Pacific may be characteristic only of the late Cenozoic and particularly the glacial stages of the Pleistocene.

Of the four principal effects which glaciation may produce on the deep sea floor (Fig. 32), only the first (increased sediment supply) tends to accumulate sediment more rapidly at a given locality; the last three act to remove or at least redistribute material. Local topographic irregularities probably determine which of these effects will predominate at any given site. One might expect, for example, that increased sediment supply should predominate in regions relatively protected from strong currents, and that solution and erosion should be most important in exposed regions where strong currents are present. The benthic population would be most abundant where food supply is greatest, with perhaps a small benthic population of suspension-feeders in the exposed regions.

As an example of variable sea floor conditions on a small scale, Fig. 33 shows a line drawing based on a reflection profile from the basin south of the deep-tow area, and indicates that local areas might conveniently be classified as either exposed or protected. This arbitrary classification might be applied to any region of the sea floor, depending on whether or not local topographic effects exposed the region to erosional processes. Fig. 34 summarizes the depositional conditions which one might expect at the sea floor in both exposed and protected regions during glacial and interglacial stages. In the exposed region, any material which accumulates during the relatively quiet interglacials is likely to be removed during the

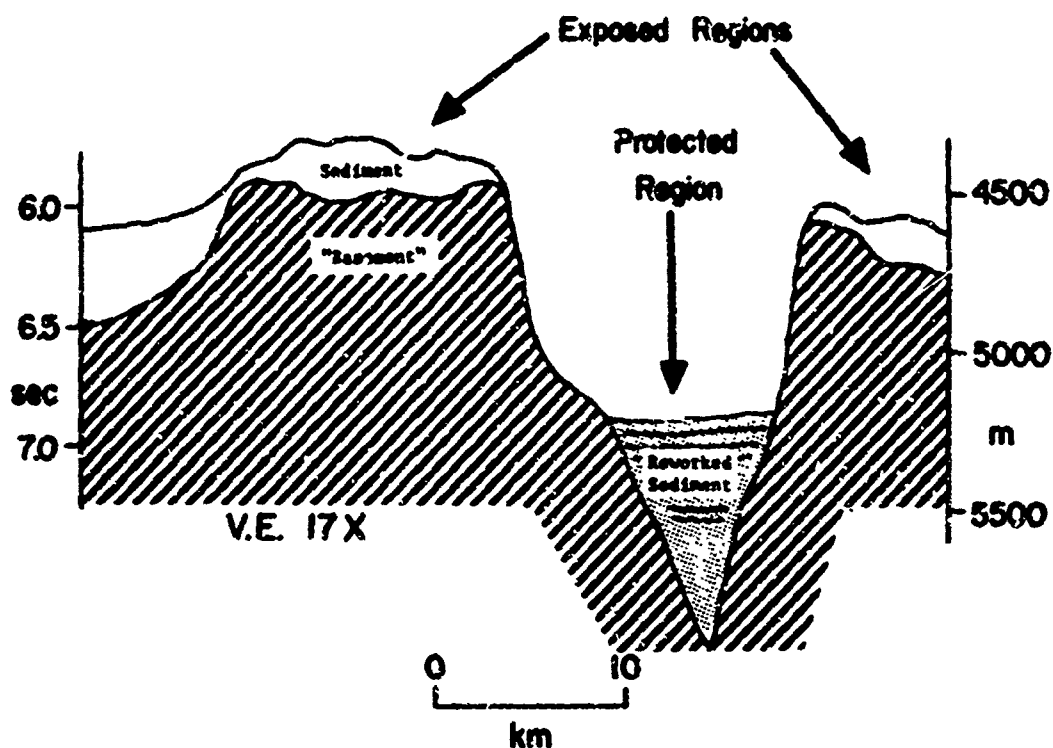


FIGURE 33 Line drawing of reflection profile from the vicinity of the deep-tow survey area, indicating the small-scale variability in depositional environments which may be characteristic of many regions where the topography is irregular.

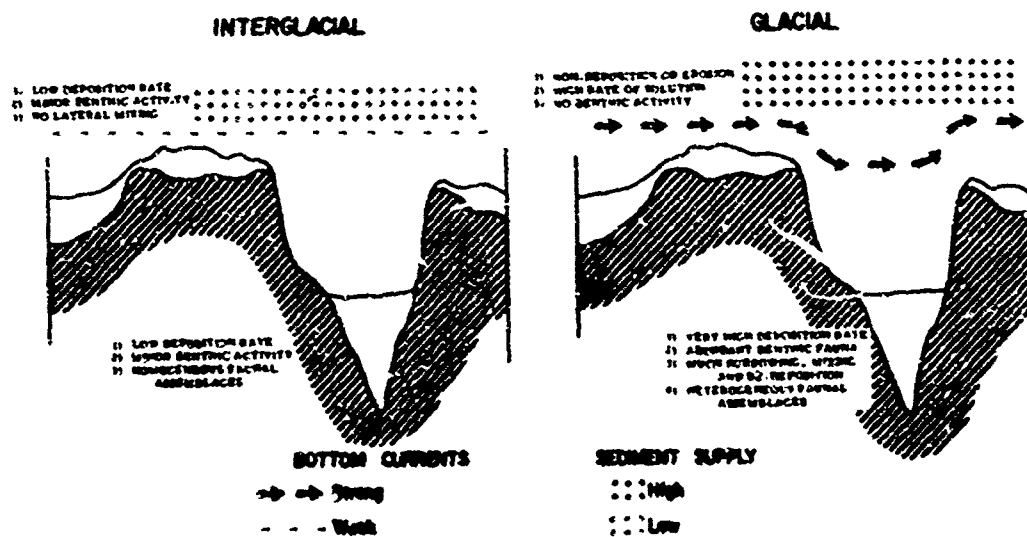


FIGURE 34 Hypothetical conditions of deposition during glacial and interglacial stages in an area consisting of relatively protected and relatively exposed regions. See text for discussion.

following glacial stage. Consequently the depositional record in exposed regions may contain hiatuses. In protected regions, however, the depositional record should be relatively complete. Depositional conditions at protected sites should alternate between periods of intense vertical and lateral mixing and high sediment supply (glacials) and relatively quiescent periods of little mixing and low deposition rates (interglacials). Sediment cores from protected regions such as this should clearly show such alternations if highly variable deposition conditions did indeed exist during the Pleistocene.

Duration of erosional events

Subaerial erosional processes commonly occur during infrequent episodic events of relatively short duration (perhaps several hours or days), and not at a uniform rate in response to a set of "average" conditions. During the time intervals which separate these events there may be little or no erosion taking place. One might consider whether the proposed intensification of bottom water flow and sediment reworking during the Pleistocene also may have been episodic in nature.

The deep ocean is relatively remote from those regions on the earth's surface where the major climatic conditions are determined. Because of its remoteness, and because of the relatively long time required for complete mixing of the world's oceans (several hundred years), surface climatic conditions are probably integrated over hundreds of years in determining the effects of these changing conditions on the deep sea floor. As a result, a brief interval of

markedly unusual climatic conditions at the surface may have no effect at all upon the deep ocean if the event is of sufficiently short duration.

It therefore appears that relatively long-term events, such as glacial/interglacial climatic oscillations, may be required in order to create significant changes in the depositional conditions on the deep sea floor. The conditions favoring intensified ocean floor erosion during glacial stages probably developed gradually, over a time scale of 10,000 to 100,000 years. The individual erosional episodes may well have occurred during brief periods, perhaps in response to tidal oscillations similar to those observed today. But the conditions which allowed intensified erosion to occur must have developed over a relatively long period of time.

REFERENCES

- Andrews, J. E., Abyssal hills as evidence of transcurrent faulting on North Pacific fracture zones, Geol. Soc. Amer. Bull., 82, 463-470, 1971.
- Arrhenius, G. O. S., Late Cenozoic climatic changes as recorded by the equatorial current system, Tellus, 2, 83-88, 1950.
- Arrhenius, G., Sediment cores from the East Pacific, Repts. Swed. Deep Sea Exp., 5, 1952.
- Arrhenius, G. O. S., Pelagic sediments, in The Sea, 3, M. N. Hill, ed., Interscience, New York, 655-727, 1963.
- Arrhenius, G., Sedimentary record of long-period phenomena, in Advances in Earth Science, P. M. Hurley, ed., M.I.T. Press, Cambridge, 155-174, 1966.
- Atwater, T. and H. U. Menard, Magnetic lineations in the northeast Pacific, Earth and Planet. Sci. Letters, 7, 445-450, 1970.

- Ballard, R. D. and K. O. Emery, Research submersibles in oceanography, Mar. Tech. Society, Washington, 1970.
- Berger, W. H., Foraminiferal ooze: solution at depths, Science, 186, 383-385, 1967.
- Berger, W. H., Planktonic foraminifera: selective solution and paleoclimatic interpretation, Deep-Sea Res., 15, 31-43, 1968a.
- Berger, W. H., Radiolarian skeletons: solution at depths, Science, 159, 1237-1238, 1968b.
- Berger, W. H., Planktonic foraminifera: selective solution and the lysocline, Mar. Geology, 8, 111-138, 1970.
- Berger, W. H. and G. R. Heath, Vertical mixing in pelagic sediments, Jour. Mar. Res., 26, 134-143, 1968.
- Berggren, W. A., A Cenozoic time scale: some implications for regional geology and paleobiogeography, Jour. Foram. Res., in press, 1971.
- Boegeman, D. E., G. J. Miller and W. R. Normark, Precise positioning for bottom samples using a relay transponder, in preparation, 1971.
- Bonatti, E. and G. Arrhenius, Eolian sedimentation in the Pacific off northern Mexico, Mar. Geology, 3, 337-348, 1965.
- Bradshaw J. S., Ecology of living planktonic foraminifera in the north and equatorial Pacific Ocean, Contr. Cushman Found. Foram. Res., 10 (2), 25-64, 1959.
- Bramlette, M. N. and W. R. Riedel, Observations on the biostratigraphy of pelagic sediments, in Micropalaeontology of the Oceans. SCCR Symposium, Cambridge Univ. Press, 665-668, 1971.
- Broecker, W. S., K. K. Turekian and B. C. Heezen, The relation of deep-sea sedimentation rates to variations in climate, Amer. J. Sci., 256, 503-517, 1958.
- Chase, T. E., H. W. Menard, and J. Mannerickx, Bathymetry of the North Pacific, Institute of Marine Resources, Scripps Inst. of Oceanography, 10 sheets, 1970.
- Cox, C. S. and H. Sandstrom, Coupling of internal and surface waves in water of variable depth, J. Oceanog. Soc. Japan, 18, 499-513, 1962.

- Curry, J. R., Late Quaternary history, continental shelves of the United States, in The Quaternary of the United States, H. E. Wright and D. G. Frey, eds., Princeton Univ. Press, 723-735, 1965.
- Damuth, J. E. and R. W. Fairbridge, Equatorial Atlantic deep-sea arkosic sands and ice-age aridity in tropical South America, Geol. Soc. Amer. Bull., 81, 189-206, 1970.
- Doebler, H. J., Savonius current meter measurements of deep ocean currents on the slope of Plantagenet Bank, Bermuda, J. Geophys. Res., 72, 511-519, 1967.
- Donn, W. L. and M. Ewing, A theory of ice ages III, Science, 152, 1706-1712, 1966.
- Edmond, J. M., An interpretation of the calcite spheres experiment (abstract), Trans. Am. Geophys. Union, 52, 256, 1971.
- Edmond, J., Y. Chung and J. G. Sclater, Pacific bottom water flow: implications of continuous deep water temperature profiles from the central North Pacific, J. Geophys. Res., in press, 1971.
- Emery, K. O. and D. A. Ross, Topography and sediments of a small area of the continental slope south of Martha's Vineyard, Deep-Sea Res., 15, 415-422, 1968.
- Emiliani, C., Isotopic paleotemperatures, Science, 154, 851-857, 1966.
- Epstein, S., R. P. Sharp and A. J. Gow, Antarctic ice sheet: stable isotope analyses of Byrd Station cores and interhemispheric climatic implications, Science, 168, 1570-1572, 1970.
- Ericson, D. B., H. Ewing and B. C. Heezen, Turbidity currents and sediments in the North Atlantic, Amer. Assoc. Petrol. Geol. Bull., 36, 489-512, 1952.
- Ericson, D. B., G. Wollin, M. Ewing and B. C. Heezen, Atlantic deep-sea sediment cores, Geol. Soc. Amer. Bull., 72, 193-286, 1961.
- Ericson, D. B. and G. Wollin, Pleistocene climates and chronology in deep-sea sediments, Science, 162, 1227-1234, 1968.
- Evans, M. W. and W. White, Internal length and time scales of motion in the Pacific North Equatorial Current, in preparation, 1971.

- Ewing, J., M. Ewing, T. Aitken and W. J. Ludwig, North Pacific sediment layers measured by seismic profiling, in The Crust and Upper Mantle of the Pacific Area, Geophys. Monograph #12, Am. Geophys. Union, Washington, 147-173, 1968.
- Fairbridge, R. W., World sea-level and climatic changes, Quaternaria, IV, 111-134, 1962.
- Fell, H. B., Biological applications of sea-floor photography, in Deep Sea Photography, J. B. Hersey, ed., Johns Hopkins Press, Baltimore, 207-221, 1967.
- Fofonoff, N. P., Some properties of sea water influencing the formation of Antarctic Bottom Water, Deep-Sea Res., 4, 32-35, 1956.
- Foster, T. D., An analysis of the cabbeling instability in sea water, Deep-Sea Res., in press, 1971.
- Francheteau, J., C. G. A. Harrison, J. G. Sclater and M. L. Richards, Magnetization of Pacific seamounts: a preliminary polar curve for the northeastern Pacific, J. Geophys. Res., 75, 2035-2061, 1970.
- Frenzel, B., The Pleistocene vegetation of northern Eurasia, Science, 161, 637-649, 1968.
- Glass, B. P., Reworking of deep-sea sediments as indicated by the vertical dispersion of the Australasian and Ivory Coast microtektite horizons, Earth and Planet. Sci. Letters, 6, 409-415, 1969.
- Gordon, A. L. and R. D. Gerard, North Pacific bottom potential temperatures, in Geological Investigation of the North Pacific, Geol. Soc. Amer. Memoir 126, J. D. Hays, ed., 23-39, 1971.
- Griggs, G. B., A. G. Carey and L. D. Kulm, Deep-sea sedimentation and sediment-fauna interaction in Cascadia Channel and on Cascadia Abyssal Plain, Deep-Sea Res., 16, 157-170, 1969.
- Hamilton, E. L., Elastic properties of marine sediments, J. Geophys. Res., 76, 579-604, 1971.
- Hays, J. D., T. Saito, N. D. Opdyke and L. H. Burckle, Pliocene-Pleistocene sediments of the equatorial Pacific: their paleomagnetic, biostratigraphic and climatic record, Geol. Soc. Amer. Bull., 80, 1481-1513, 1969.

- Hays, J. D. et al., Initial Reports of the Deep Sea Drilling Project, vol. 9, U. S. Govt. Printing Office, Washington, in press, 1971.
- Heath, G. R., Carbonate sedimentation in the abyssal equatorial Pacific during the past 50 million years, Geol. Soc. Amer. Bull., 80, 689-694, 1969.
- Heath, G. R. and T. C. Moore, Jr., Subbottom profile of abyssal sediments in the central equatorial Pacific, Science, 149, 744-746, 1965.
- Heezen, B. C., Dynamic processes of abyssal sedimentation: erosion, transportation, and redeposition on the deep-sea floor, Geophys. J. Roy. Astr. Soc., 2, 142-163, 1959.
- Heezen, B. C., Turbidity currents, in The Sea, 3, M. N. Hill, ed., Interscience, New York, 742-771, 1963.
- Heezen, B. C., D. B. Ericson and M. Ewing, Further evidence for a turbidity current following the 1929 Grand Banks earthquake, Deep-Sea Res., 1, 193-202, 1954.
- Heezen, B. C. and C. D. Hollister, Deep-sea current evidence from abyssal sediments, Mar. Geology, 1, 141-174, 1964.
- Heezen, B. C., C. D. Hollister and W. F. Ruddiman, Shaping of the continental rise by deep geostrophic contour currents, Science, 152, 502-508, 1966.
- Hjulstrom, F., Transportation of detritus by moving water, in Recent Marine Sediments, P. D. Trask, ed., Amer. Assoc. Petrol. Geol., Tulsa, 5-31, 1939.
- Hollister, C. D. and R. B. Elder, Contour currents in the Weddell Sea, Deep-Sea Res., 15, 99-101, 1969.
- Hollister, C. D. and B. C. Heezen, Ocean bottom currents, in The Encyclopedia of Oceanography, R. W. Fairbridge, ed., Reinhold Publ. Co., New York, 576-583, 1966.
- Isaacs, J. D., J. L. Reid, Jr., G. B. Schic and R. A. Schwartzlose, Near-bottom currents measured in 4 kilometers depth off the Baja California coast, J. Geophys. Res., 71, 4297-4303, 1966.

- Jacobs, S. S., A. F. Amos and P. M. Bruckhausen, Ross Sea oceanography and Antarctic Bottom Water formation, Deep-Sea Res., 17, 935-962, 1970.
- Johnson, D. A. and T. C. Johnson, Sediment redistribution by bottom currents in the central Pacific, Deep-Sea Res., 17, 157-169, 1970.
- Jones, E. J. W., M. Ewing, J. Ewing and S. Eittrheim, Influences of Norwegian Sea overflow water on sedimentation in the northern North Atlantic and Labrador Sea, J. Geophys. Res., 75, 1655-1680, 1970.
- Kaye, C. A., The effect of solvent motion on limestone solution, J. Geol., 65, 35-46, 1957.
- Kennett, J. P., Pleistocene paleoclimatic and foraminiferal biostratigraphy in subantarctic deep-sea cores, Deep-Sea Res., 17, 125-140, 1970.
- Knauss, J. A., Equatorial current systems, in The Sea, 2, M. N. Hill, ed., Interscience, New York, 235-252, 1963.
- Krause, D. C., Interpretation of echo sounding profiles, Int. Hydrog. Rev., 39, 65-123, 1962.
- Lamb, H. H. and A. Woodroffe, Atmospheric circulation during the last ice age, Quaternary Res., 1, 29-56, 1970.
- Larson, R. L., Near-bottom geologic studies of the East Pacific Rise crest, Geol. Soc. Amer. Bull., 82, 823-842, 1971.
- Laughton, A. S., Microtopography, in The Sea, 3, M. N. Hill, ed., Interscience, New York, 437-472, 1963.
- Laughton, A. S., New evidence of erosion on the deep ocean floor. Deep-Sea Res., 15, 21-23, 1968.
- Lonsdale, P. F., W. R. Normark and W. A. Newman, Sedimentation and erosion on Horizon Guyot, in preparation, 1971.
- Lowenstein, C. D., Position determination near the sea floor, in Marine Sciences Instrumentation, 4, Plenum Press, New York, 319-324, 1968.
- Luyendyk, B. P., Geological and geophysical observations in an abyssal hill area using a deeply towed instrument package, Ph.D. thesis, University of California, San Diego, 212 pp., 1969.

- Luyendyk, B. P., Origin and history of abyssal hills in the northeast Pacific ocean, Geol. Soc. Amer. Bull., 81, 2237-2260, 1970.
- Macdougall, D., Deep sea drilling: age and composition of an Atlantic basaltic intrusion, Science, 171, 1244-1245, 1971.
- McCoy, F. W., Bottom currents in the western Atlantic ocean between the lesser Antilles and the mid-Atlantic Ridge, Deep-Sea Res., 16, 179-184, 1969.
- McKenzie, D. P. and R. L. Parker, The north Pacific: an example of tectonics on a sphere, Nature, 216, 1276-1280, 1967.
- McManus, D. A., Criteria of climatic change in the inorganic components of marine sediments, Quaternary Res., 1, 72-102, 1970.
- Menard, H. W. and R. L. Fisher, Clipperton Fracture Zone in the northeastern equatorial Pacific, J. Geol., 66, 239-253, 1958.
- Miller, G. R., The flux of tidal energy out of the deep oceans, Jour. Geophys. Res., 71, 2485-2489, 1966.
- Moore, D. G., The free corer: sediment sampling without wire and winch, J. Sed. Petrol., 31, 627-630, 1961.
- Moore, T. C., Jr., Radiolaria: change in skeletal weight and resistance to solution, Geol. Soc. Amer. Bull., 80, 2103-2108, 1969.
- Moore, T. C., Jr., Abyssal hills in the central equatorial Pacific: sedimentation and stratigraphy, Deep-Sea Res., 17, 573-593, 1970.
- Moore, T. C., Jr., Radiolaria, in Initial Reports of the Deep Sea Drilling Project, vol. 8, in press, 1971.
- Moore, T. C., Jr., and G. R. Heath, Abyssal hills in the central Pacific: detailed structure of the sea floor and sub-bottom reflectors, Mar. Geology, 5, 161-179, 1967.
- Morgan, W. J., Rises, trenches, great faults, and crustal blocks, J. Geophys. Res., 73, 1959-1982, 1968.
- Mudie, J. D., W. R. Normark and E. J. Cray, Jr., Direct mapping of the sea floor using side-scanning sonar and transponder navigation, Geol. Soc. Amer. Bull., 81, 1547-1554, 1970.

- Mudie, J. D., J. A. Grow and J. R. Hutt, Microtopographic, magnetic, and bottom penetration survey of a small area of abyssal hills in the equatorial Pacific, in preparation, 1971.
- Munk, W. H., Abyssal recipes, Deep-Sea Res., 13, 707-730, 1966.
- Munk, W. H., Once again -- tidal friction, Quart. J. Roy. Astr. Soc., 9, 352-375, 1968.
- Nowroozi, A. A., M. Ewing, J. E. Nafe and M. Fleigel, Deep ocean current and its correlation with the ocean tide off the coast of northern California, J. Geophys. Res., 73, 1921-1932, 1968.
- Olausson, E., Le climat au Pleistocene et la circulation des oceans, Rev. Geogr. Phys. et Geol. Dyn., 11, 251-264, 1969.
- Owen, R. W. and B. Zeitzschel, Phytoplankton production: seasonal change in the oceanic eastern tropical Pacific, Mar. Biol., 7, 32-36, 1970.
- Parker, F. L., Distribution of planktonic foraminifera in recent deep-sea sediments, in Micropalaeontology of Marine Bottom Sediments, SCOR symposium, Cambridge Univ. Press, 289-307, 1971.
- Peterson, M. N. A., Calcite: rates of dissolution in a vertical profile in the central Pacific, Science, 154, 1542-1544, 1966.
- Phleger, F. B., Displaced foraminifera faunas, Soc. Econ. Paleont. Mineral., Spec. Publ. 2, 66-75, 1951.
- Postma, H., Sediment transport and sedimentation in the estuarine environment, in Estuaries, G. H. Lauff, ed., Publ. No. 83, Am. Assoc. Adv. Sci. (Washington), 158-179, 1967.
- Reid, J. L., Jr., ed., Oceanic Observations of the Pacific: 1955, the NORPAC Atlas, Univ. of Calif. Press, Berkeley, 1960.
- Reid, J. L., Jr., Preliminary results of measurements of deep currents in the Pacific Ocean, Nature, 221, 848, 1969.
- Reid, J. L., Jr., H. Stommel, E. D. Stroup and B. A. Warren, Detection of a deep boundary current in the western south Pacific, Nature, 217, 937, 1968.
- Rhoads, D. C. and D. K. Young, The influence of deposit-feeding organisms on sediment stability and community trophic structure, J. Mar. Res., 28, 150-178, 1970.

- Riedel, W. R., Radiolarian evidence consistent with spreading of the Pacific floor, Science, 157, 540-542, 1967.
- Riedel, W. R., The occurrence of pre-Quaternary radiolaria in deep-sea sediments, in Micropalaeontology of Marine Bottom Sediments, SCOR symposium, Cambridge Univ. Press, 567-594, 1971.
- Riedel, W. R. and B. M. Funnell, Tertiary sediment cores and microfossils from the Pacific Ocean floor, Quart. J. Geol. Soc. Lond., 120, 305-368, 1964.
- Riedel, W. R. and A. Sanfilippo, Radiolaria, in Initial Reports of the Deep Sea Drilling Project, vol. 4, 503-575, 1970.
- Riedel, W. R. and A. Sanfilippo, Cenozoic radiolaria from the western tropical Pacific, in Initial Reports of the Deep Sea Drilling Project, vol. 7, in press, 1971.
- Rubey, W. W., The force required to move particles on a stream bed, U. S. Geol. Survey Prof. Paper 189-E, 121-140, 1938.
- Ruddiman, W. F., Pleistocene sedimentation in the equatorial Atlantic: stratigraphy and faunal paleoclimatology, Geol. Soc. Amer. Bull., 82, 283-302, 1971.
- Sachs, P. L. and S. O. Raymond, A new unattached sediment sampler, J. Mar. Res., 23, 44-53, 1965.
- Sanders, H. L. and R. R. Hessler, Ecology of the deep-sea benthos, Science, 163, 1419-1424, 1962.
- Sanfilippo, A. and W. R. Riedel, Post-Eocene "closed" theoperid radiolarians, Micropaleontology, 16, 446-462, 1970.
- Seabrooke, J. M., G. L. Hufford and R. B. Elder, Formation of Antarctic Bottom Water in the Weddell Sea, Jour. Geophys. Res., 76, 2164-2178, 1971.
- Schick, G. B., J. D. Isaacs and M. H. Sessions, Autonomous instruments in oceanographic research, in Marine Sciences Instrumentation, 4, Plenum Press, New York, 203-230, 1968.
- Schmitz, W. J., A. R. Robinson and F. C. Fuglister, Bottom velocity observations directly under the Gulf Stream, Science, 170, 1192-1194, 1970.
- Schwartzlose, R. A. and J. D. Isaacs, Transient circulation event near the deep ocean floor, Science, 165, 889-891, 1969.

- Shepard, F. P., Submarine Geology (2nd ed.), Harper and Row, New York, 1963.
- Snodgrass, F., Deep sea instrument capsule, Science, 162, 78-87, 1971
- Southard, J. B., R. A. Young and C. D. Hollister, Experimental erosion of fine abyssal sediment, J. Geophys. Res., 76, in press, 1971.
- Spiess, F. N., M. S. Loughridge, M. S. McGehee and D. E. Boegeman, An acoustic transponder system, Navigation, 13, 154-161, 1966.
- Spiess, F. N., B. P. Luyendyk, R. L. Larson, W. R. Normark and J. D. Mudie, Detailed geophysical studies on the northern Hawaiian arch using a deeply towed instrument package, Mar. Geology, 7, 501-528, 1969.
- Spiess, F. N. and J. D. Mudie, Small scale topographic and magnetic features, in The Sea, 4, Part I, A. E. Maxwell, ed., Interscience, New York, 205-250, 1970.
- Tareyev, B. A., Internal baroclinic waves in flow round irregularities on the ocean floor and their effect on sedimentation processes, Oceanology, 5, 31-37, 1965.
- Tracey, J. I., Jr., et al., Initial Reports of the Deep Sea Drilling Project, vol. 8, U.S. Govt. Printing Ofc., Wash., in press, 1971.
- van Andel, Tj. H. and P. D. Komar, Ponded sediments of the mid-Atlantic Ridge between 22° and 23° north latitude, Geol. Soc. Amer. Bull., 80, 1163-1190, 1969.
- van Andel, Tj. H. et al., Deep Sea Drilling Project, Leg 16, Gentles, 16, 12-14, 1971.
- Vanoni, V. A., Measurements of critical shear stress for entraining fine sediments in a boundary layer, Calif. Inst. of Tech., Keck Lab. of Hydraulics and Water Resources, Rept. #KH-R-7, 47 pp., 1964.
- Wimbush, M. and W. Munk, The benthic boundary layer, in The Sea, 4, Part I, A. E. Maxwell, ed., Interscience, New York, 731-763, 1970.
- Wooster, W. S. and G. H. Volkmann, Indications of deep Pacific circulation from the distribution of properties at five kilometers, J. Geophys. Res., 65, 1239-1249, 1960.

PLATE 1

All figures are at a magnification of X 140.

Fig. 1	<u>Thyrsoecyrtis triacantha</u> (Ehrenberg)	E-10, 57-58 cm
Fig. 2	<u>Thyrsoecyrtis tetracantha</u> (Ehrenberg)	E-10, 0-1 cm
Fig. 3	<u>Sethochytris babylonis</u> (Clark and Campbell)	E-10, 5-7 cm
Fig. 4	<u>Cycladophora turris</u> Ehrenberg	E-10, 0-1 cm
Fig. 5	<u>Thyrsoecyrtis bromia</u> Ehrenberg	E-10, 5-7 cm
Fig. 6	<u>Thyrsoecyrtis bromia</u> Ehrenberg	E-10, 5-7 cm
Fig. 7	<u>Thyrsoecyrtis tetracantha</u> (Ehrenberg)	E-10, 57-58 cm
Fig. 8	<u>Theocampe mongolfieri</u> Ehrenberg	E-10, 0-1 cm
Fig. 9	<u>Artophormis barbadensis</u> (Ehrenberg)	E-17, 20-21 cm
Fig. 10	<u>Artophormis gracilis</u> Riedel	S-8, 22-24 cm
Fig. 11	<u>Dorcadospyris quadripes</u> Moore	S-8, 22-24 cm
Fig. 12	<u>Theocerys</u> sp.	E-17, 20-21 cm
Fig. 13	<u>Lithocyclia aristotelis</u> (Ehrenberg) group	E-10, 0-1 cm
Fig. 14	<u>Lithocyclia angustum</u> (Riedel)	E-25, 17-18 cm
Fig. 15	<u>Lithocyclia aristotelis</u> (Ehrenberg) group	E-10, 50-51 cm
Fig. 16	<u>Dorcadospyris triceros</u> (Ehrenberg)	E-19, 26-27 cm

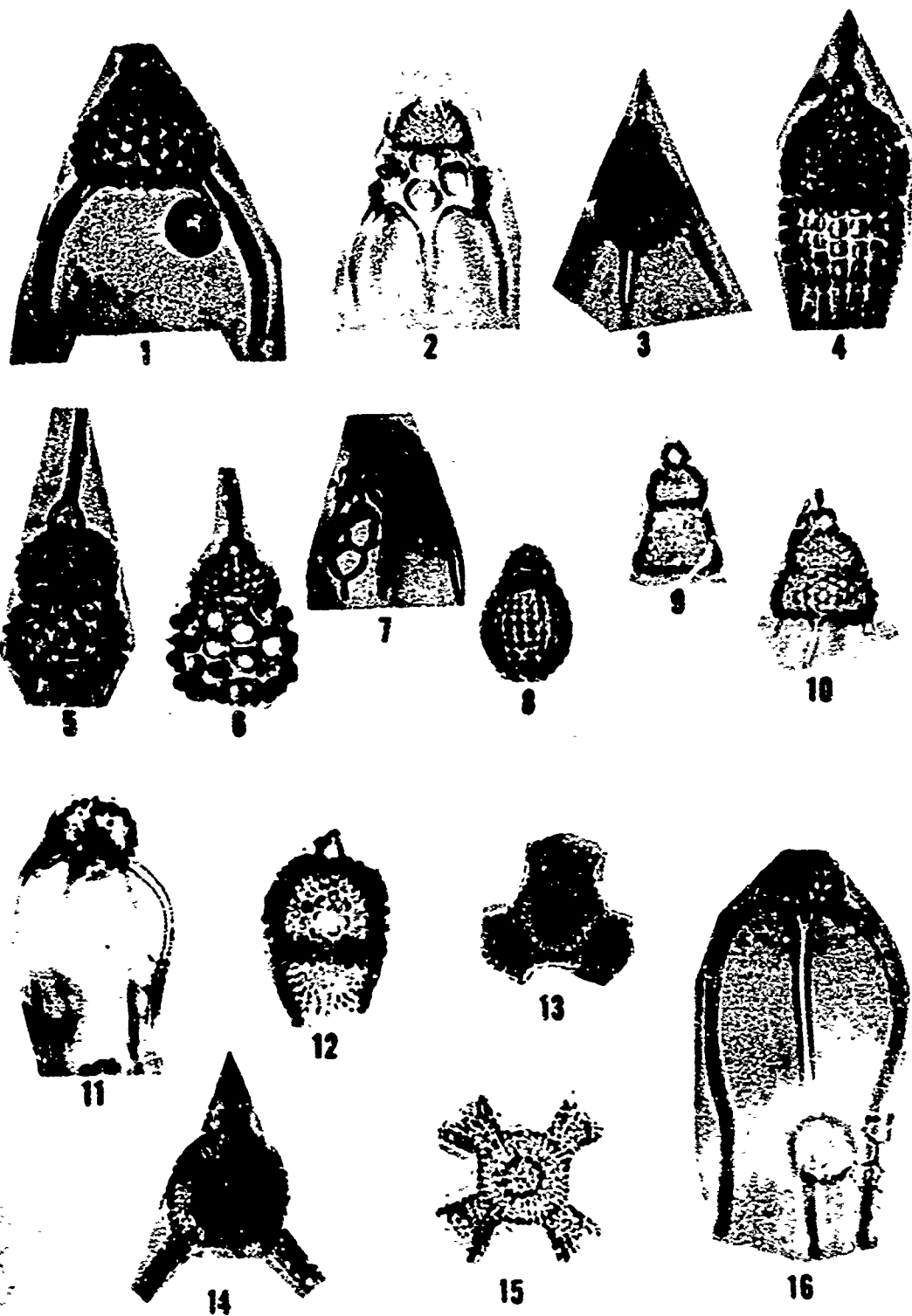


PLATE 2

Figures 1 through 10 are at a magnification of X 140.

Figures 11 through 15 are at a magnification of X 95.

- | | | |
|---------|---|------------------|
| Fig. 1 | <u>Cannartus</u> <u>prismaticus</u> (Haeckel) | S-8, 22-24 cm |
| Fig. 2 | <u>Cannartus</u> <u>tubarius</u> (Haeckel) | E-6, 45-46 cm |
| Fig. 3 | <u>Cannartus</u> <u>violina</u> Haeckel | E-3, 40-42 cm |
| Fig. 4 | <u>Cannartus</u> <u>laticonus</u> Riedel | E-5, 31-33 cm |
| Fig. 5 | <u>Ommatartus</u> <u>antepenultimus</u> Riedel and Sanfilippo | E-27, 110-112 cm |
| Fig. 6 | <u>Ommatartus</u> <u>hughesi</u> (Campbell and Clark) | E-27, 110-112 cm |
| Fig. 7 | <u>Cyclampteryum</u> (?) <u>milowi</u> Riedel and Sanfilippo | E-14, 1-2 cm |
| Fig. 8 | <u>Cyclampteryum</u> <u>pegetrum</u> Sanfilippo and Riedel | S-8, 22-24 cm |
| Fig. 9 | <u>Cyclampteryum</u> <u>leptetrum</u> Sanfilippo and Riedel | E-6, 45-46 cm |
| Fig. 10 | <u>Cyclampteryum</u> <u>tanythorax</u> Sanfilippo and Riedel | E-5, 31-33 cm |
| Fig. 11 | <u>Dorcadospyris</u> <u>ateuchus</u> (Ehrenberg) | S-8, 22-24 cm |
| Fig. 12 | <u>Dorcadospyris</u> <u>simplex</u> (Riedel) | E-6, 45-46 cm |
| Fig. 13 | <u>Dorcadospyris</u> <u>alata</u> (Riedel) | E-5, 31-33 cm |
| Fig. 14 | <u>Dorcadospyris</u> <u>papilio</u> (Riedel) | S-7, 11-13 cm |
| Fig. 15 | <u>Dorcadospyris</u> <u>dentata</u> Haeckel | E-3, 40-42 cm |

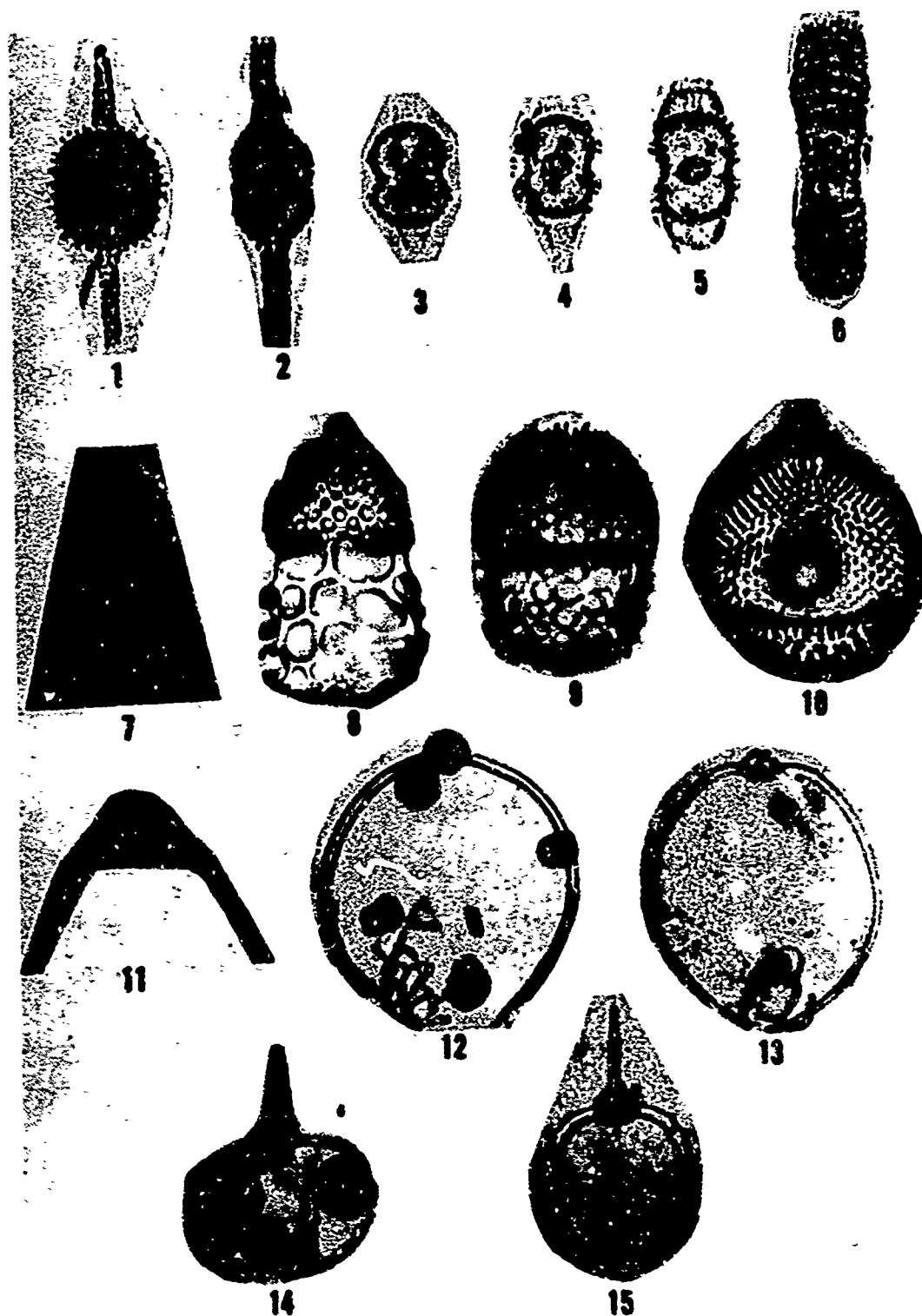


PLATE 3

All figures are at a magnification of X 140.

- | | | |
|---------|--|------------------|
| Fig. 1 | <u>Theocyrtis tuberosa</u> Riedel | E-10, 0-1 cm |
| Fig. 2 | <u>Theocyrtis annosa</u> (Riedel) | S-23, 3-5 cm |
| Fig. 3 | <u>Calocycletta robusta</u> Moore | S-6, 17-19 cm |
| Fig. 4 | <u>Calocycletta costata</u> (Riedel) | E-4, 41-42 cm |
| Fig. 5 | <u>Lychnocanium bipes</u> Riedel | S-7, 11-13 cm |
| Fig. 6 | <u>Calocycletta virginis</u> Haeckel | E-11, 21-22 cm |
| Fig. 7 | <u>Calocycletta virginis</u> Haeckel | E-18, 7-8 cm |
| Fig. 8 | <u>Stichocorys delmontensis</u> (Campbell and Clark) | E-27, 110-112 cm |
| Fig. 9 | <u>Stichocorys wolffii</u> Haeckel | E-3, 40-42 cm |
| Fig. 10 | <u>Cyrtocapsella cornuta</u> Haeckel | E-6, 45-46 cm |
| Fig. 11 | <u>Cyrtocapsella tetrapera</u> Haeckel | E-5, 31-33 cm |
| Fig. 12 | <u>Stichocorys delmontensis</u> (Campbell and Clark) | E-16, 45-46 cm |
| Fig. 13 | <u>Lithopera renzae</u> Sanfilippo and Riedel | E-5, 14-16 cm |
| Fig. 14 | <u>Lithopera renzae</u> Sanfilippo and Riedel | E-5, 31-33 cm |
| Fig. 15 | <u>Lithopera neotera</u> Sanfilippo and Riedel | E-27, 140-142 cm |

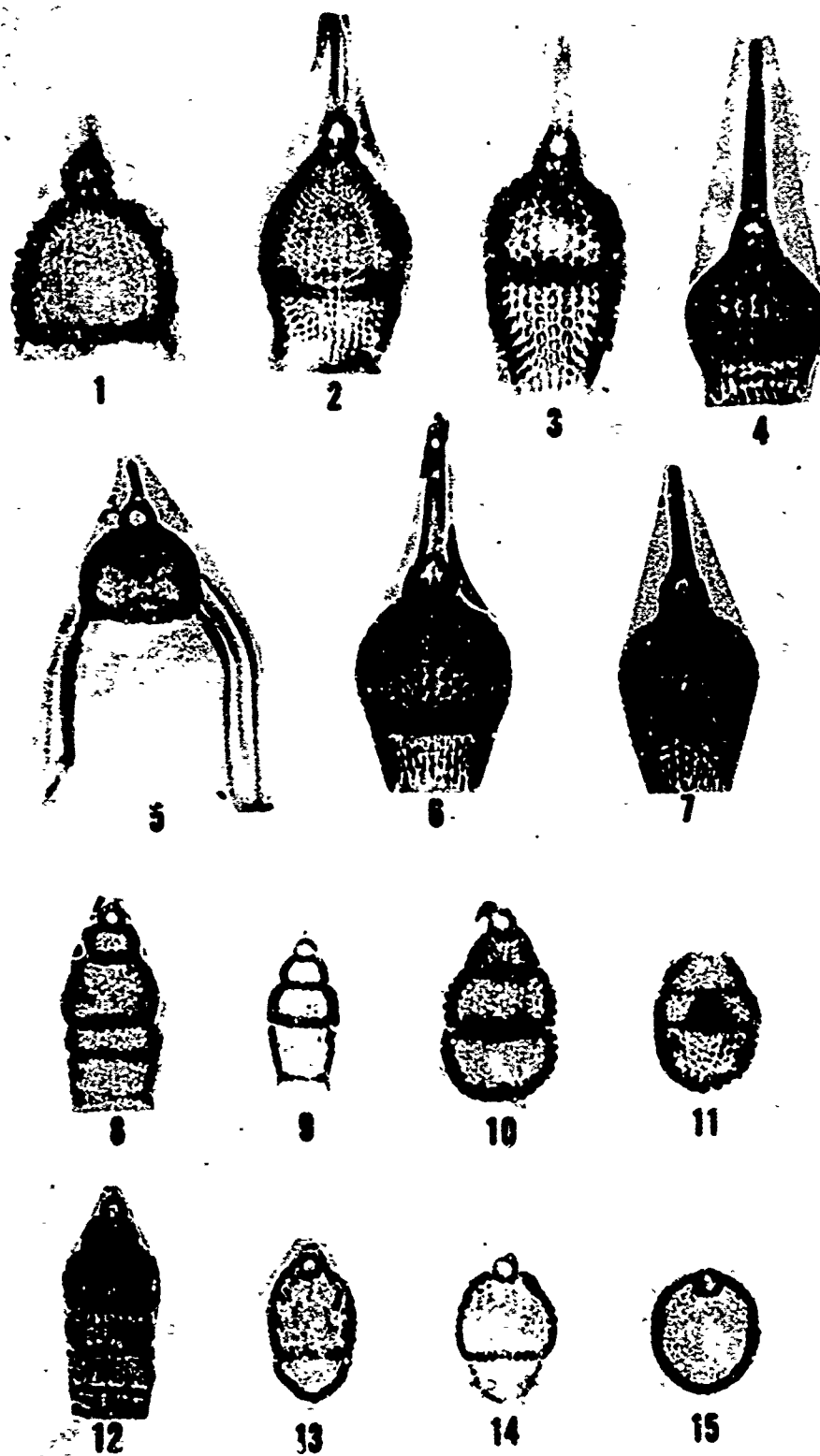


PLATE 4

FREE-FALL CORES: PROFILE I



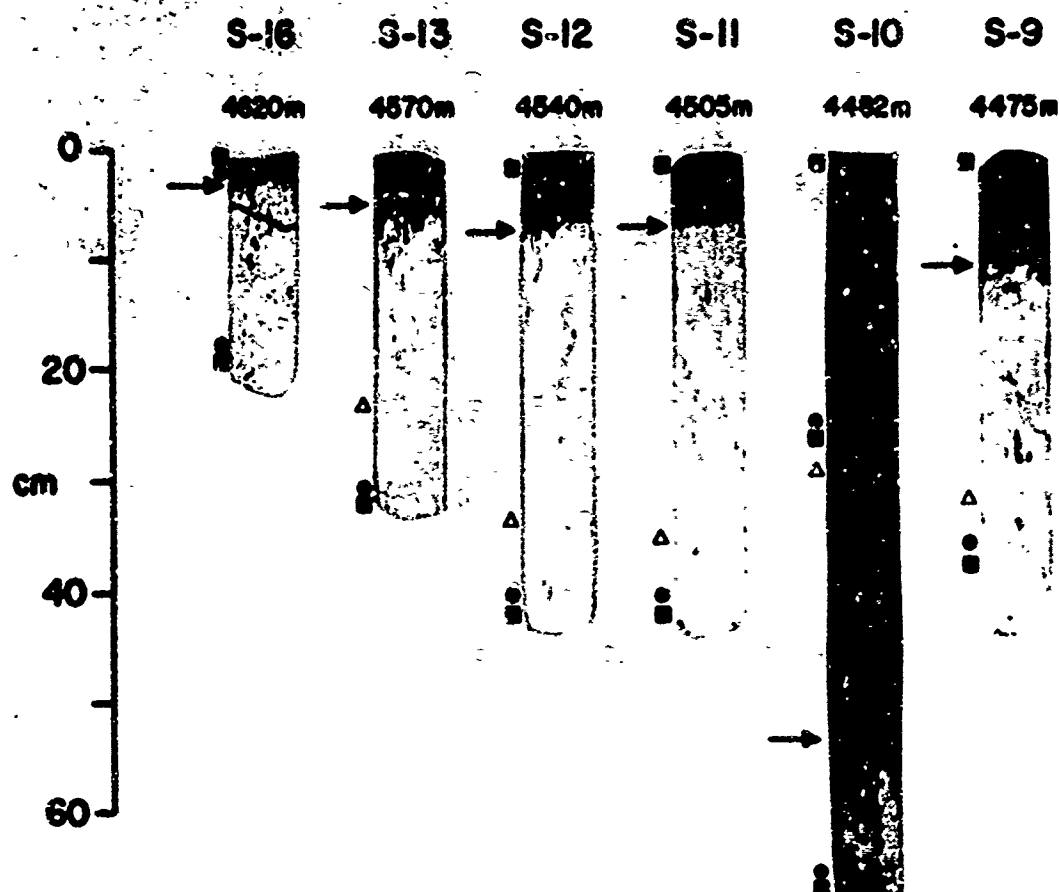
Samples Taken

- Radiolaria
- Foraminifera
- △ Physical properties

→ Holocene - M. Tertiary
unconformity

PLATE 5

FREE-FALL CORES: PROFILE II



Samples Taken

- Radiolaria
- Foraminifera
- △ Physical properties

→ Holocene - M. Tertiary
unconformity

PLATE 6

FREE-FALL CORES: PROFILE III

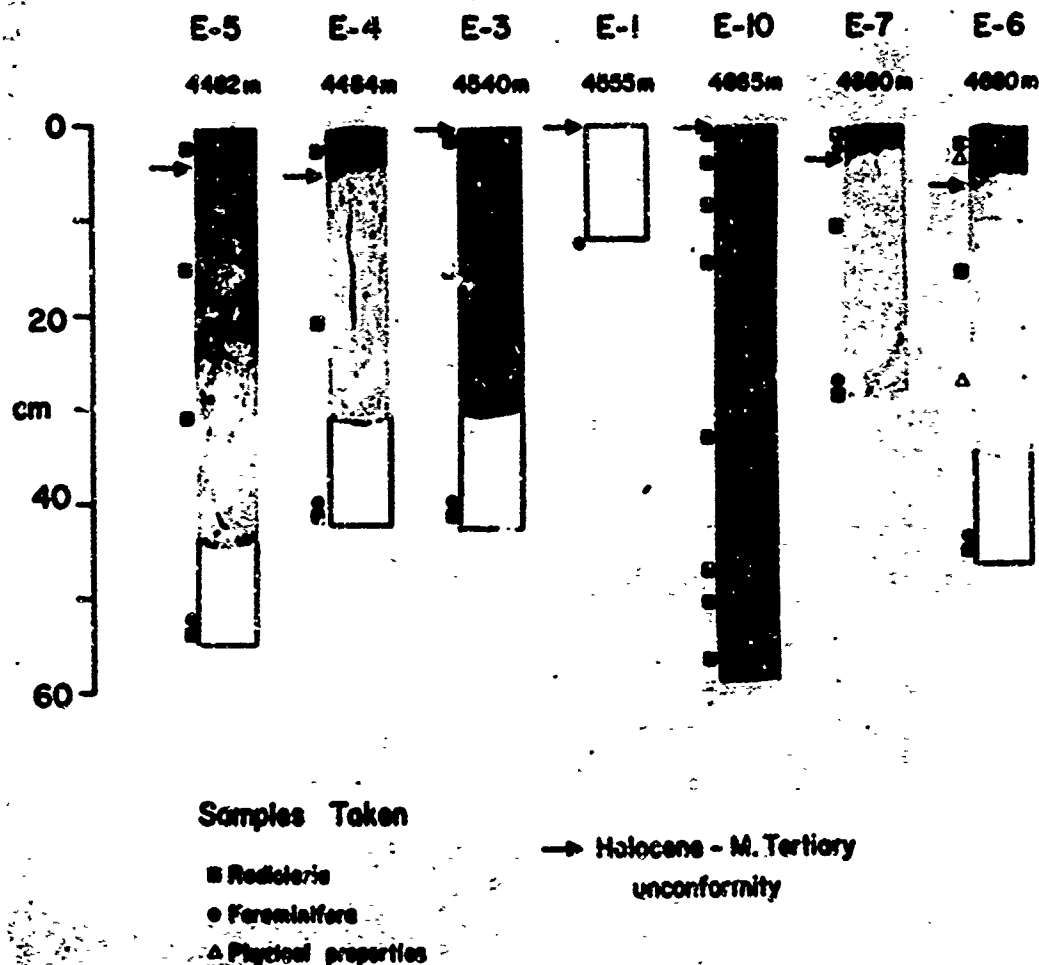
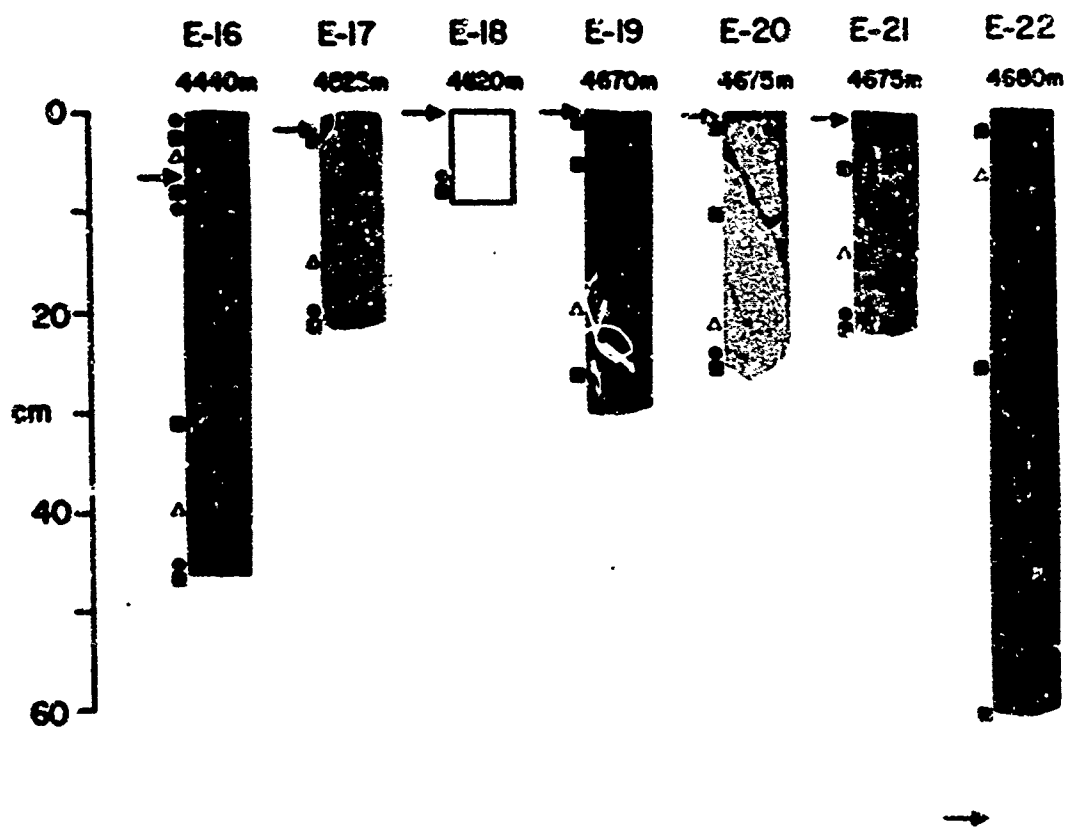


PLATE 7

FREE-FALL CORES: PROFILE IV



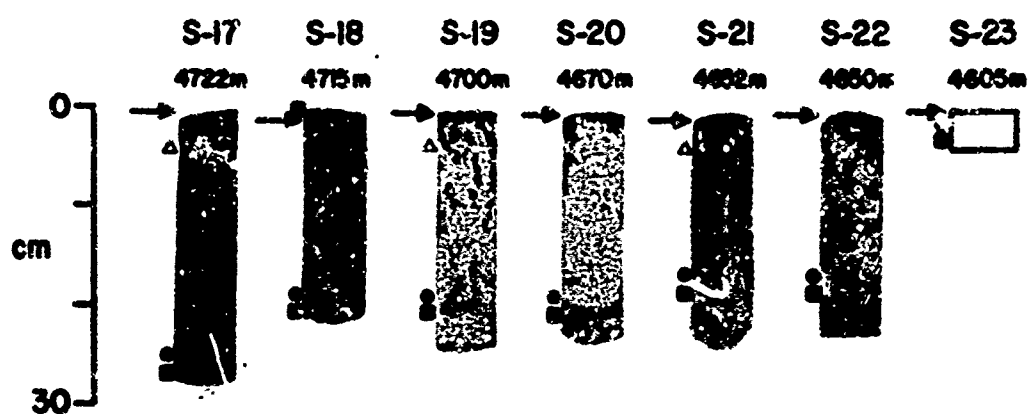
Samples Taken

- Radiolaria
- Foraminifera
- △ Physical properties

→ Holocene - M. Tertiary
unconformity

PLATE 8

FREE-FALL CORES: PROFILE V



Samples Taken

- Radiolaria
- Foraminifera
- △ Physical properties

→ Holocene - M. Tertiary
unconformity

PLATE 9

PISTON CORES

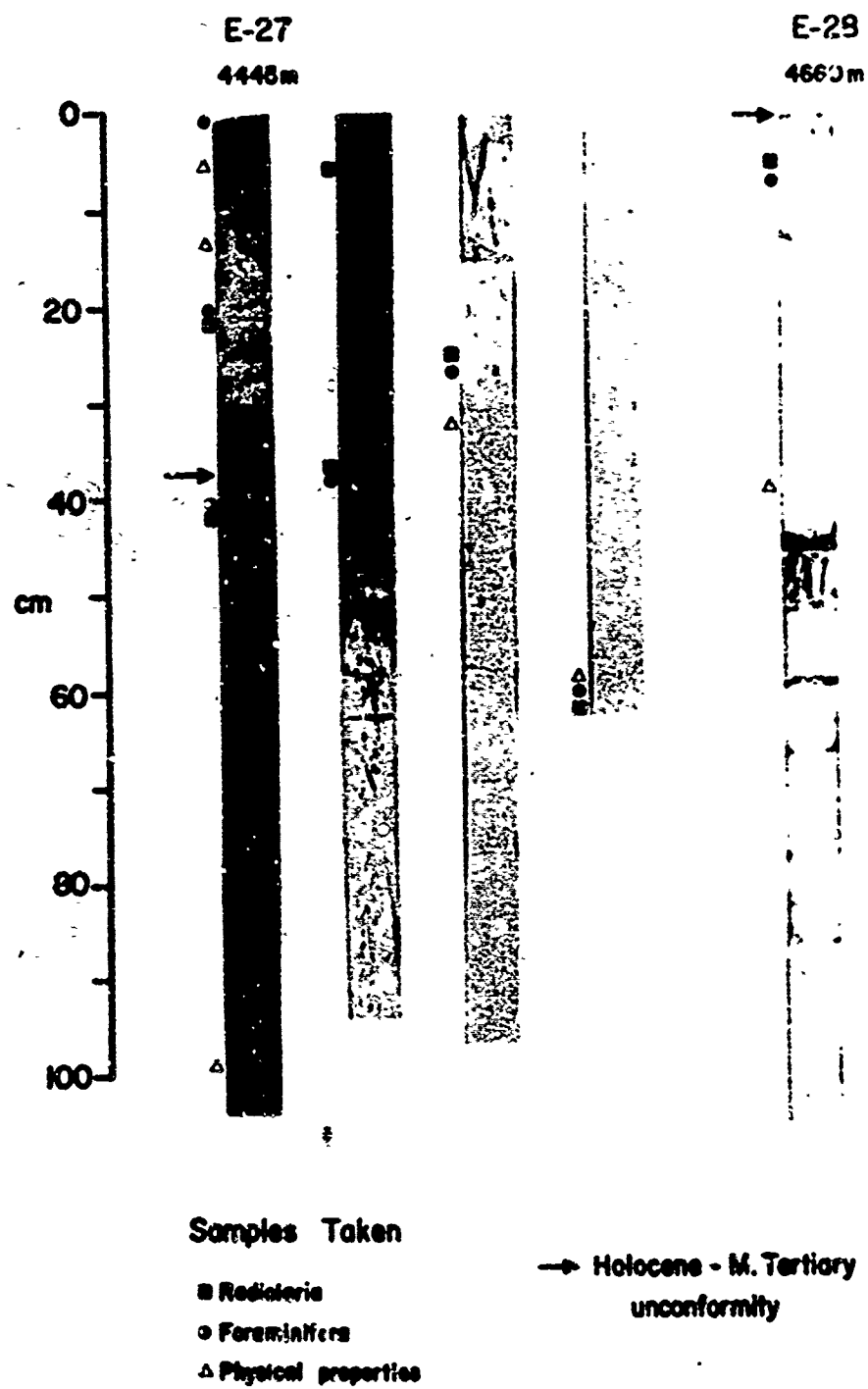
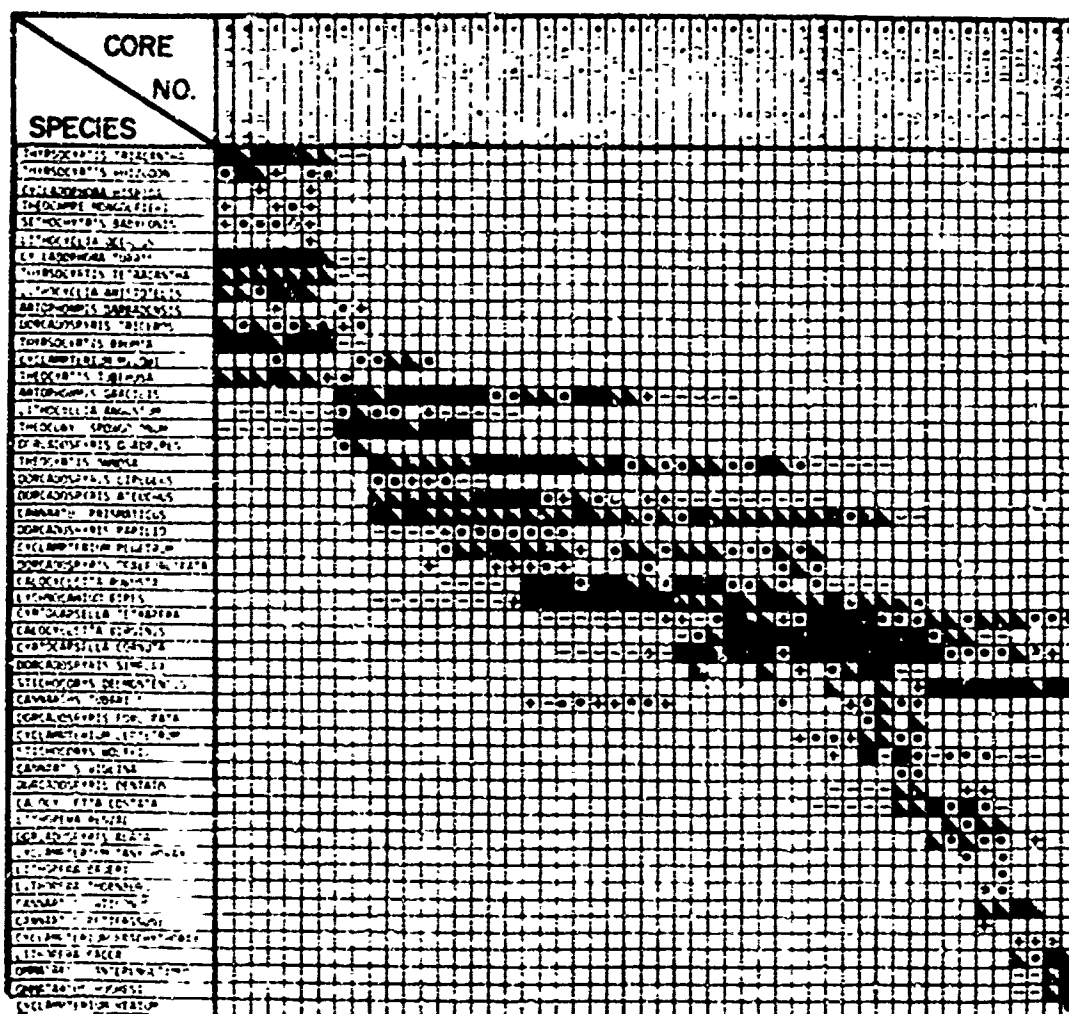


PLATE 10

SPECIES	CORE NO.	
	1	2
CLONCHADINA AMPLIAPUTERA	8-17	8-22 cm
CLONCHADINA CORTANI	8-23	1-10 cm
CLONCHADINA DISTANS	8-24	13-15 cm
CLONCHADINA LUNATA	8-25	1-8 cm
CLONCHADINA LUNATA	8-26	1-8 cm
CLONCHADINA LUNATA	8-27	1-8 cm
CLONCHADINA LUNATA	8-28	1-8 cm
CLONCHADINA LUNATA	8-29	1-8 cm
CLONCHADINA LUNATA	8-30	1-8 cm
CLONCHADINA LUNATA	8-31	1-8 cm
CLONCHADINA LUNATA	8-32	1-8 cm
CLONCHADINA LUNATA	8-33	1-8 cm
CLONCHADINA LUNATA	8-34	1-8 cm
CLONCHADINA LUNATA	8-35	1-8 cm
CLONCHADINA LUNATA	8-36	1-8 cm
CLONCHADINA LUNATA	8-37	1-8 cm
CLONCHADINA LUNATA	8-38	1-8 cm
CLONCHADINA LUNATA	8-39	1-8 cm
CLONCHADINA LUNATA	8-40	1-8 cm
CLONCHADINA LUNATA	8-41	1-8 cm
CLONCHADINA LUNATA	8-42	1-8 cm
CLONCHADINA LUNATA	8-43	1-8 cm
CLONCHADINA LUNATA	8-44	1-8 cm
CLONCHADINA LUNATA	8-45	1-8 cm
CLONCHADINA LUNATA	8-46	1-8 cm
CLONCHADINA LUNATA	8-47	1-8 cm
CLONCHADINA LUNATA	8-48	1-8 cm
CLONCHADINA LUNATA	8-49	1-8 cm
CLONCHADINA LUNATA	8-50	1-8 cm
CLONCHADINA LUNATA	8-51	1-8 cm
CLONCHADINA LUNATA	8-52	1-8 cm
CLONCHADINA LUNATA	8-53	1-8 cm
CLONCHADINA LUNATA	8-54	1-8 cm
CLONCHADINA LUNATA	8-55	1-8 cm
CLONCHADINA LUNATA	8-56	1-8 cm
CLONCHADINA LUNATA	8-57	1-8 cm
CLONCHADINA LUNATA	8-58	1-8 cm
CLONCHADINA LUNATA	8-59	1-8 cm
CLONCHADINA LUNATA	8-60	1-8 cm
CLONCHADINA LUNATA	8-61	1-8 cm
CLONCHADINA LUNATA	8-62	1-8 cm
CLONCHADINA LUNATA	8-63	1-8 cm
CLONCHADINA LUNATA	8-64	1-8 cm
CLONCHADINA LUNATA	8-65	1-8 cm
CLONCHADINA LUNATA	8-66	1-8 cm
CLONCHADINA LUNATA	8-67	1-8 cm
CLONCHADINA LUNATA	8-68	1-8 cm
CLONCHADINA LUNATA	8-69	1-8 cm
CLONCHADINA LUNATA	8-70	1-8 cm
CLONCHADINA LUNATA	8-71	1-8 cm
CLONCHADINA LUNATA	8-72	1-8 cm
CLONCHADINA LUNATA	8-73	1-8 cm
CLONCHADINA LUNATA	8-74	1-8 cm
CLONCHADINA LUNATA	8-75	1-8 cm
CLONCHADINA LUNATA	8-76	1-8 cm
CLONCHADINA LUNATA	8-77	1-8 cm
CLONCHADINA LUNATA	8-78	1-8 cm
CLONCHADINA LUNATA	8-79	1-8 cm
CLONCHADINA LUNATA	8-80	1-8 cm
CLONCHADINA LUNATA	8-81	1-8 cm
CLONCHADINA LUNATA	8-82	1-8 cm
CLONCHADINA LUNATA	8-83	1-8 cm
CLONCHADINA LUNATA	8-84	1-8 cm
CLONCHADINA LUNATA	8-85	1-8 cm
CLONCHADINA LUNATA	8-86	1-8 cm
CLONCHADINA LUNATA	8-87	1-8 cm
CLONCHADINA LUNATA	8-88	1-8 cm
CLONCHADINA LUNATA	8-89	1-8 cm
CLONCHADINA LUNATA	8-90	1-8 cm
CLONCHADINA LUNATA	8-91	1-8 cm
CLONCHADINA LUNATA	8-92	1-8 cm
CLONCHADINA LUNATA	8-93	1-8 cm
CLONCHADINA LUNATA	8-94	1-8 cm
CLONCHADINA LUNATA	8-95	1-8 cm
CLONCHADINA LUNATA	8-96	1-8 cm
CLONCHADINA LUNATA	8-97	1-8 cm
CLONCHADINA LUNATA	8-98	1-8 cm
CLONCHADINA LUNATA	8-99	1-8 cm
CLONCHADINA LUNATA	8-100	1-8 cm

PLATE 11



■ COMMON
 ▲ FEW
 • RARE
 + PRESENT
 - ABSENT

APPENDIX I

BOTTOM PHOTOGRAPHS

FIGURE A-1

Bottom photograph from camera run C, showing large circular mounds of sediment 50 to 100 cm in width and several tens of cm in height. The mounds were probably formed by a burrowing organism.



FIGURE A-2

Bottom photograph from camera run C, showing what may be an outcropping of igneous material. Alternatively, the dark material may be a manganese oxide coating which formed on the erosion surface which overlies the Tertiary sediments.



FIGURE A-3

Bottom photograph from camera run D. The organism in the upper left corner is probably a holothurian (see Fell, 1967, fig. 19-3).

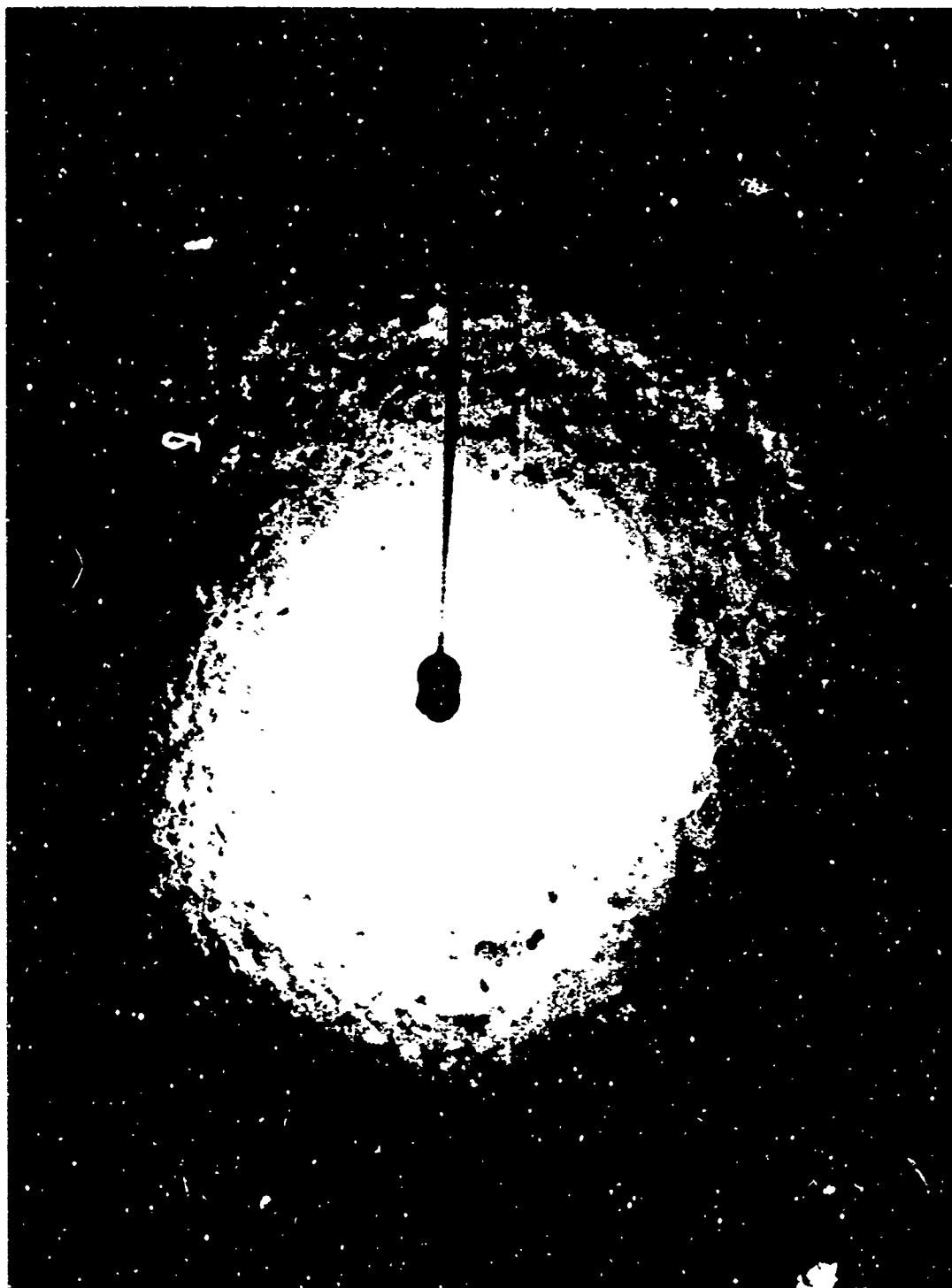


FIGURE A-4

Bottom photograph from camera run K, showing several types of structures created by the activity of benthic organisms. The sea floor is covered with small pits and craters which are barely visible in this photograph. Near the right edge of the photograph there is a somewhat larger crater, with a single straight furrow extending outward from it. A structure indicative of horizontal burrowing by a relatively large organism is present near the top of the picture. Width of the field of view is approximately 3 meters.

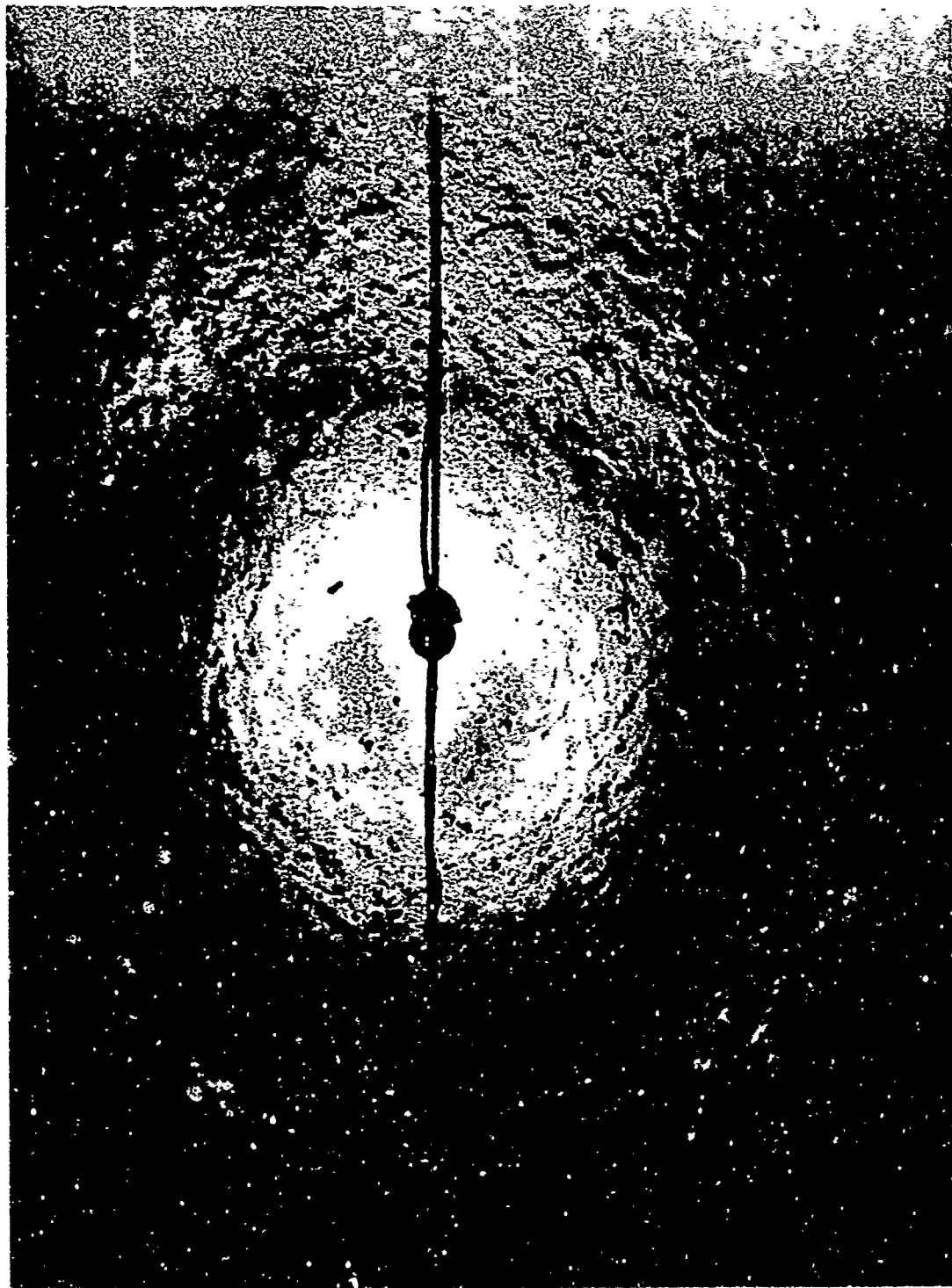


FIGURE A-5

Bottom photograph from camera run K, showing many small craters, pits, and meandering narrow grooves. Some of the grooves may have been formed by organisms such as those illustrated by Ewing and Davis (1967, Figs. 24-40 through 24-44).

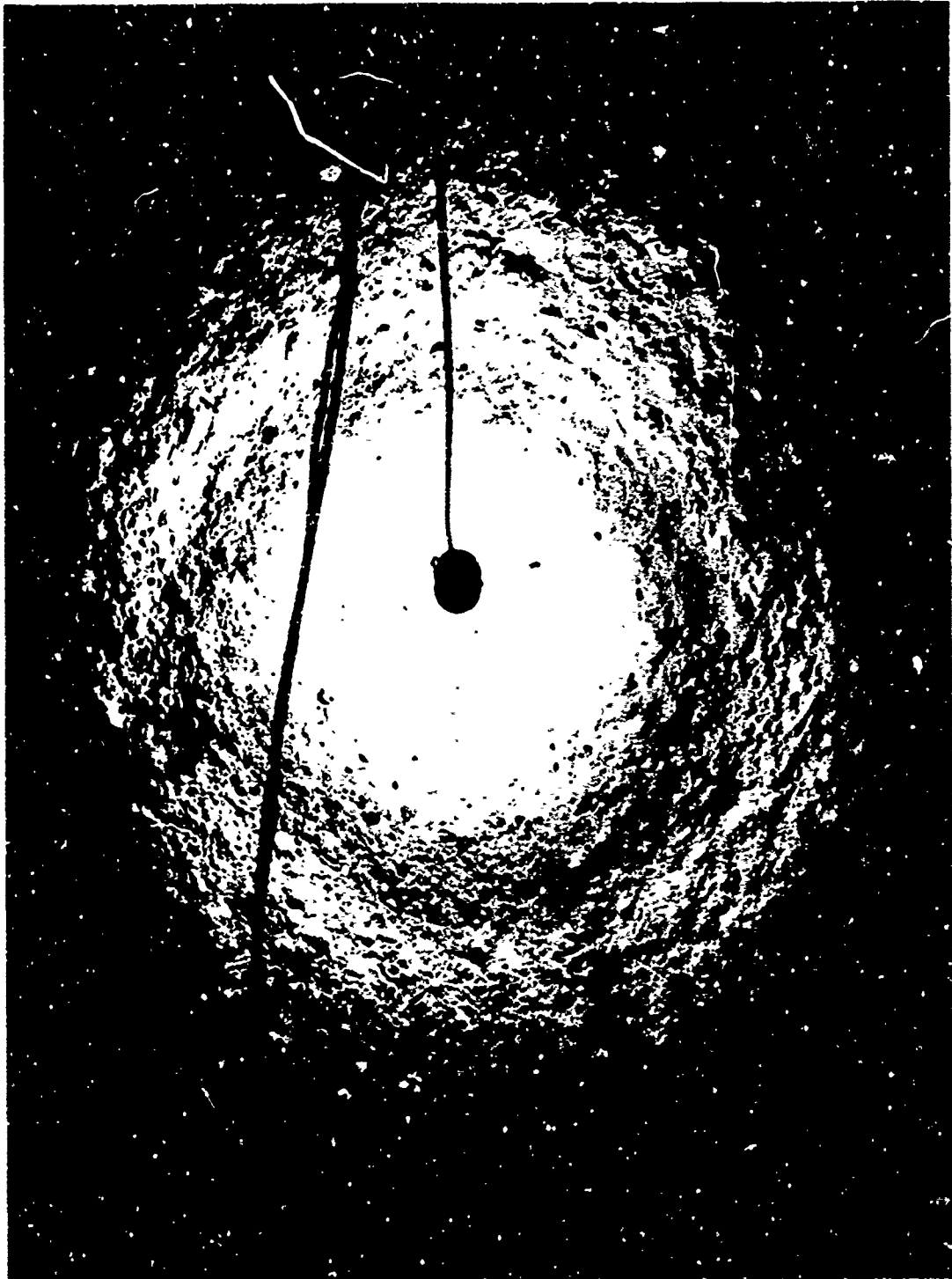


FIGURE A-6

Bottom photograph from camera run K. The meandering path of a burrowing organism can be seen in the upper-right corner of the photograph. The circular cloud of fine-grained sediment beneath the strobe light was put into suspension when the light struck bottom just before the picture was taken. Width of the field of view is approximately 3 meters.

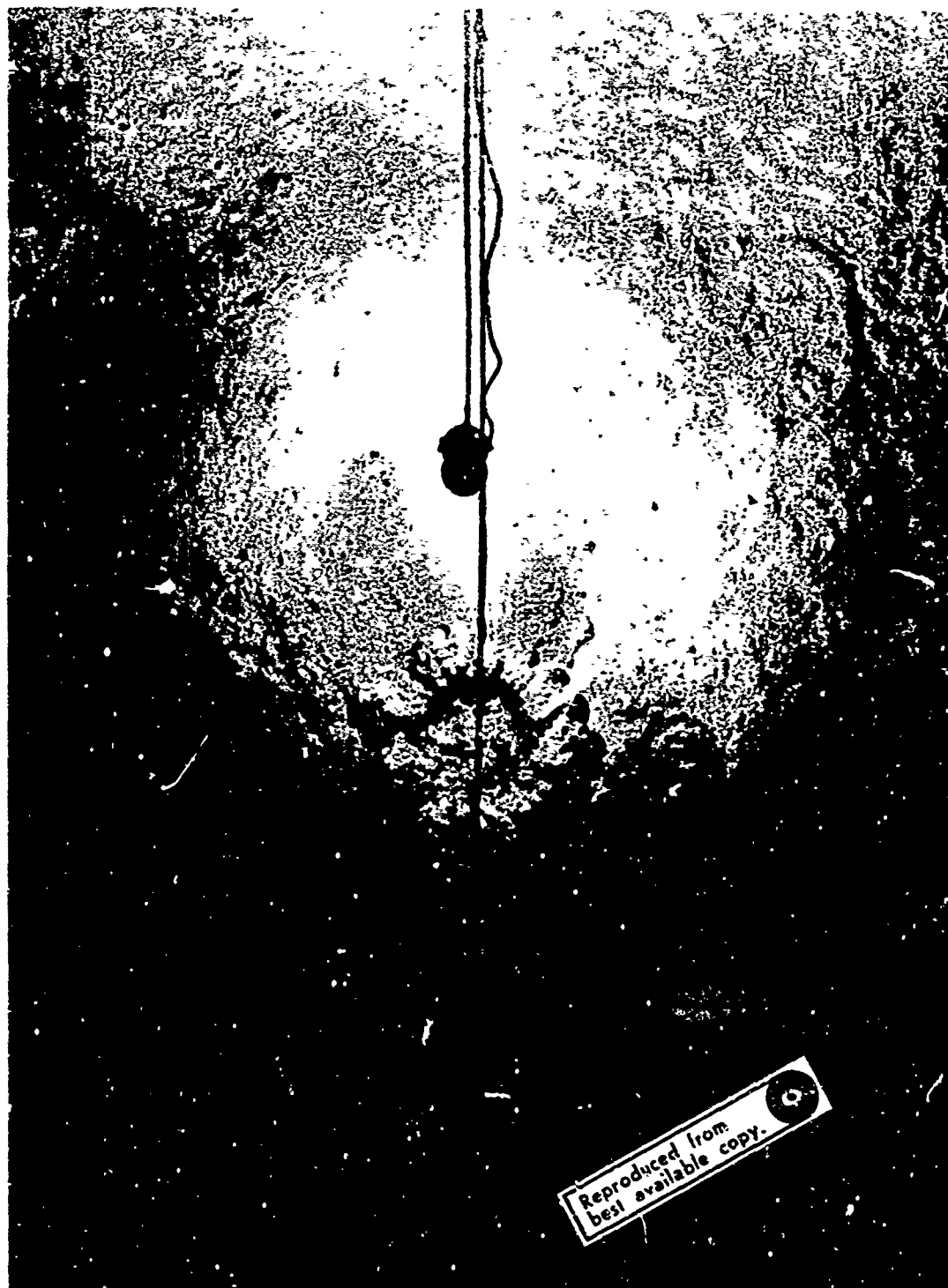


FIGURE A-7

Bottom photograph from camera run K, showing several features indicative of benthic activity. Pits and craters of variable size cover the bottom. Below and to the left of the strobe light is a set of narrow grooves radiating from a central lump (see Ewing and Davis, 1967, Figs. 24-53 through 24-61). A faecal structure appears near the left edge of the photograph.

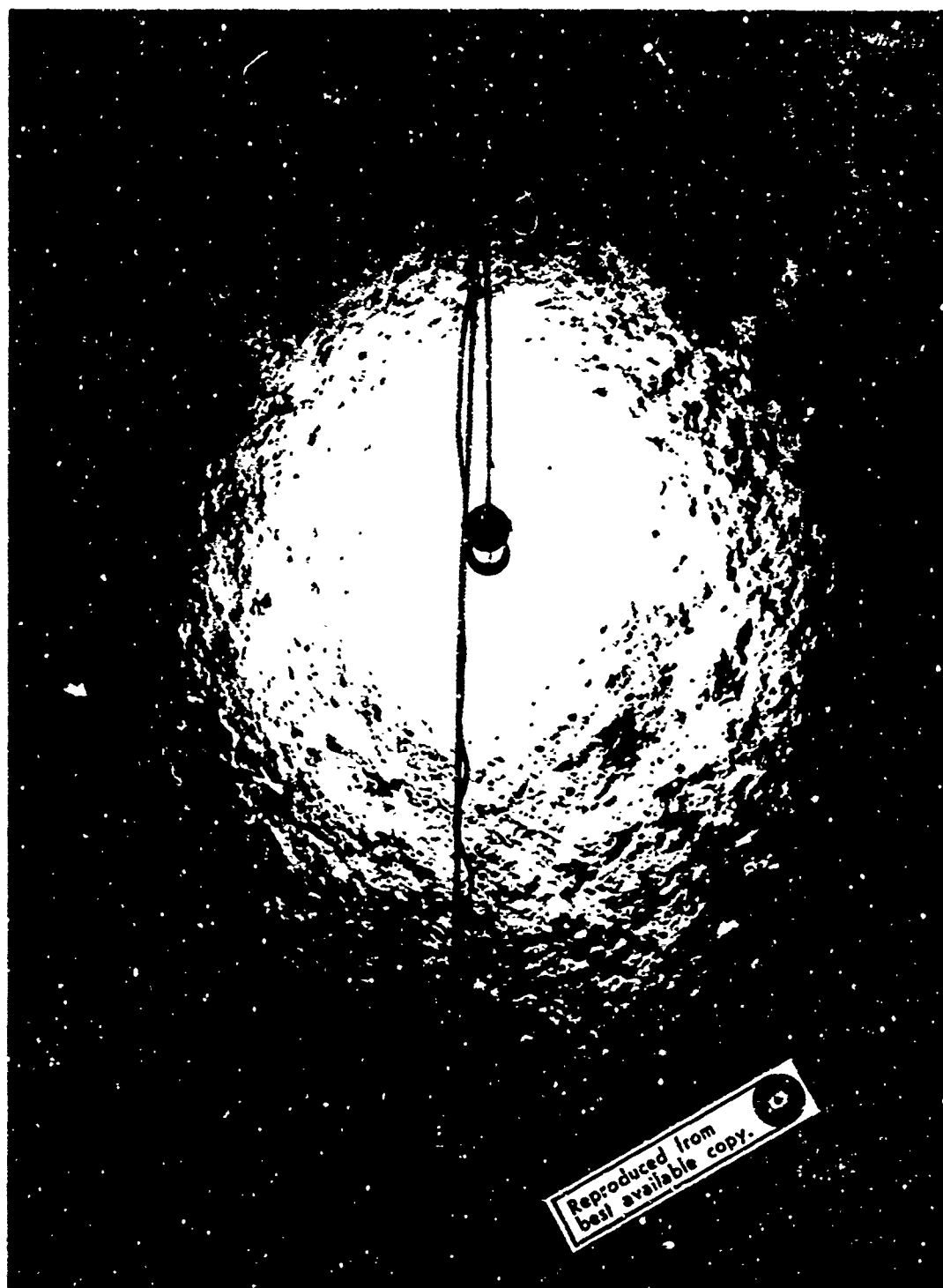


FIGURE A-8

. ttom photograph from camera run K. The dark, irregular fragments may be igneous in origin, or may be manganese oxide coatings. Between the fragments are numerous small pits and meandering trails, indicative of benthic activity.

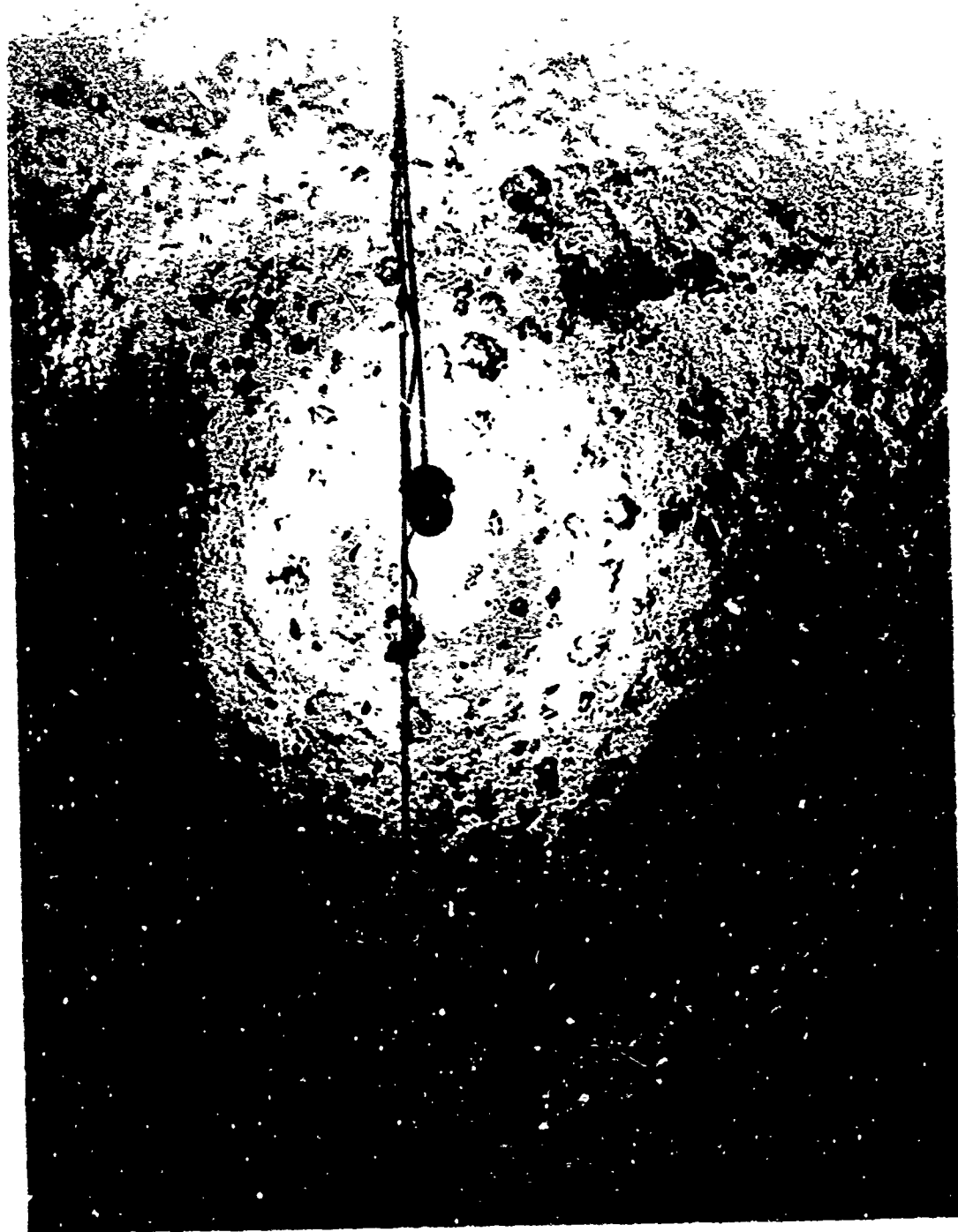
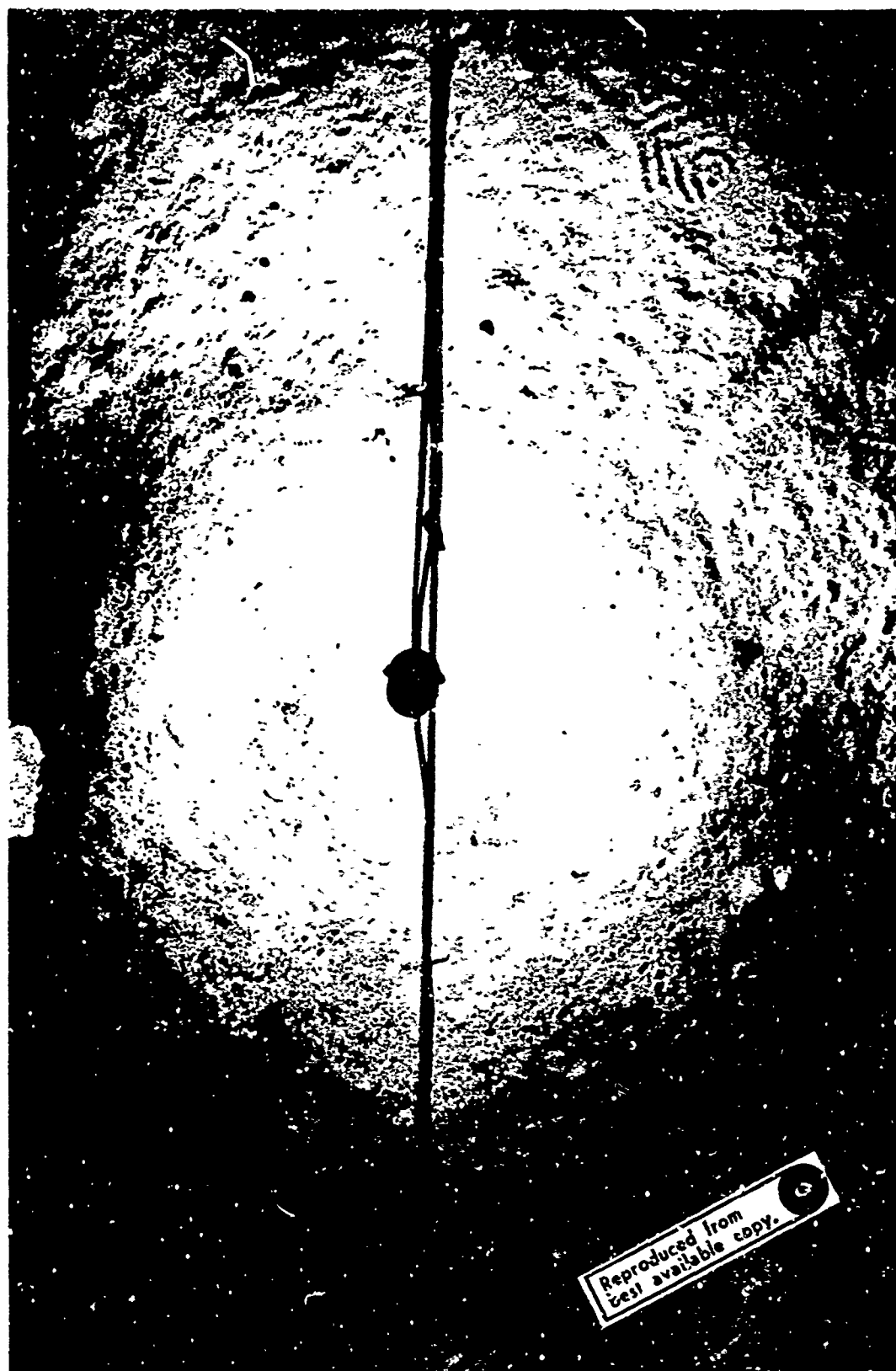


FIGURE A-9

Bottom photograph from camera run M. Two sets of radiating grooves around a central lump can be seen to the right of the strobe light. Near the top of the photograph is a meandering ridge, perhaps formed by an organism of the type illustrated by Ewing and Davis (1967, Figs. 24-3 and 24-4). Width of the field of view is approximately 3 meters.



APPENDIX II

CURRENT METER DATA

Preceding page blank

TABLE 6a

Listing of data obtained by bottom current meters. Instrument #5
recorded current direction only. Speeds indicated are in cm/sec.

DAY	TIME	#2		#3		#4		#5
		Direction	Speed	Direction	Speed	Direction	Speed	Direction
17 OCTOBER	0000	015°	5.6					
		035°	5.4					
		022°	4.9					
		032°	5.4	090°	4.2			
		045°	4.7	090°	5.2	040°	4.8	
	0600	050°	4.7	100°	4.8	058°	4.5	
		049°	5.4	100°	7.0	058°	4.8	105°
		042°	8.8	096°	7.4	057°	4.8	100°
		048°	8.0	105°	5.5	053°	7.0	079°
		055°	8.0	065°	6.6	055°	7.3	068°
	1200	049°	6.0	072°	8.6	060°	7.4	060°
		035°	6.4	072°	7.4	054°	5.8	050°
		049°	4.3	081°	7.0	044°	4.6	068°
		025°	5.3	055°	3.8	050°	4.8	085°
		040°	5.4	100°	3.4	050°	4.5	075°
	1800	050°	4.9	090°	6.2	052°	5.5	120°
		055°	4.1	090°	6.2	062°	4.8	110°
		070°	3.9	100°	7.0	070°	4.5	110°
		078°	4.5	110°	6.6	080°	4.2	126°
		072°	4.1	104°	6.2	080°	4.2	135°
18 OCTOBER	0000	059°	4.5	107°	5.8	072°	3.8	135°
		058°	4.7	100°	6.6	058°	3.8	120°
		044°	4.5	084°	5.8	050°	3.8	100°
		033°	4.5	068°	5.2	040°	3.8	095°
	0600	018°	4.3	078°	5.5	035°	3.8	105°
		010°	5.1	068°	5.2	025°	4.2	095°
		040°	5.3	071°	5.2	030°	5.2	055°
		038°	6.6	072°	5.8	040°	5.2	049°
		040°	5.8	067°	7.0	035°	6.2	107°
	1200	042°	6.0	072°	7.0	040°	6.6	078°
		048°	4.9	068°	7.0	055°	6.6	072°
		054°	5.3	071°	6.6	058°	6.2	075°
		052°	5.1	080°	6.6	060°	6.2	078°
		049°	4.3	074°	7.0	060°	5.2	080°
	1800	045°	4.1	100°	5.8	054°	4.5	089°
		035°	3.3	080°	3.4	054°	3.8	095°
		026°	2.9	122°	3.0	042°	3.8	098°
		020°	3.1	084°	3.0	040°	3.4	098°
		028°	3.4	095°	3.4	040°	3.4	095°
		036°	4.5	085°	4.8	050°	3.8	112°
		035°	3.7	079°	6.2	060°	4.5	115°
		041°	3.3	120°	4.8	065°	4.5	120°
		059°	3.1	086°	4.2	060°	3.8	135°
		081°	3.1	031°	4.8	060°	3.4	125°
		088°	2.9	095°	5.5	075°	3.4	125°
		082°	2.2	086°	4.8	095°	2.6	125°
		030°	3.4	124°	4.3	080°	2.6	125°
		022°	5.1	095°	5.5	040°	3.8	120°

TABLE 6b

Listing of data obtained by bottom current meters. Instrument #5 recorded current direction only. Speeds indicated are in cm/sec.

DAY	TIME	#2		#3		#4		#5
		Direction	Speed	Direction	Speed	Direction	Speed	Direction
19 OCTOBER	0000	014°	6.4	062°	4.2	030°	5.5	090°
		010°	5.4	065°	4.5	030°	6.2	055°
		025°	6.4	078°	4.8	030°	6.6	050°
		009°	6.0	070°	5.5	035°	6.2	035°
		042°	5.8	073°	7.4	030°	7.0	075°
		032°	5.4	084°	6.2	040°	5.6	090°
	0600	050°	4.1	090°	5.2	050°	5.5	100°
		050°	2.9	096°	5.8	050°	4.8	103°
		050°	3.1	098°	6.6	065°	3.4	115°
		057°	4.7	120°	5.5	070°	3.0	116°
		050°	4.5	111°	5.2	050°	3.8	114°
		035°	3.9	105°	5.8	050°	3.8	105°
	1200	013°	4.9	109°	4.2	035°	3.8	095°
		009°	6.8	100°	7.2	020°	4.5	087°
		020°	6.2	030°	0.8	025°	5.2	080°
		023°	4.1	110°	1.7	035°	4.8	075°
		037°	2.1	125°	2.2	043°	3.4	077°
		055°	2.9	110°	2.6	040°	3.4	100°
	1800	030°	2.1	103°	5.2	046°	2.6	125°
		068°	2.9	110°	5.5	045°	2.2	130°
		066°	2.7	116°	6.2	095°	1.7	135°
		039°	2.7	131°	2.2	070°	2.2	130°
		035°	2.2	155°	2.2	050°	1.7	127°
		020°	3.7	101°	3.4	030°	2.6	120°
20 OCTOBER	0000	010°	4.3	180°	0.8	012°	3.8	095°
		010°	4.3	025°	1.7	008°	3.4	065°
		001°	4.3	055°	1.7	008°	2.4	080°
		001°	4.3	020°	2.2	008°	3.4	058°
		001°	4.9	060°	2.6	010°	3.8	067°
		002°	3.3	075°	2.6	010°	3.8	078°
	0600	008°	3.3	095°	2.2	010°	3.0	105°
		020°	2.4	115°	3.4	028°	2.6	115°
		070°	1.1	111°	4.8	050°	1.7	127°
		075°	1.1	119°	3.1	028°	1.3	128°
		043°	2.1	128°	2.2	080°	1.3	130°
		029°	3.1	096°	2.2	050°	1.7	121°
	1200	033°	3.1	095°	3.4	035°	3.0	121°
		015°	3.7	096°	2.6	035°	3.4	116°
		008°	3.9	085°	2.2	025°	2.6	114°
		008°	2.9	086°	3.0	020°	3.4	113°
		355°	2.7	040°	3.0	020°	3.0	100°
		343°	2.1	085°	2.2	010°	3.0	116°
	1800	359°	1.1	055°	3.0	008°	2.2	135°
		000°	0.8	073°	3.0	023°	1.3	140°
		008°	0.8	093°	2.2	030°	1.3	152°
		000°	1.1	100°	2.6	030°	0.8	146°
		355°	1.5	090°	3.4	003°	0.8	149°
		002°	2.4	070°	3.8	000°	1.7	149°

TABLE 6c

Listing of data obtained by bottom current meters. Instrument #5 recorded current direction only. Speeds indicated are in cm/sec.

DAY	TIME	#2		#3		#4		#5
		Direction	Speed	Direction	Speed	Direction	Speed	Direction
21 OCTOBER	0000	001°	2.4	070°	4.2	003°	2.6	135°
		001°	3.9	080°	3.4	002°	3.0	114°
		004°	6.0	060°	3.0	002°	4.2	112°
		005°	6.2	050°	3.4	010°	5.9	072°
		005°	4.9	032°	3.4	012°	5.5	064°
		007°	3.1	142°	1.3	020°	4.5	032°
		008°	2.7	130°	1.3	016°	2.6	099°
	0600	010°	2.2	125°	1.3	026°	1.7	130°
		019°	2.4	120°	3.0	030°	2.6	133°
		024°	2.7	128°	3.0	026°	3.0	155°
		016°	3.4	150°	1.3	038°	2.6	104°
		013°	4.3	112°	1.7	025°	2.2	093°
		008°	4.7	096°	1.7	018°	2.6	103°
		010°	4.9	085°	2.2	019°	4.2	082°
	1200	003°	6.2	045°	3.4	017°	4.5	055°
		359°	7.4	033°	3.4	008°	5.8	019°
		000°	5.8	025°	3.0	007°	5.8	010°
		000°	3.7	032°	2.6	007°	3.0	018°
		000°	3.3	060°	2.6	010°	3.0	100°
		000°	2.4	089°	2.2	021°	2.2	122°
		000°	1.5	095°	1.7			135°
	1800	005°	0.8	096°	2.2			141°
		005°	1.3	119°	2.6			150°
		013°	2.7					
	0000	009°	4.7					
		004°	5.8					
		004°	6.8					
		001°	6.4					
		000°	6.4					
		000°	6.0					
		000°	5.4					
22 OCTOBER	0600	355°	3.3					
		358°	3.4					

Scientific personnel on R/V THOMAS WASHINGTON during EQUATOR
expedition, October 1969:

C. Ingram, R. Hitchcock, M. D. Benson, H. R. Kaye, R. W. Cooke,
J. T. Donovan, M. Elston, D. E. Boegeman, P. H. Rapp,
C. D. Lowenstein, F. N. Spiess, D. A. Johnson, M. G. Dinkelman,
F. W. Stone, J. Pew.

Not pictured: C. Isaacs, W. B. F. Ryan

